9860064
Udo Schilcher

Inhomogeneous Node Distributions and Interference in Wireless Networks

DISSERTATION

zur Erlangung des akademischen Grades
Doktor der technischen Wissenschaften

Alpen-Adria-Universität Klagenfurt
Fakultät für Technische Wissenschaften

Univ.-Prof. Dr.-Ing. Christian Bettstetter
Institute of Networked and Embedded Systems
University of Klagenfurt

Prof. Dr. Martin Haenggi
Dept. of Electrical Engineering
Dept. of Applied and Comp. Math.
University of Notre Dame

July 2011

Ich erkläre ehrenwörtlich, dass ich die vorliegende wissenschaftliche Arbeit selbstständig angefertigt und die mit ihr unmittelbar verbundenen Tätigkeiten selbst erbracht habe. Ich erkläre weiters, dass ich keine anderen als die angegebenen Hilfsmittel benutzt habe. Alle aus gedruckten, ungedruckten oder dem Internet im Wortlaut oder im wesentlichen Inhalt übernommenen Formulierungen und Konzepte sind gemäß den Regeln für wissenschaftliche Arbeiten zitiert und durch Fußnoten bzw. durch andere genaue Quellenangaben gekennzeichnet.

Die während des Arbeitsvorganges gewährte Unterstützung einschließlich signifikanter Betreuungshinweise ist vollständig angegeben.

Die wissenschaftliche Arbeit ist noch keiner anderen Prüfungsbehörde vorgelegt worden. Diese Arbeit wurde in gedruckter und elektronischer Form abgegeben. Ich bestätige, dass der Inhalt der digitalen Version vollständig mit dem der gedruckten Version übereinstimmt.

Ich bin mir bewusst, dass eine falsche Erklärung rechtliche Folgen haben wird.

(Unterschrift)	(Ort, Datum)

Acknowledgements

I would like to thank my supervisor, Prof. Christian Bettstetter, who always helped me focusing on the positive side of my research, and my second examiner, Prof. Martin Haenggi, who immediately accepted to review this thesis. I also would like to thank my colleagues at the Institute of Networked and Embedded Systems, especially Michael Gyarmati, Günther Brandner, Sérgio Crisóstomo, Helmut Adam, and Wilfried Elmenreich for interesting and helpful discussions during the years of research, and Johannes Klinglmayr for sharing his lunch time with me. Very warm thanks go to Kornelia, the good spirit of our institute. Without each of you I would not have kept my motivation up for such a long time.

Further, I would like to express my gratitude and close friendship to my dear friends Tanja & Sigi, Wolfi, Holger (let's headbang), Karin, Robert, Heli the geek, Sonja & Walter, Zaiga & Markus, Thomas, and Stefan for distracting me from work. You reminded me that there is more in the world than wireless networks.

I also want to say thank you to my fighting friends at the Traditional Taekwondo Club Poggersdorf and at the Academic Karate Club Klagenfurt. Ossu!

Last but not least, I would like to thank my family, especially my parents Brunhilde and Ernst, who made all this possible; and to the one, who gave a sense to everything: Manuela. You are mine!

Inhomogeneous Node Distributions and Interference in Wireless Networks

Many research and engineering tasks in the area of wireless communications necessitate simulation based studies of wireless networks. If such simulations should be beneficial, many different aspects of the network and its environment have to be modeled as realistically as possible. The thesis at hand contributes to two groups of such models: the spatial distribution of nodes and the interference model.

When regarding spatial node distributions, many research work is based on a uniform distribution. One of the reasons for that is the lack of an easy-to-use model that generates inhomogeneous node distributions. As shown, e.g., in Chapter 5, the node distribution has great influence on the performance of different protocols. Hence, the node distribution applied in a simulation study should closely reflect the node distribution of the real scenario, which is rarely a uniform distribution. We propose a model for synthesizing inhomogeneous node distributions, a metric for measuring inhomogeneity, and a mobility model for inhomogeneously distributed mobile nodes in Chapter 3 of this thesis, to counteract this lack within the research community.

In Chapter 4, we give attention to interference in wireless networks. We have to mention that not only the strength of interference, but also its temporal and spatial behavior has strong influence on the performance of many communication protocols. Hence, to analyze these protocols it is necessary to calculate the temporal and spatial correlation of interference. We contribute to this issue by deriving closed-form expressions for the temporal correlation of interference in several scenarios.

Finally, in Chapter 5 we conduct a simulation based study to compare time and space-time diversity methods with conventional communication protocols. The results of this study show that the performance of a wireless network is to a great extent determined by the interference present in the network. It is therefore advantageous to reduce the interference as much as possible.

Inhomogene Knotenverteilungen und Interferenz in kabellosen Netzwerken

Viele Forschungs- und Entwicklungstätigkeiten im Bereich kabelloser Kommunikation erfordern simulationsgestützte Untersuchungen. Damit solche Simulationen zu den gewünschten Resultaten führen, müssen viele verschiedene Aspekte sowohl des zu simulierenden Netzwerks als auch von dessen Umgebung so realistisch wie möglich modelliert werden. Die vorliegende Doktorarbeit trägt zu dieser Modellierung in zwei Bereichen bei: in der Modellierung der räumlichen Knotenverteilung und bei Interferenzmodellen.

Betrachtet man die Knotenverteilung, so sieht man, dass viele Forschungsarbeiten auf einer zweidimensionalen Gleichverteilung der Knoten basieren. Eine der Ursachen dafür ist, dass es keine einfach zu verwendenden Modelle zur Erzeugung von inhomogenen Knotenverteilungen gibt. Wie z.B. in Kapitel 5 ersichtlich, hat die Verteilung der Knoten großen Einfluss auf die Leistung verschiedener Protokolle. Somit ist es wichtig, dass die Verteilung der Knoten in der Simulation jene in realen Szenarien möglichst genau widerspiegelt. In Kapitel 3 der vorliegenden Arbeit schlagen wir ein Modell für die Synthese von inhomogenen Knotenverteilungen, ein Maß für Inhomogenität sowie ein Mobilitätsmodell für inhomogen verteilte Knoten vor, um diesem Problem entgegenzuwirken.

Kapitel 3 beschäftigt sich mit Interferenz in kabellosen Netzwerken. Es ist festzustellen, dass nicht nur die Stärke, sondern auch die zeitliche und räumliche Veränderung der Interferenz großen Einfluss auf die Performanz von Kommunikationsprotokollen hat. Daher ist zur Analyse solcher Protokolle eine genaue Kenntnis der zeitlichen und räumlichen Korrelation von Interferenz essentiell. Die vorliegende Arbeit leistet dazu den Beitrag, eine geschlossene Formel für die zeitliche Korrelation in verschiedenen Szenarien herzuleiten.

In Kapitel 5 wird schließlich eine simulationsbasierte Studie durchgeführt, die verschiedene Diversity-Techniken mit konventionellen Kommunikationsprotokollen vergleicht. Das Ergebnis dieser Studie lässt den Schluß zu, dass die Übertragungsleistung in einem Netzwerk in erster Linie von der vorhandenen Interferenz bestimmt wird. Daher ist es von Vorteil Methoden anzuwenden, welche die Interferenz so weit wie möglich reduzieren.

Contents

1 Introduction **1**

2 Modeling Wireless Networks **3**

2.1 Node Distribution 5
2.2 Node Mobility 8
2.3 Wireless Channel 10
2.4 Digital Modulation over AWGN Channels 15
2.5 Medium Access 16
2.6 Data Traffic 20
2.7 Interference 21
2.8 Transmission Methods 24

3 Inhomogeneous Distribution of Nodes **27**

3.1 A Model for Inhomogeneous Node Distributions 27
3.1.1 Introduction of the Model 28
3.1.2 Stochastic Properties of the Distribution 29
3.1.2.1 Percentage of Nodes Remaining 30
3.1.2.2 Expected Number of Previous Neighbors 30
3.1.2.3 Survival Probability of the Nearest Neighbor 31
3.1.2.4 Survival of Other Neighbors 33
3.1.2.5 Nearest Neighbor Distance 35
3.1.2.6 Distance to Other Neighbors 36
3.1.3 Visualization for Different Parameters 37
3.2 Measuring Inhomogeneity 39
3.2.1 A Grid-Based Inhomogeneity Measure 40
3.2.1.1 Definitions 40
3.2.1.2 Derivation of the Inhomogeneity Measure 41
3.2.1.3 Basic Properties of $\psi(z)$ 42
3.2.1.4 Minimum and Maximum of ψ 43
3.2.1.5 Visualization 45

3.2.2 Comparison Between the Measure and Human Perception of Inhomogeneity . . . 45
3.2.2.1 General Results . . . 46
3.2.2.2 Perception of Linear Operations . . . 46
3.3 Related Work for Inhomogeneous Node Distributions . . . 47
3.3.1 Models for Inhomogeneous Node Distribution . . . 47
3.3.2 Measuring Inhomogeneity . . . 48
3.3.3 Mobility Models . . . 49

4 Temporal Correlation of Interference **51**
4.1 Correlation between Interference of Disjoint Node Sets . . . 52
4.2 Temporal Correlation of Interference . . . 54
4.2.1 The Non-Random Case $(0, 0, 0)$. . . . 57
4.2.2 The Cases Without Correlation; Cases $(0, 0, 1)$, $(0, 1, 0)$, and $(0, 1, 1)$. . . . 57
4.2.3 The Correlation for Independent Node Distributions; Cases $(1, j, k)$. . . . 57
4.2.4 The Correlation Caused by the Node Distribution; Cases $(2, j, k)$ with $j, k \in \{0, 1\}$. . . . 57
4.2.5 The Correlation Caused by the Traffic; Cases $(0, 0, 2)$ and $(0, 1, 2)$. . . . 58
4.2.5.1 Fixed Channel . . . 58
4.2.5.2 Random Independent Channel . . . 61
4.2.6 The Correlation Caused by Node Distribution and Traffic; Cases $(2, j, 2)$, $j = 0, 1$ . . . 62
4.2.7 The Correlation Caused by Fading; Cases $(0, 2, 0)$, $(2, 2, 0)$. . . . 64
4.2.8 The Correlation Caused by Fading Under Random Traffic; Cases $(2, 2, 1)$, $(0, 2, 1)$. . . . 65
4.2.8.1 Random Node Locations . . . 66
4.2.8.2 Nonrandom Node Locations . . . 66
4.2.9 The Correlation Caused by Fading and Traffic; Case $(0, 2, 2)$. . . . 69
4.2.10 The Correlation Caused by Node Distribution, Fading, and Traffic; Case $(2, 2, 2)$. . . . 74
4.3 Related Work for Interference Models and Analysis . . . 75
4.3.1 Interference Models . . . 75
4.3.2 Analytical Work on Interference Correlation . . . 76
4.3.3 Practical Work on Interference and its Correlation . . . 76

5 Case Study: Analysis of the Overall Network Throughput **79**

5.1 Simulation Setup 79
5.2 Simulation Results 81
5.3 Related Work for Network Capacity Analysis 84
5.3.1 Analysis of the Network Capacity 84
5.3.2 The Impact of Cooperative Diversity 84
5.3.3 Interference Related Capacity Analysis 87
5.3.4 Network Capacity in Sparse Networks 87

6 Conclusion and Future Work **89**

A Simulations of Inhomogeneous Node Distributions **91**

List of Symbols **93**

List of Own Publications **99**

Curriculum Vitae **101**

Bibliography **103**

List of Figures

2.1 Different models for simulation of a wireless network and their interconnections. . . . 4
2.2 Deriving the pdf of the distance between N_1 and a randomly chosen node. . . . 7
2.3 Throughput for different MAC protocols (for CSMA $a = 0.01$). . . . 17
2.4 The hidden terminal problem. . . . 19
2.5 The exposed terminal problem. . . . 20

3.1 Spatial distributions and thinning. . . . 28
3.2 Border effect in the thinning algorithm. . . . 29
3.3 Neighborhoods and common areas. . . . 31
3.4 Pdfs of the nearest neighbor distance before and after the thinning process. . . . 35
3.5 Simulations with fixed k and increasing r. . . . 37
3.6 Simulations with fixed r and increasing k. . . . 38
3.7 Simulations with increasing r and k. . . . 39
3.8 Multiple thinning. . . . 39
3.9 Different inhomogeneity values for a moved cluster. . . . 41
3.10 Inhomogeneity values for different distributions. . . . 45
3.11 Effect of linear operations on human perception. . . . 46

4.1 Interference correlation in case $(0, 0, 2)$. . . . 60
4.2 Interference correlation in case $(0, 1, 2)$. . . . 61
4.3 Interference correlation in case $(2, 0, 2)$. . . . 64
4.4 Interference correlation in case $(2, 2, 1)$. . . . 66
4.5 Interference correlation in case $(0, 2, 1)$. . . . 68
4.6 Interference correlation in case $(0, 2, 2)$. . . . 73
4.7 Interference correlation in case $(2, 2, 2)$. . . . 74

5.1 Successful transmissions in Scenario 1. . . . 81
5.2 Relative success frequencies for Scenarios 1-4. . . . 82

5.3 Relative success frequencies for Scenarios 1 and 3. 83
5.4 Relative success frequencies for Scenarios 2 and 4. 83

List of Tables

2.1 Bit and symbol error probabilities of different modulation schemes [Gol05]. 16

3.1 Answers in the online survey. 46
3.2 Effect of linear operations in online survey. 47

4.1 Correlation of interference – summary of results. 56
4.2 Blocks for node behavior. 69

5.1 Simulation scenarios 80
5.2 Simulation parameters 81

A.1 Comparison of simulated and calculated values, part 1. 91
A.2 Comparison of simulated and calculated values, part 2. 92

Chapter 1

Introduction

The development of new methods, technologies, and protocols for wireless networks is very time and cost intensive. It must be ensured that newly developed techniques are comprehensively tested before they are deployed in real devices. Hence, there is a huge demand for performance assessment tools such as testbeds and simulators. Especially simulators are the means of choice by many researchers as they are cost efficient, highly flexible, and accurate. Newly developed methods are easily integrated into a simulator allowing for quick performance tests.

The simulation of wireless networks raises the need for a broad range of different models: the radio channel, the distribution of the nodes, mobility and many other aspects have to be part of the simulator. Each aspect has to be modeled as realistically as possible since the accuracy of the models highly impacts the accuracy of the simulation results. These results only become meaningful if accurate models are applied. The development of these models is therefore a very important field of research within the community of wireless networks.

While many of the models needed for simulators are already comprehensively investigated, others are not. One important aspect of modeling wireless networks that still needs further insights is to answer the following question: How should the nodes of a network be placed to realistically reflect the placement of the participants of a real network? The classical approach would be to uniformly distribute the nodes on a given area. This approach is very easy to handle, since it is implemented in all simulation tools and it simplifies all further mathematical analysis. It, however, lacks realism since our daily experience tells us that people and hence their devices concentrate on certain spots of interest while other places are rarely visited by anyone. At these spots of interest most of the users form clusters leaving just a few users isolated. These clusters could model, e.g., people in classes, meetings, offices, etc. They should not be fixed over time, but nodes should be able to change their clusters as, e.g., real users would change their group when going from one meeting to another. Hence, there is a need for having a model that distributes the nodes of a network in an inhomogeneous manner. Such a model should incorporate the aspects of the behavior of real users as described above.

A further issue in wireless networks that still lacks research is the modeling of interference. Interference denotes the impact of concurrent transmissions on each other. The amount of interference as well as its temporal and spatial behavior, i.e., whether interference is fast or slowly changing over time and space, heavily influence the performance of many different protocols and mechanisms. A research topic of increasing interest is therefore to analyze the temporal and spatial correlation of interference in a wireless network. In this field mainly Haenggi and Ganti have published analytical results in [HG09, GH09a, Hae09]. Despite their interesting contributions there are still open issues to address: First, they only considered the node locations as source of interference correlation while there might be others. Second, the impact of the interference correlation on existing communication protocols has to be investigated.

The thesis at hand contributes to the above mentioned research questions threefold: First, a comprehensive overview of all models needed for the simulation of a wireless network and the most common approaches to each of them is presented in Chapter 2. Second, in Chapter 3 we contribute to the modeling of inhomogeneous node distributions. We propose a model for inhomogeneously distributing the nodes of a network. This model has the advantages that it is easy to implement and that it exhibits nice stochastic properties. Further, a metric for measuring the inhomogeneity of a given node distribution is introduced. Such a metric is necessary to compare synthetic node distributions to real distributions of users with regard to their inhomogeneity. Third, Chapter 4 contributes to the analysis of the temporal correlation of interference. In this chapter we derive analytical expressions for the temporal correlation of interference for three different sources of correlation: the node locations, the wireless channel, and the traffic.

Chapter 5 of the thesis applies the models discussed above by conducting a simulation based study on the performance of diversity techniques. It compares the overall network performance of time and space-time diversity with conventional communication methods. The results show that the performance of the network is mainly determined by the interference present at the destination nodes. Hence, it is preferable to apply techniques that minimize interference over approaches that try to increase the throughput of a single link without considering the impact of interference. Chapter 6 finally concludes this thesis and gives a short overview of open issues and further research steps.

Preliminary results of this thesis have been obtained in cooperation with M. Gyarmati, G. Brandner, and C. Bettstetter. They are published in [1, 2, 9] and are currently under review in [10]. Note that publications by the author of this thesis are referenced by numbers (e.g. [2]) while all others are referenced alphanumerically (e.g. [HG09]).

Chapter 2

Modeling Wireless Networks

When developing new methods, protocols, or technologies for wireless networks it is necessary to have means to assess their performance. While testbeds and prototypes are best in terms of realism, their construction and setup procedures are usually very time and cost intensive. Therefore, computer based simulations of wireless networks are the method of choice for performance assessment by many researchers. Their advantages are manifold: They are usually cheap, quickly implemented, and very flexible. Any new update in the method under investigation can be easily integrated into the simulation tool.

The major disadvantage of simulation based analysis is, however, that it may lack realism in several aspects. This lack arises from the fact that all environmental factors that have influence on the wireless network have to be represented via a mathematical model. These factors are, e.g., the wireless channel, the locations and movements of the nodes, and the data traffic. In Figure 2.1 we give an overview of the most important models needed when simulating wireless networks. Some of the environmental factors cannot be reproduced in each and every detail, but have to be approximated by some statistical model. Therefore, the realism of the simulations mainly depend on the accuracy of the applied models. In the following we show the relations between all models shown in Figure 2.1 and give a detailed overview of the different approaches to each of them.

When simulating a wireless network, one of the major questions to be answered is: What is the probability that a given transmission succeeds? Equivalently, we can ask for the *outage probability*, which is the probability that a transmission fails. Answering this question is a highly sophisticated task since it depends on many different parameters and models.

The success of a given transmission mainly depends on the *signal to interference and noise ratio* (SINR). Hence, the following three parameters determine the success of a transmission:

1. The received signal power is determined by the channel and the transmission power, which are described by the channel model. We can further subdivide

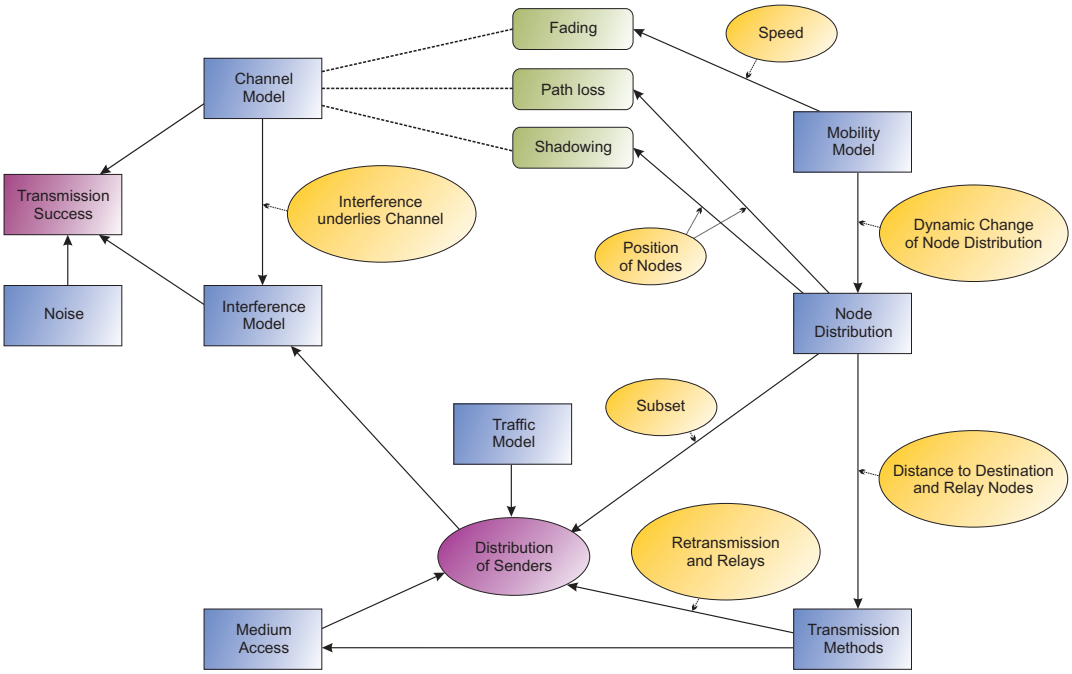

Figure 2.1: Different models for simulation of a wireless network and their interconnections.

the channel model according to the three major effects occurring in wireless communication: The first is the *path loss model* that describes the decrease of the signal strength with distance. The second model describes *shadowing*, the decrease of the signal strength due to obstacles. Finally, the third model describes the effects of *fading*, which is the influence of the multipath propagation due to reflection, scattering, and diffraction on the signal strength.

2. The channel model has not only influence on the received signal strength, but also on the *interference power*. For a given transmission interference is defined as the power arriving at the destination from the sending nodes of all other concurrent transmissions. On their paths from the interfering nodes to the destination these signals also underly the same effects as the signal from the source and are hence similarly effected by it.

3. The noise power is determined by system parameters as bandwidth and does not depend on other models.

The interference additionally depends on the number and *distribution of sending nodes*. This distribution is determined by mainly four influence factors: First, the *traffic model* has huge influence on the distribution of senders since it selects which nodes are trying to transmit a message. It could range from purely random choice to modeling an application that raises large spatial dependencies on the traffic

generation. Second, the *medium access* (MAC) protocol also determines the distributions of the senders. If, e.g., CSMA/CA is used there is at least a given distance between two sending nodes due to its channel reservation mechanism; for ALOHA protocols this is not the case. Third, the transmission method may trigger additional transmissions, e.g., due to retransmission of lost packets. The connection between the transmission methods and the MAC protocol in Figure 2.1 indicates that the transmission methods may be implemented as part of the MAC layer in the network stack and influence the behavior of the MAC protocol itself. As an example, cooperative relaying protocols may raise the need for longer channel reservations to allow the additional relaying message to take place [AEBS09]. Finally, fourth, the *node distribution* itself is a huge influence factor on the distribution of senders, since the senders are always a subset of the set of all nodes. If the node distribution is modeled via a stochastic point process, the distribution of senders could be interpreted as a *thinning* of this process.

Finally, the *node distribution* has some influence on the transmission methods (e.g. it determines if there are good relay nodes for cooperative relaying); and it has also a huge impact on path loss (over the distance distribution) and on shadowing. It is influenced or even determined by the mobility model for obvious reasons. The *mobility model* additionally influences several parameters of fading whose characteristics significantly depend on the nodes' speed.

In the following sections we provide a more detailed description of each of the models appearing in Figure 2.1. Additionally, we specify the models and parameters used for the analytical work in the following chapters.

2.1 Node Distribution

When simulating a wireless network, the spatial distribution of the nodes is of essential importance. In first place the node distribution determines the distribution of the distances to the neighbors of a node. As a further consequence it influences, on the one hand, local parameters, e.g., the channel quality between a given node and its neighbors (see [Sch05]). This behavior connects the node distribution to the channel model and is further described in Section 2.3. On the other hand, it influences global network parameters, e.g., the connectivity of the network (see [Bet02, DTH02] and [5]).

Before going into detail on nodes distributions, we define the Poisson point process [DVJ03].

Definition 2.1. Let $N(a_i, b_i]$ denote the number of events of a stochastic point process within the interval $(a_i, b_i]$ with $a_i < b_i \leq a_{i+1}$. If the equation

$$\mathbb{P}\big(N(a_i, b_i] = n_i,\ i = 1, \ldots, k\big) = \prod_{i=1}^{k} \frac{\big(\lambda(b_i - a_i)\big)^{n_i}}{n_i!}\, \mathrm{e}^{-\lambda(b_i - a_i)}\,. \tag{2.1}$$

holds, the stochastic point process is called a *Poisson point process*. The symbol λ is called the *intensity* of the process.

A Poisson point process possesses the following properties:

- The number of points in each finite interval $(a_i, b_i]$ follows a Poisson distribution with mean value $\lambda(b_i - a_i)$.
- The distance between a point and its nearest neighbor, both in the same finite interval $(a_i, b_i]$, follows an exponential distribution with mean value $\lambda(b_i - a_i)$.
- The numbers of points in disjoint intervals are stochastically independent.
- The distributions are stationary, i.e., they depend only on the lengths $b_i - a_i$ of the intervals, not on the values of a_i and b_i.

Let $\mathcal{N}$ denote a Poisson point process with intensity λ. Nodes are located at all points in $\mathcal{N}$. For easier notation, $x \in \mathcal{N}$ further denotes both the point of the process as well as the node located at this point.

For some investigations it is reasonable to consider a bounded area instead of an infinite point process. Let therefore A denote an area of size $a \times b$, where $a = b$ if necessary. A can be regarded as a subarea of $\mathcal{N}$ where the number of nodes n is a random number following a Poisson distribution. Then $\lambda = \frac{n}{A}$ is called the density of the nodes within A.

Let $\mathcal{S}$ denote the set of all sending nodes, which is a subset of $\mathcal{N}$. The node distribution together with the traffic model determines the distribution of sending nodes and thus indirectly the spatial distribution of the interference. Last but not least, the node distribution has a major influence on certain transmission methods. As an example one could think of relay selection strategies in cooperative relaying. For more details on that refer to Section 2.8.

As we have seen the distance between two nodes is of great importance. We introduce two different distance measures that both are often used in simulations. Usually, the distance between two nodes $x, y \in \mathcal{N}$ is measured by means of the Euclidean metric, which is defined as

$$d(x, y) \coloneqq \sqrt{(x_1 - y_1)^2 + (x_2 - y_2)^2}\,. \tag{2.2}$$

The major advantage of this metric is that it best represents the real world. When using a bounded area A, however, border effects may arise that may degrade the quality of simulation results dramatically. This different behavior of nodes located near the boundaries of the area A stems from the fact that these nodes have a lower number of neighbors (see [SB03, Bet04]). An easy way to avoid border effects is the use of a wrap-around distance metric that assumes a border of A to be connected to

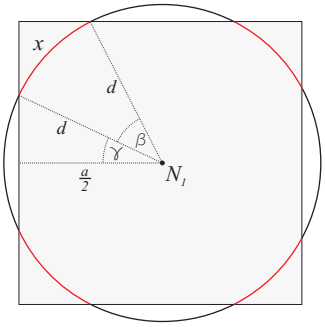

Figure 2.2: Deriving the pdf of the distance between N_1 and a randomly chosen node.

its opposite border (see [Cre91]). This metric is defined as

$$\begin{aligned} d_w(x,y) \quad := \quad & \min\Big(\sqrt{(x_1-y_1)^2+(x_2-y_2)^2}, \sqrt{(x_1-y_1-a)^2+(x_2-y_2)^2}, \\ & \sqrt{(x_1-y_1+a)^2+(x_2-y_2)^2}, \sqrt{(x_1-y_1)^2+(x_2-y_2-b)^2}, \\ & \sqrt{(x_1-y_1)^2+(x_2-y_2+b)^2}, \sqrt{(x_1-y_1-a)^2+(x_2-y_2-b)^2}, \\ & \sqrt{(x_1-y_1-a)^2+(x_2-y_2+b)^2}, \sqrt{(x_1-y_1+a)^2+(x_2-y_2-b)^2}, \\ & \sqrt{(x_1-y_1+a)^2+(x_2-y_2+b)^2}\Big) . \end{aligned} \tag{2.3}$$

Although this metric successfully avoids all border effects, it is to some degree unrealistic since in real world applications wrap-around distances almost never occur. Even the avoidance of the border effects can reduce the realism of a simulation, since they may occur in real systems. Hence, an analysis of the impact of the border effects is sometimes preferable over the avoidance of them (see, e.g., [BZ02]).

Next, we are going to derive the probability density function (pdf) of the distance between a given node N_1 and a randomly chosen node N_i when the wrap-around metric (2.3) is applied. Let therefore n nodes be uniformly distributed on an area $A = a^2$ and N_1 be an arbitrary but fixed node. Due to the wrap-around metric we can, without loss of generality, place N_1 in the middle of A, i.e., at the position $(\frac{a}{2}, \frac{a}{2})$.

The probability for $d_w(N_1, N_i) = d$ is proportional to the circumference of the circle with radius d around N_1, as long as $d \leq \frac{a}{2}$. For larger distances, this circle is no longer a subset of A, as can be seen in Figure 2.2. Therefore, the pdf is proportional to the sum of the red parts of the circle in Figure 2.2, which we denote by $4x$. To compute the value of x we use the fact that $\gamma = \arccos\left(\frac{a}{2d}\right)$ and $\beta = \frac{\pi}{2} - 2\gamma$. Thus, $x = d\beta$, where the angle β is measured in radian. When integrating the resulting function considering the bounds 0 to $\frac{1}{\sqrt{2}}$, the result is a^2 since we sum over all parts of the circles within A and thus calculate the area of A. Hence, we have to normalize

the function in order to get a proper pdf. In summary we have

$$f_{d(N_1,N_i)}(d) = \begin{cases} \frac{2d\pi}{a^2} & \text{for } 0 \leq d \leq \frac{a}{2} \\ \frac{2d}{a^2}\left(\pi - 4\arccos\left(\frac{a}{2d}\right)\right) & \text{for } \frac{a}{2} < d \leq \frac{a}{\sqrt{2}}\,. \end{cases} \tag{2.4}$$

Although a Poisson point process simplifies mathematical analysis, it is sometimes necessary to apply an inhomogeneous node distribution [AGL09a, AGLM10, AGL09b]. There are several different methods to create inhomogeneous node distributions $\mathcal{T}$. One class of methods is based on *thinning* of a homogeneous node distributions or of a Poisson point process. The term thinning refers to the removal of some nodes of the process. If this thinning is conducted based on some spatial dependencies, the resulting node distribution is inhomogeneous. As an example, the method for generating an inhomogeneous distribution $\mathcal{T}$, which is introduced in Section 3.1.1, is based on thinning a Poisson point process or uniform distribution.

An alternative approach is to follow a *two step method*: First, the cluster centers are distributed on the area A with some distribution, which could be a uniform distribution or a grid distribution as in [LH06]. Second, all other nodes are placed around these cluster centers according to some placement strategy. This placement strategy could be to uniformly distribute the nodes within a circle around the cluster centers, as in [AM01]. Alternatively, they could be distributed according to a Gaussian distribution around the cluster centers [VWAH06].

It is also possible to apply an inhomogeneous Point process to place the nodes. As an example, a Cox process could be applied [Cox55], which is similar to a Poisson point process but with the intensity λ being a random variable. Note that the simplest case of a Cox process for which the intensity is randomly selected once and then kept constant over the whole area still gives a uniform node distribution. If an inhomogeneous node distribution is desired, the intensity has to be randomly selected as a function of the location, possibly with some spatial dependencies. Therefore, the structure of the resulting distribution (e.g. the number of clusters, their locations) is mainly based on the value of λ as a function of the position, and hence it is determined by the spatial dependencies of λ.

The number of nodes within $\mathcal{T}$ is furtheron denoted by n'.

2.2 Node Mobility

In many real world scenarios the nodes are moving, which introduces the need for a mobility model in a simulation environment. The area of mobility models is a well-investigated field with a huge variety of different approaches and solutions. The most basic and therefore often used models are briefly described in this section.

The most commonly used mobility model in research on wireless networks is the *random waypoint* (RWP) model [JM96, BHPC04, BRS03]. A node moving according to the RWP model can be described by a stochastic process $i \mapsto (P_i, V_i, T_{p,i})$ with

the time index $i \in \mathbb{N}$. For each i, a node chooses a location (*waypoint*) P_i inside the simulation area and moves with a constant speed V_i toward this waypoint. When the waypoint is reached, the node rests for a pause time $T_{p,i}$ and then starts over. The waypoints are chosen from a two-dimensional uniform distribution. In the simplest form of RWP, a node chooses the speed from a uniform distribution, i.e. $V_i \in [v_{\min}, v_{\max}]$, and it uses always the same pause time $T_{p,i} = T_p \, \forall i$. Each node moves independently from other nodes.

Another frequently used approach is the *random direction* (RD) model [Bet01, NTLL05]. A node moving according to the RD model is generally described by a stochastic process $i \mapsto (\Phi_i, V_i, T_i, T_{p,i})$. A node chooses a direction angle Φ_i and then moves with speed V_i for a certain movement time T_i. After pausing for a period $T_{p,i}$ it starts over. Often, the speed is chosen from a uniform distribution, the movement time is set to a fixed value (i.e. $T_i = \tau \, \forall i$), and the pause time is always zero. Similar to the RWP model, each node moves independently from other nodes.

A different approach is taken by the *random walk* (RW) mobility model. This mobility model is strongly connected to Brownian motion first described mathematically by Einstein [Ein56]. Its main application is in modeling the movement of users in a cellular network. Here, a node located in a certain cell is able to move to a predefined number of neighboring cells. In each time step the node stays within its cell with a given probability or moves to one of the neighboring cells with a given transition probability. This process is usually modeled via a Markov chain (see, e.g., [JZH98, CS01]).

There are also other mobility models with spatial dependencies, which are well-suited when users move in groups (e.g. firefighters, military). As an example we can take the *reference point group* (RPG) mobility model [HGPC99]. It can be described as follows: some reference nodes (group leaders) move according to the RWP model. The group members and their waypoints are uniformly distributed on a disk with fixed radius around their group leader. Furthermore, their velocities are set in a way that they arrive at their next waypoint at the same time as their group leader.

A mobility model that tries to preserve a predefined inhomogeneity of the nodes' distribution, which is called *inhomogeneous random waypoint (IRWP) model* is introduced in [3]. This model can also be used to change the inhomogeneity value of the node distribution over time, which may help determining the influence of the inhomogeneity on some measurand.

In the thesis at hand we apply the RWP and RD mobility model. The reason to choose these models is that they are most commonly used in simulation based analysis since they are very simple to implement. Additionally, especially the RWP model is usually natively supported by network simulation tools such as ns-2 and OPNET. We compare these two models with our IRWP model regarding several aspects of the distribution of the nodes and its trend during simulation time.

2.3 Wireless Channel

The nodes are communicating via electromagnetic waves radiated by antennas. In the following we will describe how this radiation can be mathematically described regarding propagation and signal strength at the receiver. We start by considering free space propagation, i.e. sender S and receiver D are located within a three dimensional empty space. Additionally, we assume that each node has the same transmission power p_t. Then, the propagation of the electromagnetic wave radiated by the transmitting antenna can be described by *Friis' equation* (see [Fri46], and [Mad08] pg. 133)

$$p_r = p_t \, g_t \, g_r \left(\frac{v_c}{4\pi \, f_0 \, d} \right)^2 , \tag{2.5}$$

where p_r is the signal power received by an antenna located at a distance d apart from the sender. The symbol v_c denotes the speed of light and f_0 indicates the center frequency of the transmission. The terms g_r and g_t denote the antenna gains of the receiving and transmitting antennas, respectively. Antenna gain is defined as the fraction of the power radiated by a given antenna in the direction toward the receiving station and the power radiated by an isotropic antenna fed with the same signal. Isotropic antennas are radiating / receiving with the same signal strength in all directions. Obviously, isotropic antennas have $g_r = g_t = 1$. For other antennas the gain is usually higher since they focus the transmitted power to directions that are used for communication (see [Sch05] pg. 17).

Friis' equation (2.5) can be generalized for higher path loss exponents $\alpha > 2$, which gives the *simplified path loss model* (see [Gol05] pg. 46). For a given destination the power received from its source node at a distance d in free space is given by (see [Sch05])

$$\mathbb{E}(p_r) = p_t \, g_t \, g_r \, g_{ref} \left(\frac{d}{d_{ref}} \right)^{-\alpha} , \tag{2.6}$$

where g_{ref} is the reference gain at a distance d_{ref} and α denotes the path loss exponent. Note that if we set $\alpha = 2$ and $g_{ref} = p_t \, g_t \, g_r \left(\frac{v_c}{4\pi \, f_0 \, d_{ref}} \right)^2$, Equation (2.6) is equivalent to Friis' equation (2.5). In free space we have $\alpha = 2$, whereas in areas with more obstacles, which can reflect electromagnetic waves, this exponent is set to a higher value. In cities reasonable values can go up to $\alpha = 5$ and beyond (see [Gol05] pg. 47).

In the following, without loss of generality we assume $g_t = g_r = 1$, $g_{ref} = 1$, and $d_{ref} = 1\,\mathrm{m}$. In order to be able to cope with distances smaller than the reference distance d_{ref}, we calculate the path loss by $l(d) \coloneqq \min(1, d^{-\alpha})$. Then, Equation (2.6) simplifies to

$$\mathbb{E}(p_r) = p_t \, l(d) = p_t \, \min(1, d^{-\alpha}) \tag{2.7}$$

with the distance d normalized to meters.

If the transmission is not carried out in free space but in a space with obstacles, we have to distinguish between the average reception power and the instantaneous

reception power. In the following we describe how to model the average reception power. Due to the obstacles that may be located within the transmission path, the signal is degraded and hence the pathloss exponent is increased.

Additionally, the reception power at the receiver not only depends on its distance to the transmitter but also on the positions of receiver, transmitter and the obstacles and may fluctuate as these entities move. This effect is called *shadowing*. Therefore, the instantaneous reception power is a random variable with its mean value given in Equation (2.7). The value of the instantaneous power varies slowly in time and space due to the large size and slow movement of the obstacles, which is the reason that it is sometimes referred to by *slow fading*. These fluctuations $g_s^{(\mathrm{dB})} = 10\log(g_s)$ measured in dB can be fairly well approximated by a Gaussian distribution, i.e. its pdf is given by

$$f_{g_s^{(\mathrm{dB})}}(x) = \frac{1}{\sqrt{2\pi\sigma_s^2}}\,\mathrm{e}^{-\frac{x^2}{2\sigma_s^2}}\,, \tag{2.8}$$

where σ_s^2 denotes the variance of shadowing. Its value is an indicator for the severeness of the shadowing and is a parameter of the environment. Typical values range from 6 dB to 10 dB (see [Sch05]). Hence, in linear scale the gain g_s caused by shadowing follows a lognormal distribution. If we incorporate shadowing in Equation (2.7), we have

$$p_r = p_t\, l(d)\, g_s\,. \tag{2.9}$$

In this work shadowing is not considered since it is not relevant for the investigations presented in this work. Hence, we set $g_s \equiv 1$ and therefore apply Equation (2.7) instead of Equation (2.9).

If obstacles are present in the communication environment, they cause additional effects besides shadowing that have great influence on the transmissions: they reflect, diffract, and scatter the electromagnetic waves. Due to these reflections many copies of the same signal arrive at the receiver. Unfortunately, they may have slightly different shapes due to the different paths they take and they arrive at different points in time. This leads to some effects that negatively influence the quality of the received signal.

The first and most obvious effect that occurs is the *delay spread* of the transmitted signal due to the different path lengths. Since the multiple copies of the signal arrive at different points in time, the beginning and ending of the transmitted symbols may become blurred. Hence, especially for high data rates consecutive symbols may interfere with each other leading to *inter-symbol interference*. This effect limits the maximum achievable data rate significantly.

To explain the second effect we have to recall the behavior of electromagnetic waves sent / received by a moving node. As is well known from physics the frequency of a wave changes if the source or sink move toward / away from each other. This effect is called *Doppler effect* (see [GV93], pg. 164). If the destination is moving toward the source, the frequency gets higher and vice versa. Hence, the resulting

frequency at the receiver is

$$f_0' = f_0 \left(1 + \frac{v_0 \cos\beta}{v_c}\right) , \tag{2.10}$$

where f_0 denotes the transmission frequency, v_0 denotes the speed of the destination, and β denotes the angle between the moving direction and the connecting line of source and destination.

If only one signal path is present between the sender and the receiver, the Doppler effect is easy to compensate: The receiving node just tunes its transceiver to the frequency f_0'. In a multi-path environment, however, the Doppler effect has a negative impact on the received signal that cannot be compensated easily. Here, the signals coming from the different paths arrive at different angles. Therefore, the Doppler shift is different for each of them resulting in a broadening of the bandwidth of the signal, which is called the *frequency spread* of the received signal.

The third effect is called *fading*, which is caused by the superposition of multiple copies of the same signal due to reflection on obstacles. As the paths of the signals have different lengths the copies of the signal have slightly different phases. Therefore, they could constructively or destructively superimpose, depending on the length of the paths they take from the transmitter to the receiver. Even slight movements of one of these two (in the magnitude of the wavelength) or slight changes in the transmission frequency may completely change the signal quality.

Different models have been proposed to model the effects of fading. In the following we give an overview of the most important. The first model is the Rayleigh fading model (see [Gil65, Cla68]). Here we assume due to the central limit theorem (see [PP02], pg. 278) that the in-phase and the quadrature components of the signal are zero mean Gaussian distributed. Let X and Y denote the in-phase and quadrature components of the signal, respectively. Then we have $X, Y \sim N(0, \sigma^2)$ and the signal envelope $\sqrt{X^2 + Y^2}$ follows a Rayleigh distribution with parameter σ^2, i.e. its pdf is

$$f_{\sqrt{X^2+Y^2}}(x) = \frac{x}{\sigma^2}\, \mathrm{e}^{-\frac{x^2}{2\sigma^2}} , \tag{2.11}$$

where the average received power is $\mathbb{E}(p_r) = 2\sigma^2$. The instantaneous reception power, which is the squared value of the signal envelope, is then $p_r = X^2 + Y^2$ and can thus be written as

$$p_r = p_t\, l(d)\, h^2 , \tag{2.12}$$

where the channel state h is Rayleigh distributed and hence h^2 is exponentially distributed with expected value $\mathbb{E}(h^2) = 1$, i.e., its pdf is

$$f_{h^2}(x) = \frac{1}{\mathbb{E}(h^2)}\, \mathrm{e}^{-\frac{x}{\mathbb{E}(h^2)}} = \mathrm{e}^{-x} . \tag{2.13}$$

Note that we have to select $\mathbb{E}(h^2) = 1$ such that the expected value of the reception power is $\mathbb{E}(p_r) = p_t\, d^{-\alpha}$.

The Rayleigh fading model is accurate for transmissions that have no dominant line-of-sight path in the received signal. If there is a dominant line-of-sight path present in the received signal, the in-phase and quadrature components still follow a Gaussian distribution, but with non-zero mean. Here, the Rician fading model is more suitable (see, e.g., [Ric44]), which assumes that the signal envelope follows a Rician distribution with pdf

$$f_{\sqrt{X^2+Y^2}}(x) = \frac{x}{\sigma^2}\,\mathrm{e}^{-\frac{x^2+\nu^2}{2\sigma^2}} I_0\left(\frac{x\nu}{\sigma^2}\right)\,, \tag{2.14}$$

where $I_0(z)$ denotes the modified Bessel function of the first kind of order zero, i.e.

$$I_0(z) = \sum_{i=0}^{\infty} \frac{1}{i!\,\Gamma(i+1)} \left(\frac{z}{2}\right)^{2i}\,, \tag{2.15}$$

with $\Gamma(z) = \int_0^\infty t^{z-1}\mathrm{e}^{-t}\,\mathrm{d}t$ being the Gamma function. The term ν^2 denotes the average power of the line-of-sight components and $2\sigma^2$ is the average power of all non-line-of-sight components of the received signal. Therefore, the average received power is given by $\mathbb{E}(p_r) = \nu^2 + 2\sigma^2$. Mind that if $\nu = 0$, i.e. the power of the line-of-sight component of the received signal is very small, this function is equal to the Rayleigh distribution presented in Equation (2.11).

Rayleigh and Rician fading models are very well approximating the behavior of real channels. In some scenarios there is, however, a more general model needed, as some measurements have shown (see [Ric44]). Therefore, Nakagami introduced a new fading model in [Nak60]. For this model the pdf of the signal envelope is given by

$$f_{\sqrt{X^2+Y^2}}(x) = \left(\frac{m}{\mathbb{E}(p_r)}\right)^m \frac{2x^{2m-1}}{\Gamma(m)}\,\mathrm{e}^{-\frac{mx^2}{\mathbb{E}(p_r)}}\,. \tag{2.16}$$

The parameter m is modeling the severeness of fading, where a smaller value indicates a more harsh fading environment. If $m = \infty$ no fading is present; for $m = 1$ the pdf reduces to Rayleigh fading as in Equation (2.11); if we set $m = \frac{(\nu+1)^2}{2\nu+1}$ the Nakagami distribution is approximating Rician fading with parameter ν. If $m < 1$ Nakagami fading has a stronger impact on the received signal than Rayleigh fading. The instantaneous reception power for Nakagami fading thus has the form

$$f_{p_r}(x) = \left(\frac{m}{\mathbb{E}(p_r)}\right)^m \frac{x^{m-1}}{\Gamma(m)}\,\mathrm{e}^{-\frac{mx}{\mathbb{E}(p_r)}}\,. \tag{2.17}$$

Independent on the model used to describe the severeness of fading, we want to analyze the time-variant behavior of it. We already mentioned above that the channel changes when either the source or the destination move a bit. Hence, the changing speed of the channel depends mainly on the speed of the nodes.

If we assume that the delay spread is much smaller than the inverse bandwidth B^{-1}, the received signal $r(t)$ is of the form (see [Gol05], Section 3.2).

$$r(t) = r_I(t)\cos(2\pi f_0 t) - r_Q(t)\sin(2\pi f_0 t)\,, \tag{2.18}$$

where the components are given by

$$r_I(t) = \sum_{n=1}^{N} a_n(t)\cos(\phi_n(t)) \,, \tag{2.19}$$

$$r_Q(t) = \sum_{n=1}^{N} a_n(t)\sin(\phi_n(t)) \,. \tag{2.20}$$

The sums are taken over all N multipath components. Note that $a_n(t)$ denotes the amplitude of the n^{th} multipath component and the phase is given by $\phi_n(t) = 2\pi f_0 \tau_n(t) - \phi_{D_n} - \phi_0$. Here, $\tau_n(t)$ denotes the delay and ϕ_{D_n} the Doppler shift of the n^{th} component and ϕ_0 indicates the phase offset.

Next, we consider two important functions, which characterize the temporal behavior of the received signal strength.

Definition 2.2. The autocorrelation of the in-phase component $r_I(t)$ is defined as

$$F_{r_I}(\Delta t) = \mathbb{E}(r_I(t) r_I(t+\Delta t)) \,, \tag{2.21}$$

and analogue for the quadrature component $r_Q(t)$. The crosscorrelation of the signal is defined as

$$F_{r_I, r_Q}(\Delta t) = \mathbb{E}(r_I(t) r_Q(t+\Delta t)) \,. \tag{2.22}$$

If we assume uniform scattering from all directions [Cla68] we get

$$F_{r_I}(\Delta t) = F_{r_Q}(\Delta t) = p_r \, I_0\left(2\pi f_0 \frac{v_0 \cos\beta}{v_c} \, \Delta t\right) \,, \tag{2.23}$$

where $I_0(z)$ is the Bessel function as defined in Equation (2.15) and $f_0 \frac{v_0 \cos\beta}{v_c}$ is the Doppler shift frequency as in Equation (2.10). Additionally, we have $F_{r_I, r_Q}(\Delta t) = 0$.

The *autocorrelation function* of the received signal $r(t)$ is then given by (see [Gol05], Section 3.2.1)

$$\begin{aligned} F_r(\Delta t) &= \mathbb{E}(r(t) r(t+\Delta t)) \\ &= F_{r_I}(\Delta t)\cos(2\pi f_0 \Delta t) + F_{r_I, r_Q}(\Delta t)\sin(2\pi f_0 \Delta t) \\ &= p_r \, I_0\left(2\pi f_0 \frac{v_0 \cos\beta}{v_c} \Delta t\right) \cos(2\pi f_0 \Delta t) \,. \end{aligned} \tag{2.24}$$

Then, the channel coherence time c' is defined as the largest time interval Δt for which the autocorrelation function $F_r(\Delta t)$ is non-zero. Hence, for two time instants that are more than c' apart we can assume that the channel is uncorrelated.

In the rest of this work we assume a Rayleigh fading environment, which has mainly two reasons: First, the Rayleigh fading model is the most often used model in investigations regarding wireless networks. Therefore, by applying this model our results can by easily compared to results presented in related literature. Second, the

Rayleigh fading model is mathematically easy allowing analytical results to be quickly derived and represented by closed form expressions. The same results are usually much harder to derive for other fading models, if this is possible at all. The Rayleigh fading model is, however, still of great realism in many scenarios, hence representing a good compromise between realism and simplicity for modeling a multipath fading environment.

2.4 Digital Modulation over AWGN Channels

In the following we calculate the power of noise in wireless channels and its impact on transmissions with different modulation schemes. Noise is injected into the received signal mainly at the receiver. We only consider thermal noise caused by the receiver electronics operated at room temperature. This noise follows a white Gaussian random process with mean zero and power spectral density $\frac{N_0}{2}$. Therefore, such a channel is called *additive white Gaussian noise* (AWGN) channel.

The noise has a uniform power spectral density over the whole bandwidth $2B$ of the transmission. Therefore, the overall noise power is given by $\frac{N_0}{2}2B = N_0 B$, where $N_0 = \kappa T$ in $\frac{\mathrm{W}}{\mathrm{Hz}}$ with $\kappa = 1.381 \cdot 10^{-23} \frac{\mathrm{J}}{\mathrm{K}}$ (see [GV93], pg. 193) being Boltzmann's constant and T being the temperature in K. Note that $N_0 B$ is measured in W. Hence, the signal to noise power ratio (SNR) is given by

$$\mathrm{SNR} = \frac{p_r}{N_0 B} \,. \tag{2.25}$$

Let T_s and T_b denote the duration of a symbol and the duration of a bit in seconds, respectively. Then, the energy per symbol can be calculated by $E_s = p_r T_s$ and the energy per bit by $E_b = p_r T_b$. Therefore, we can rewrite the SNR by

$$\mathrm{SNR} = \frac{E_s}{N_0 B\, T_s} = \frac{E_b}{N_0 B\, T_b} \,. \tag{2.26}$$

For performance analysis of different modulation schemes we need the SNR per symbol γ_s and the SNR per bit γ_b. These quantities are defined as

$$\gamma_s := \frac{E_s}{N_0} \,; \qquad \gamma_b := \frac{E_b}{N_0} \,. \tag{2.27}$$

If pulse shaping is applied for which $T_s = \frac{1}{B}$, we have $\mathrm{SNR} = \gamma_s$.

To be able to transmit a signal over a wireless channel we have to modulate it using one of several different modulation schemes. An comprehensive overview of these schemes can be found, e.g., in [Gol05]. The bit and symbol error probabilities of the most important modulation schemes can be found in Table 2.1. Note that $\bar{\gamma}_b$ and $\bar{\gamma}_s$ denote the mean bit and symbol error probability, respectively. We have to apply these average values for amplitude modulation schemes since when using them the energy is not the same for each symbol due to different signal amplitudes.

Table 2.1: Bit and symbol error probabilities of different modulation schemes [Gol05].

Modulation scheme	$p_b(\gamma_b)$	$p_s(\gamma_s)$
BFSK	$p_b = \frac{1}{2}\operatorname{erfc}\left(\sqrt{\frac{\gamma_b}{2}}\right)$	$p_s = \frac{1}{2}\operatorname{erfc}\left(\sqrt{\frac{\gamma_s}{2}}\right)$
BPSK	$p_b = \frac{1}{2}\operatorname{erfc}\left(\sqrt{\gamma_b}\right)$	$p_s = \frac{1}{2}\operatorname{erfc}\left(\sqrt{\gamma_s}\right)$
QPSK, 4-QAM	$p_b \approx \frac{1}{2}\operatorname{erfc}\left(\sqrt{\gamma_b}\right)$	$p_s \approx \operatorname{erfc}\left(\sqrt{\frac{\gamma_s}{2}}\right)$
M-PAM	$p_b \approx \frac{M-1}{M\log_2(M)}\operatorname{erfc}\left(\sqrt{\frac{3\bar{\gamma}_b\log_2(M)}{M^2-1}}\right)$	$p_s = \frac{M-1}{M}\operatorname{erfc}\left(\sqrt{\frac{3\bar{\gamma}_s}{M^2-1}}\right)$
M-PSK	$p_b \approx \frac{1}{\log_2(M)}\operatorname{erfc}\left(\sqrt{\gamma_b\log_2(M)}\sin\left(\frac{\pi}{M}\right)\right)$	$p_s \approx \operatorname{erfc}\left(\sqrt{\gamma_s}\sin\left(\frac{\pi}{M}\right)\right)$
M-QAM	$p_b \approx \frac{2}{\log_2(M)}\operatorname{erfc}\left(\sqrt{\frac{3\bar{\gamma}_b\log_2(M)}{2(M-1)}}\right)$	$p_s \approx 2\operatorname{erfc}\left(\sqrt{\frac{3\bar{\gamma}_s}{2(M-1)}}\right)$

To allow different data rates while keeping the bandwidth constant (see Section 2.8), we apply different modulation schemes. The default modulation scheme applied in this work is QPSK (quadrature phase shift keying). Let furtheron b_r denote the data rate in bit per second when QPSK is applied. QPSK is preferred over BPSK (binary phase shift keying) since it provides a twice as high data rate at the same bandwidth and the same bit error probability. If a doubled data rate is needed, we use 16-QAM (quadrature amplitude modulation) within this thesis.

We decided to apply QPSK and M-QAM modulation schemes since they are frequently used in current wireless technologies, such as WLAN in the 802.11n standard [Wlan09], WiMAX in the 802.16j standard [Wimax09], and LTE [3GPP10].

2.5 Medium Access

In a wireless network each node that wants to transmit a data packet has to gain access to the shared channel. This channel access is controlled via a medium access control (MAC) protocol. The most simple of these protocols is *(pure) ALOHA* [Abr70], where the node simply starts a transmission if it has to send a packet. Therefore, it may happen that the transmissions of two nodes overlap in time. Then, in general both packets cannot be received correctly and are lost, which we call a *collision*. If such a collision occurs, the corresponding nodes wait a random time and then retransmit the lost packets. The random waiting time is necessary to reduce the probability that the retransmitted packets collide again.

In the following analysis of MAC protocols we assume that packets that do not collide are successfully received. We define the throughput of a MAC protocol as the fraction of time in which a successful transmission is conducted. Then the throughput Θ of a MAC protocol is given by the traffic load L multiplied with the probability

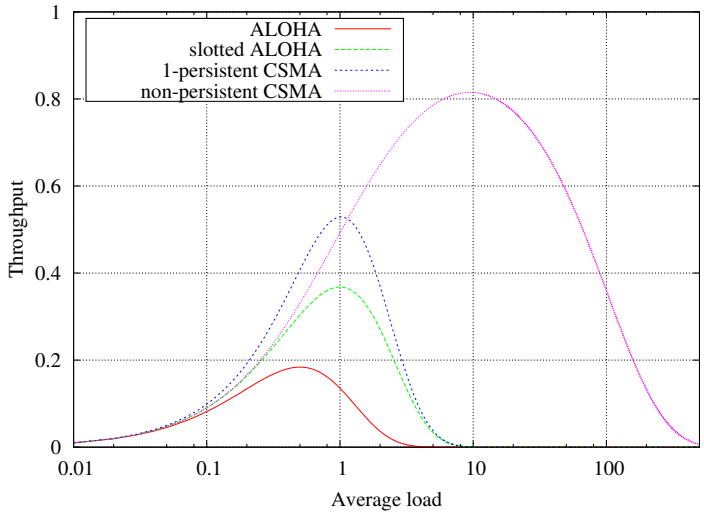

Figure 2.3: Throughput for different MAC protocols (for CSMA $a = 0.01$).

that no collision occurs $1 - p_{col}$, i.e.

$$\Theta = L(1 - p_{col}) \,. \tag{2.28}$$

Let δ denote the time duration of a single packet being transmitted. When a node starts its transmission at time instant 0 a collision occurs if and only if another node starts its transmission within the time interval $(-\delta, \delta)$.

As described in Section 2.6 we assume that traffic is produced by a Poisson arrival process with intensity λ_T. Therefore, the number of packets that arrive within a time interval of length t follows a Poisson distribution with the probabilities

$$\mathbb{P}(X = k) = \frac{(\lambda_T t)^k}{k!} \, \mathrm{e}^{-\lambda_T t} \,. \tag{2.29}$$

The traffic load is defined as the expected number of packets per packet duration, which is given by $L = \lambda_T \delta$. Thus, the probability that no collision occurs is equal to the probability that no transmission request occurs within the time interval $(-\delta, \delta)$, which is given by $1 - p_{col} = \mathrm{e}^{-2\delta\lambda_T} = \mathrm{e}^{-2L}$. Hence, the throughput of ALOHA is given by

$$\Theta = L \, \mathrm{e}^{-2L} \,. \tag{2.30}$$

The throughput as a function of the traffic load is plotted in Figure 2.3. As can be seen its maximum value occurs at a load of $L = 0.5$ and is about 18%.

As an improvement of the ALOHA protocol time can be subdivided into intervals of equal length δ (the length of a packet), which are called time slots. The resulting protocol is called *slotted ALOHA*. Here, a node is allowed to start its transmission only at the beginning of a time slot. Assume a node starts its transmission at time instant 0. Then a collision only occurs if another packet arrives within the time

interval $(-\delta, 0)$, since then the corresponding node would start a transmission at time instant 0. This increases the probability that no collision occurs to $1 - p_{col} = \mathrm{e}^{-\delta\lambda_T} = \mathrm{e}^{-L}$, giving a throughput of

$$\Theta = L\,\mathrm{e}^{-L}\,. \tag{2.31}$$

The throughput of slotted ALOHA is also plotted in Figure 2.3. As can be seen, the maximum throughput occurs at a load of $L = 1$ and is about 36% which is twice as high as for pure ALOHA. The major disadvantage of slotted ALOHA is that it can only be applied if all nodes are perfectly synchronized. This synchronization produces additional communication overhead and is therefore not applicable for several scenarios. For an extensive overview of different aspects of synchronization please refer to [TAB07, Tyr10, TAB10, KBT09, KB10].

The next MAC protocol we analyze is the *carrier sense multiple access* (CSMA) protocol. Here, a node that wants to send a packet is first sensing the channel. If no other node is currently transmitting, the node immediately starts its transmission. If there is, however, another node transmitting, there are several possibilities depending on which variant of CSMA is used: For *p-persistent CSMA* the node waits until the channel gets unoccupied; it then starts its transmission with probability p. Hence, for 1-persistent CSMA the node starts its transmission immediately when the channel gets unoccupied. This variant suffers from the problem that in high load situations usually more than one node is waiting until the channel gets unused. Therefore, they start their transmissions simultaneously leading to a collision.

To decrease the probability of a collision after the channel gets unoccupied, another variant of CSMA can be applied: A node encountering an occupied channel waits for a random time (random backoff) and then senses the channel again. If it is free, the node starts its transmission, otherwise another random backoff period is initiated, etc. This method is called *non-persistent CSMA*.

Let a denote the propagation delay in relation to the packet duration δ. Then, the throughput for 1-persistent CSMA is given by (see [TK85, TH80])

$$\Theta = \frac{L\,\mathrm{e}^{-L(1+2a)}\left(1 + L + aL\left(1 + L + \frac{aL}{2}\right)\right)}{L\,(1+2a) - (1 - \mathrm{e}^{-aL}) + (1 + aL)\,\mathrm{e}^{-L(1+a)}}\,. \tag{2.32}$$

For non-persistent CSMA, a higher maximum throughput can be achieved, as can be seen in (see [Hea06])

$$\Theta = \frac{L\,\mathrm{e}^{-aL}}{L\,(1+2a) + \mathrm{e}^{-aL}}\,. \tag{2.33}$$

A plot of both equations can be found in Figure 2.3. As can be seen in the figure, the maximum throughput of 1-persistent CSMA with $a = 0.01$ is at about 52% for a load of $L = 1$, which outperforms both ALOHA variants. For non-persistent CSMA the maximum achiveable throughput is even higher at about 81% for a load $L \approx 9.5$.

Whatever type of CSMA protocol is used, it is still possible that a collision occurs. If, e.g., two or more nodes sense the channel unused simultaneously and then starting their transmissions at the same time they collide. If a collision occurs, the packet has to be retransmitted. To avoid this situation, there are two extensions of the CSMA protocol:

In CSMA with *collision detection* (CSMA/CD) a node that is transmitting a packet always simultaneously senses the channel, if there is any other node transmitting at the same time. In case of a collision at least one of the sending nodes is therefore noticing the problem and starting to send a jamming signal. This signal informs all other nodes that a collision has occurred, which makes them stop their transmissions immediately. Then, they wait a random time (the so-called *back-off time*) and then start the CSMA protocol again by sensing the channel. The throughput of 1-persistent CSMA/CD with the same definition for a as above is given by (see [TK85])

$$\Theta = \frac{L\,(1+L)\,\mathrm{e}^{-L(1+2a)} + L\,\mathrm{e}^{-L(b+a)}\left(\left(\frac{bL}{2}\right)\left(1-\mathrm{e}^{-2aL}\right) - \frac{aL}{2}\,\mathrm{e}^{-2aL}\right)}{\mathrm{e}^{-L(1+a)} + L\,\mathrm{e}^{-aL} + \left(1-\mathrm{e}^{-aL}\right)(1+(b+a)\,L) + \frac{1-\mathrm{e}^{-2aL}}{2}\,\mathrm{e}^{-bL}}\,, \tag{2.34}$$

where b denotes the fraction of the duration of a transmission aborted by the collision detection mechanism and the duration of a successful transmission δ.

The CSMA/CD protocol is very effective in terms of throughput. Therefore, it has been applied in Ethernet defined in the 802.3 standard [Eth05]. It is, however, not applicable for wireless channels, since a wireless transceiver transmits with a power of several milliwatts while the received signal from another node is in the order of nanowatts. Hence, due to its limited dynamic range, it would not detect any collision.

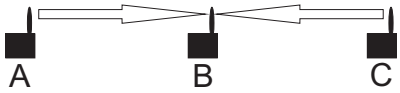

Figure 2.4: The hidden terminal problem.

In wireless networks with CSMA also the *hidden terminal problem* may occur, as depicted in Figure 2.4. Assume nodes A and C want to send a message to node B, and node C is starting its transmission first. Then due to the fact that node A is outside the communication range of node C, it is not able to sense the ongoing transmission. Therefore, it will start its transmission, which causes a collision. Due to this problem, for wireless channels another extension to CSMA has been introduced, that tries to avoid collisions: The CSMA protocol with *collision avoidance* (CSMA/CA).

When applying CSMA/CA a node that has a packet to transmit first sends a *request to send* (RTS) packet to its destination node. If the destination receives the RTS packet correctly, it responds with a *clear to send* (CTS) message. Since both the RTS and the CTS message contain the length of the data packet to send, all

nodes within the radio range of either the sender or the receiver are informed about the initiating transmission and its duration and stay quiet. Note that collisions are still possible since, e.g., two RTS packets could collide. The probability for that is, however, low since these RTS packets are relatively short.

The obvious disadvantage of CSMA/CA is that it produces signaling overhead by introducing the RTS and CTS messages. This overhead is especially problematic if only *very small data packets* have to be transmitted. Here, the advantage of the reduced collision probability becomes very small, since the RTS and CTS packets are not significantly shorter than the data packets. Hence, in such scenarios it is advantageous to prefer one of the protocols described above over CSMA/CA. An analysis of the throughput of CSMA/CA can be found, e.g., in [ZA02, PKC+05, HC96].

Since the CSMA/CA protocol is especially designed for wireless transmissions, it is applied in wireless technologies as, e.g. WLAN [Wlan09] and low-rate wireless personal area networks (LR-WPAN) 802.15.4 [Wpan06].

Figure 2.5: The exposed terminal problem.

Note that all CSMA variants and extensions described above may suffer from the *exposed terminal problem* as depicted in Figure 2.5. Assume that node C is already transmitting a packet to node D. If node B wants to send a packet to its destination it first senses the channel, which results in a random backoff due to the transmission of node C. It might be the case, however, that node A is outside the range of node C and node D is outside the range of node B. Hence, if node B would start its transmission, no collision would occur. Therefore, some available bandwidth is wasted.

As medium access (MAC) protocol we apply slotted ALOHA throughout the work at hand, unless otherwise stated. The reasons for selecting ALOHA are the following: First, it is the easiest protocol to implement and analyze. Second, it allows an unbiased analysis of some effects in wireless networks such as interference, which is heavily affected by the MAC protocol. Third, it leads to scenarios where interference is not completely avoided, but instead the behavior of transmitters is adapted to the current interference state [9, 10].

2.6 Data Traffic

The traffic model describes when a packet arrives at a given node that is intended to be sent to some other node. It is usually modeled via a stochastic arrival process, e.g., a Poisson arrival process. Although such an approach is analytically simple it is for some scenarios not reflecting the real world [PF95]. Alternatively, some models

try to model real traffic generated by a given application, e.g., HTTP [Mah97, CB97], FTP [DJC+92], Video [KM98, DDKS00], and Network games [Fär02]. These type of models are, however, very specific as the traffic behaves completely different for different applications. The need for special models reflecting the behavior of real users is especially important for the analysis of cellular networks [MBM09, HR86]. A good overview of different traffic models can be found in [Ada97].

A very simple traffic model is the *greedy source*. There, each node always has a packet to send. If it is able to send the packet, a new one is generated immediately. Hence, this model is well suited to simulate network overload situations; but it lacks realism.

A very widely used method is to model traffic via a Poisson arrival process where in each time slot each of the n nodes in $\mathcal{N}$ sends a packet with probability p. Here, the number of nodes starting a transmission within a given time slot follows a Poisson distribution with intensity $\lambda_T = pn$, as in Equation (2.29). The set of all active senders is denoted by $\mathcal{S}$. Note that $\mathcal{S}$ is generated by thinning the Poisson point process $\mathcal{N}$.

The length s of a single transmission in time slots is assumed to be the same for all transmissions. Hence, an expected fraction of $\mathbb{E}(S) = ps$ nodes is transmitting simultaneously in each time slot. If not mentioned otherwise, we assume $s = 1$.

The destination is randomly selected from the nodes within transmission range. Two possible strategies are applied when selecting the destination: Using the first strategy, the selection is conducted by a purely random choice without considering the state of the selected node. If the second strategy is applied, the destination is selected out of all idle nodes, i.e., the nodes that currently do not send nor receive.

The transmission range is determined using the path loss model presented in Equation (2.7) and the receiver sensitivity $p_r^{\min}$ without considering fading. Hence, the destination must be located within a maximum range of

$$d_{\max} = \left(\frac{p_t}{p_r^{\min}}\right)^{\frac{1}{\alpha}} \tag{2.35}$$

apart from the source node. If we assume uniformly distributed nodes, the distance $d(S, D)$ between the source S and the destination D is a random value due to the random selection of D. It is distributed according to the pdf

$$f_{d(S,D)}(d) = \frac{2d}{d_{\max}^2}\,. \tag{2.36}$$

2.7 Interference

Consider a source node S that transmits a data packet to its destination D. Then, all sending nodes except the source node are considered to be interferers. Let $I(x)$ denote the interference power of node x arriving at the destination node D. Since

the sending powers of these nodes are adding up as they arrive at D, the overall interference power is the sum

$$I(\mathcal{S}) = \sum_{x \in \mathcal{S}} I(x) \tag{2.37}$$

of exponentially distributed random variables $I(x)$. Let $n_s := |\mathcal{S}|$ denote the number of transmitting nodes at a given point in time. The expected values $\mathbb{E}(I(x))$ are in general different, as the distances of the interfering nodes to the destination $d(x, D)$ are different. Therefore, the sum $I(\mathcal{S})$ follows a generalized Erlang distribution (for a definition see [Neu81], pp. 41ff and [DVJ08], pg. 111), which is a special case of the phase-type (PH) distribution. The corresponding pdf is given by

$$f_{p_I}(x) = -\beta \, \mathrm{e}^{x\Theta} \, \Theta \mathbf{1}_{n_s} \, , \tag{2.38}$$

with $\beta = (1, 0, \ldots, 0)$ and $\mathbf{1}_{n_s} = (1, \ldots, 1)$ being vectors of length n_s, and Θ representing the $(k \times k)$-matrix

$$\Theta := \begin{pmatrix} -\frac{1}{\bar{p}_{r,1}} & \frac{1}{\bar{p}_{r,1}} & 0 & \cdots & 0 \\ 0 & -\frac{1}{\bar{p}_{r,2}} & \frac{1}{\bar{p}_{r,2}} & \cdots & 0 \\ \vdots & \ddots & \ddots & \ddots & \vdots \\ 0 & \cdots & 0 & -\frac{1}{\bar{p}_{r,n_s-1}} & \frac{1}{\bar{p}_{r,n_s-1}} \\ 0 & \cdots & 0 & 0 & -\frac{1}{\bar{p}_{r,n_s}} \end{pmatrix} . \tag{2.39}$$

Next, we derive the mean value of the interference power $I(\mathcal{S})$ in a single time slot (see also [GH09a]). As described in Section 2.6, we assume that a fraction p of the nodes start a transmission in each time slot. The duration of each transmission is s time slots. In the case that the nodes are uniformly distributed the density of the senders is given by $sp\lambda$. Hence, we have

$$\begin{aligned} \mathbb{E}(I(\mathcal{S})) &= \sum_{x \in \mathcal{S}} \bar{p}_{r,x} \\ &= \mathbb{E}\left(\sum_{x \in \mathcal{S}} p_t l(d(x, D)) h_x^2 \right) \\ &= p_t \, \mathbb{E}\left(\sum_{x \in \mathcal{S}} l(d(x, D)) \right) \\ &= p_t \, sp\lambda \int_{\mathbb{R}^2} l(d(x, D)) \, \mathrm{d}x \\ &\overset{\alpha > 2}{=} p_t \, sp\lambda \, \frac{\alpha}{\alpha - 2} \pi \, . \end{aligned} \tag{2.40}$$

The third equality holds since $\mathbb{E}(h_x^2) = 1$ and the random variables $l(d(x, D))$ and h_x^2 are independent. The fourth equality holds due to Campbell's theorem (see Chapter 10.2 in [PP02] or Chapter 6 in [DVJ03]). Note that the integral does only converge for $\alpha > 2$. The last equality shows a closed form expression for $\alpha \in \mathbb{N}$.

Its variance is given by

$$\mathrm{var}(I(\mathcal{S})) = \sum_{x \in \mathcal{S}} \bar{p}_{r,x}^2 \,. \tag{2.41}$$

The overall interference power has a similar negative influence on the decoding process of a signal at the receiver than noise. Thus, when considering interference the quality of the received signal is measured by the signal to interference and noise ratio (SINR), which is given by

$$\mathrm{SINR} = \frac{p_r}{I(\mathcal{S}) + N_0 B} \,. \tag{2.42}$$

Similar to Equation (2.26) we can rewrite the SINR by substituting $E_s = p_r T_s$ and $E_b = p_r T_b$ yielding

$$\mathrm{SINR} = \frac{E_s}{(I(\mathcal{S}) + N_0 B) T_s} = \frac{E_b}{(I(\mathcal{S}) + N_0 B) T_b} \,. \tag{2.43}$$

When computing the bit error probability and fading has to be considered, the SINR has to be substituted into the bit error probability formulas in Table 2.1 (see [Ham02]).

Since interference has a negative impact on transmissions, different techniques are applied to counteract interference. The first method is to introduce a MAC protocol that reserves space around receivers and transmitters. Within this reserved area, no other node is allowed to transmit. Hence, there is a minimum distance between two simultaneous transmissions, reducing the interference effect one of them could cause on the other. Note, however, that if many interferers are transmitting, the maximum allowed level of interference can still be exceeded.

Another approach is to minimize the interference caused by each transmission. One approach is to apply power control for this purpose. Here, the transmission power is adjusted just high enough to allow the destination to receive the signal. The selection of the transmission method also influences the interference power caused by each transmission, as discussed in [9]. Hence, another approach for minimizing the interference is to choose an appropriate transmission method. In spread spectrum communication systems there are additional methods to counteract interference. First, spread spectrum communication itself is a countermeasure for narrowband interference [Kal96]. Second, there are additional countermeasures: For example, DiPietro presented a method to mitigate narrow-band interference based on the fast Fourier transformation (FFT) in [DiP89].

A simple model to estimate the overall interference power at a destination node, which is based on multiple circles, is presented by Schilcher *et al.* in [7]. The temporal correlation of interference for consecutive time slots is analyzed in Chapter 4.

In the rest of the work we assume that the channel state h^2 does not change significantly during a single time slot (block fading). In scenarios where no fading is present we set $h^2 \equiv 1$. Let furtheron c denote the channel coherence time in time slots.

2.8 Transmission Methods

With the term *transmission method* we summarize all parts of the behavior of the nodes sending a packet that are one abstraction level above the node-to-node link or channel access. In the OSI layer architecture of networks the transmission methods would reside partly within the link layer and partly within the network layer. The major task is to handle the event that a transmission of a packet from a source node to its destination is unsuccessful.

In this work four different transmission methods are applied:

1. *Direct transmission:* When using this method the source node sends the data packet directly to its destination at a data rate b_r. If the packet gets lost during transmission (e.g. due to fading) the transmission is considered to be failed, i.e., no retransmission method is considered. This method serves as the reference model.

2. *Double data rate transmission:* As the name suggests, this method is similar to *direct transmission* except that the data rate is doubled to $2b_r$ by applying a higher modulation scheme, e.g. 16-QAM instead of QPSK as described in Section 2.4. As a consequence the duration of each transmission is halved, therefore also reducing the expected overall interference by a factor of two, as follows immediately from Equation (2.40).

3. *Time diversity:* (See, e.g., [Ali96].) Here, the source is exploiting time diversity by sending each packet twice. For fairness reasons the data rate is doubled ($2b_r$) to preserve the same overall transmission energy per bit. Due to these assumptions, the overall duration of the transmission process is equal to that in *direct transmission*. The states of the channels of the two transmissions can be stochastically dependent or independent depending on the channel coherence time c in relation to the time between the two transmissions. Note that retransmitting each packet is an extremal case considered for analysis reasons only. In practice a node would only retransmit a packet if the first attempt has been unsuccessful.

4. *Cooperative Relaying:* (See, e.g., [Ala98, LW00, LWT01].) This method starts similarly as in *double data rate transmission*: The source node is transmitting its data packet directly to the destination with doubled data rate $2b_r$.The neighboring nodes, however, try to receive the packet as well. By forwarding the packet again, one of these neighboring nodes, which is called the relay, may help the destination node to correctly decode the message. Due to the two distinct paths the message travels on its way from the source to the destination the communication partners can exploit the diversity gain. This gain arises from the fact that the states of the channels from source to destination and from relay to destination are stochastically independent due to their spatial diversity. If the relay is located between source and destination, there might

be an additional multihop gain also improving the overall performance of the network.

When categorizing different cooperative diversity schemes, there are several criteria that can be applied. The first criteria determines the behavior of the relay nodes. One possibility is that the relay node tries to decode the message and retransmits the decoded data. This variant is called *decode and forward*. The alternative variant would be that the relay node simply amplifies the received analog signal and retransmits it, which is called *amplify and forward*. Both variants have their advantages and disadvantages; an analysis of them can be found, e.g., in [LL10, XJZ+10, IK09, YB07, ZYC+09].

The second criteria is whether relaying is done for each transmission or only if the direct transmission from the source to the destination fails. For the investigations in this work we apply relaying for each transmission since we again try to analyze the extremal case.

A third criteria is how the acting relay node is selected out of the potential relays. The simplest variant is to randomly select the relay out of the set of potential relays that are able to receive and decode the original message correctly. An analysis of this method is presented in Chapter 5. To implement the random selection of the relay in a protocol some signaling messages have to be exchanged such that each of the potential relay nodes knows whether it is the relay or not. One possible approach to perform relay selection is introduced in [BBV08]. There, several short time slots are reserved, in which each potential relay transmits a message with a certain probability. This probability is different for each of these slots. It is selected in a way that it maximizes the probability that the first potential relay that decides to send a message does not suffer from a collision. Hence, the potential relay that responds first is selected to be the acting relay.

Alternatively, there could be very sophisticated relay selection protocols that try to choose the best relay according to a certain criteria as, e.g., the position of the relay in relation to the source and destination nodes, the measured channel state, or a combination of them [ABS09, MYAB09, ABS08, AEBS09]. The selection of the relay could also be done with the same approach as in [BBV08] by incorporating a quality measure for the relays. This measure increases the sending probability for *good relays* such that it is more likely that such a well suited potential relay responds first. Note that if the set of potential relays is empty, there is no relay transmission taking place.

The last criteria determines when the relay node is selected. There are mainly two possibilities: The relay selection process is executed as part of each transmission, which is called *relay selection on demand*. The advantage of this method is that if the direct transmission succeeds and thus no relaying is necessary, also the relay selection process can be omitted. Additionally it is very well suited for fast changing channels where for each transmission a different relay has to be selected. The alternative approach is to *pre-select a relay*, which

can support a series of transmissions until the channels have changed and a new relay has to be selected. The advantage of this approach is that the relay selection procedure is not executed for each transmission reducing the signaling overhead significantly.

Depending on the scenario we apply one or more of these transmission methods in this thesis. Further, we provide a comprehensive simulation based comparison of all four transmission methods.

Chapter 3

Inhomogeneous Distribution of Nodes

In this chapter we introduce a model for inhomogeneously distribute the nodes on a given simulation area and a measure for assessing the inhomogeneity of a given node distributions. Preliminary results have been obtained in cooperation with M. Gyarmati, G. Brandner, and C. Bettstetter. They have been published in [1, 2].

3.1 A Model for Inhomogeneous Node Distributions

To assess the performance of wireless networks via simulation we need different types of models that determine the behavior of different entities of the simulated scenario. While most of these models have been deeply investigated (see Chapter 2), the *spatial distribution* of the nodes still provides room for improvement.

Since real-world node distributions are hard to obtain, it is advantageous to have a model that allows the generation of artificial random distributions. The easiest possibility is to distribute the nodes uniformly. This method has, however, the drawback that it is not very realistic for many scenarios since real world entities, e.g., human beings in an working environment, do not behave like that. Instead, they work in groups together forming clusters in the distribution of their locations.

To overcome this drawback, we propose a model (see [1]) that allows to synthetically generate *inhomogeneous* (or *non-uniform*) random distributions, which is presented in Section 3.1.1. The model is based on the well-known concept of *thinning* of a homogeneous node distribution [Cre91, SKM95]. This approach is flexible, yet simple to implement and not restricted to certain scenarios. We also derive some important stochastic properties of the inhomogeneous distribution such as number of surviving nodes and the probability distribution of the distance to the nearest neighbor of a node.

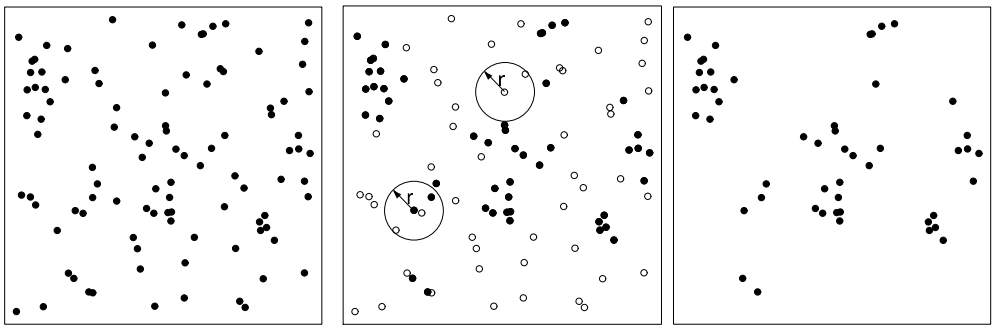

(a) Uniform distribution. (b) Thinning process. (c) Non-uniform distribution.

Figure 3.1: Spatial distributions and thinning.

3.1.1 Introduction of the Model

In the following we introduce a method that allows the generation of inhomogeneous random distributions of nodes. This method can generate its distributions for both bounded and infinitely-large areas. The generation of an inhomogeneous distribution on a *bounded area* A consists of two steps:

1. We generate a uniform random node distribution $\mathcal{U}$, i.e., we uniformly distribute n nodes on a given area A.
2. We remove some of the nodes according to a certain algorithm. This *thinning* of $\mathcal{U}$ yields a non-uniform node distribution $\mathcal{T}$.

The thinning algorithm consists of the following steps: For each node, we determine the number of nodes located within a *neighborhood range* r around its position. The nodes within this circle are called the node's *neighbors*. A node is marked to be thinned if it has less than k neighbors; Otherwise it is marked to be preserved. After each node has been classified, the nodes marked to be thinned are eventually removed. Alternatively, we can think of a node to be retained if its k^{th} nearest neighbor is at most a distance r away. Note that the algorithm does not depend on the order in which the nodes are processed.

Example 3.1. An example is illustrated in Figure 3.1(a), where $n = 100$ initial nodes are uniformly distributed on a square area with side length $\sqrt{A} = 5$ length units. Figure 3.1(b) shows the neighborhood circle of radius $r = 0.5$ length units of two nodes. Nodes are removed if they have less than $k = 3$ neighbors within their circles. The nodes shown as solid dots are marked to be preserved, and the nodes shown as circles are marked to be removed. In this example, there are $n' = 50$ remaining nodes, which are shown in Figure 3.1(c).

During thinning of the nodes a *border effect* occurs: The expected number of neighbors is lower for nodes close to the border of A and these nodes are therefore

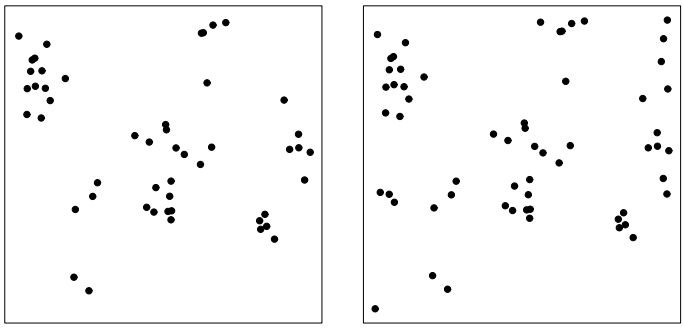

(a) Normal distance. (b) Wrap-around distance.

Figure 3.2: Border effect in the thinning algorithm.

more likely to be removed. This effect is similar to the border effect occurring in the analysis of connectivity in ad-hoc networks (see [SB03, Bet04]). To avoid this effect, a wrap-around distance metric can be used in place of the standard Euclidean distance metric, as defined in Equation (2.3). With this metric, a node at a border of A is considered to be close to a node at the opposite border of A. Hence, these two nodes can be neighbors.

Example 3.2. Figure 3.2 demonstrates the border effect using the same initial distribution as in Example 3.1. In the wrap-around case (Figure 3.2(b)), more nodes located close to the border survive the thinning process. In this example, there are $n' = 60$ remaining nodes when applying the wrap-around distance metric compared to $n' = 50$ remaining nodes with Euclidean distance metric.

The same thinning algorithm can be applied to nodes distributed on an *infinite area* according to a stationary Poisson point process. In fact, a homogeneous distribution $\mathcal{N}$ generated by a Poisson process can be regarded as the limiting case of a uniform distribution $\mathcal{U}$ in which $n \to \infty$ and $A \to \infty$ but the node density $\lambda = \frac{n}{A}$ remains constant. If we apply thinning to $\mathcal{N}$ and regard a subarea of size A', stochastically essentially the same node pattern will emerge as if thinning is applied to $\mathcal{U}$ under the following conditions:

- The wrap-around distance metric has to be applied.
- $\mathcal{U}$ contains a random number of nodes that follows a Poisson distribution with expected value λ.

3.1.2 Stochastic Properties of the Distribution

In the following we are going to derive some important stochastic properties of an inhomogeneous node distribution $\mathcal{T}$ being generated by the thinning algorithm presented above. The probability density function (pdf) of the distance of a node to

its nearest neighbor in $\mathcal{T}$ is, e.g., an essential distance property that has significant impact on network connectivity (see [Bet04]). We consider only the case where no border effects occur assuming a Poisson process generating the underlying homogeneous distribution $\mathcal{N}$. The results also hold, however, on bounded areas if a wrap-around distance model is applied.

3.1.2.1 Percentage of Nodes Remaining

Theorem 3.1. *Let $\mathcal{T}$ denote the resulting distribution when applying the thinning algorithm on a uniform node distribution $\mathcal{U}$ with parameters r and k. Then the expected number of nodes remaining in an area of size A is given by*

$$\mathbb{E}(n') = \lambda\, A\, \mathbb{P}(N \textit{ survives}) = \lambda\, A \left(1 - \frac{\Gamma(k, \lambda\, r^2\pi)}{(k-1)!}\right) . \tag{3.1}$$

Proof. Let $\mathcal{N}$ denote a Poisson point process with intensity λ and the random variable K denote the number of neighbors of a node $N \in \mathcal{N}$. Per definition of a Poisson point process, K follows a Poisson distribution, i.e., $\mathbb{P}(K = i) = P_\mu(i) \coloneqq \frac{\mu^i}{i!}\mathrm{e}^{-\mu}$. The constant μ represents the expected number of neighbors of N, i.e., $\mu = \lambda\, r^2\pi$. The probability for a node N to be removed is thus given by $\mathbb{P}(N \text{ removed}) = \mathbb{P}(K < k) = \sum_{i=0}^{k-1} \mathbb{P}(K = i)$.

Using the incomplete Gamma function $\Gamma(k, \mu) \coloneqq (k-1)!\ \mathrm{e}^{-\mu} \sum_{i=0}^{k-1} \frac{\mu^i}{i!}$, we obtain

$$\mathbb{P}(N \text{ removed}) = \frac{\Gamma(k, \mu)}{(k-1)!} . \tag{3.2}$$

The probability that a node N is not removed, i.e., it survives the thinning process is

$$\mathbb{P}(N \text{ survives}) = 1 - \mathbb{P}(N \text{ removed}) = 1 - \frac{\Gamma(k, \mu)}{(k-1)!} = 1 - \frac{\Gamma(k, \lambda\, r^2\pi)}{(k-1)!} . \tag{3.3}$$

□

3.1.2.2 Expected Number of Previous Neighbors

Let N_0 denote a node that survives the thinning operation. The number of neighbors K_0 that this node had in the original distribution $\mathcal{N}$ is no longer Poisson distributed due to the condition that N_0 survives. For all $i \geq k$ we have

$$\mathbb{P}(K_0 = i \mid N_0 \text{ survives}) = \mathbb{P}(K_0 = i \mid K_0 \geq k) = \frac{\mathbb{P}(K_0 = i \wedge K_0 \geq k)}{\mathbb{P}(K_0 \geq k)} = \frac{P_\mu(i)}{1 - \frac{\Gamma(k,\mu)}{(k-1)!}} . \tag{3.4}$$

The expected number of previous neighbors of a surviving node is then

$$\mathbb{E}(K_0) = \frac{\Gamma(k-1, \mu)(k-1) - \Gamma(k)}{\Gamma(k, \mu) - \Gamma(k)}\, \mu\, , \tag{3.5}$$

with $\Gamma(k) = (k-1)!$.

3.1.2.3 Survival Probability of the Nearest Neighbor

Let N_0 denote a surviving node and N_1 denote its nearest neighbor, i.e., the node that has the smallest distance to N_0 in $\mathcal{N}$. We are going to derive the probability that the nearest neighbor of a surviving node also survives, i.e., the conditional probability $\mathbb{P}(N_1 \text{ survives} \mid N_0 \text{ survives})$.

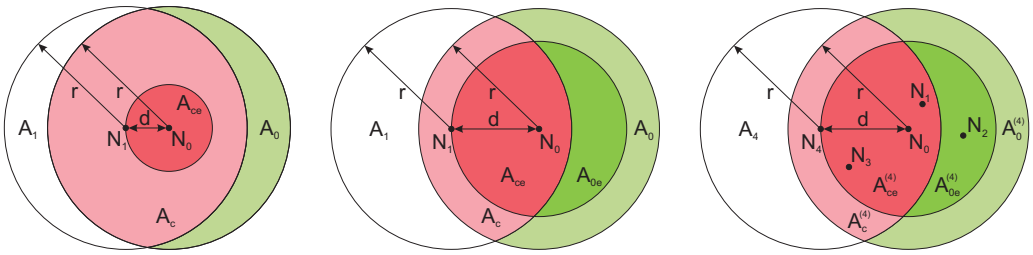

(a) Empty neighborhood circle in common area.

(b) Empty neighborhood circle exceeding common area.

(c) Neighborhood and common areas of N_0 and N_4.

Figure 3.3: Neighborhoods and common areas.

We start with deriving the number of common neighbors of N_0 and N_1.

Lemma 3.1. *Let d_1 denote the distance between N_0 and N_1, and let the random variable K_c denote the number of common neighbors of these nodes. Then we have*

$$\begin{aligned} \mathbb{P}\left(K_c = j \mid N_0 \textit{ survives}\right) &= \mathbb{P}\left(K_c = j \mid K_0 \geq k\right) = \\ &= \sum_{i=k}^{\infty} B_{i,p_{com}}(j)\ \mathbb{P}\left(K_0 = i \mid N_0 \textit{ survives}\right)\ . \end{aligned} \tag{3.6}$$

The corresponding probability p_{com} is given by

$$p_{com} = \frac{A_c - A_{ce}}{(r^2 - d_1^2)\,\pi}\ . \tag{3.7}$$

Proof. Node N_0 has K_0 neighbors in $\mathcal{N}$. Some of these K_0 neighbors are located in the area A_c (see Figure 3.3(a)). The probability for an arbitrary chosen neighbor of N_0 to be also a neighbor of N_1 is furtheron denoted by p_{com}. If we assume that K_0 is known, K_c follows a binomial distribution, i.e. $\mathbb{P}(K_c = j \mid K_0 = i) = B_{i,p_{com}}(j) := \binom{i}{j} p_{com}^{j}\ (1 - p_{com})^{i-j}$ for all $j \leq i$. The probability $\mathbb{P}\left(K_c = j \mid N_0 \text{ survives}\right)$ is the weighted sum over all possible values of K_0. Since N_0 survives the thinning ($K_0 \geq k$), we get the result in Equation (3.6).

Next, we derive an expression for the probability p_{com}. Since N_1 is the nearest neighbor of N_0, there are no nodes within a circle of radius d_1 around N_0. If $d_1 \leq \frac{r}{2}$ this *empty circle* lies completely within A_c and is called A_{ce} (see Figure 3.3(a)). Otherwise, if $d_1 > \frac{r}{2}$ it lies partly in A_c and partly in A_0. These two parts are denoted with A_{ce} and A_{0e}, respectively (see Figure 3.3(b)). Note that A_c and A_0

still denote the total areas as in Figure 3.3(a). Given these definitions, a neighbor of N_0 lies in A_c with probability

$$p_{com} = \frac{A_c - A_{ce}}{(r^2 - d_1^2)\,\pi}\,. \tag{3.8}$$

□

Theorem 3.2. *Let N_1 be the nearest neighbor of a given node N_0. The survival probability of N_1 under the condition that N_0 survives the thinning is given by*

$$\begin{aligned}\mathbb{P}(N_1 \textit{ survives} \mid N_0 \textit{ survives}) \;=\; & \int_0^r \sum_{i=k}^{\infty} \left(\sum_{j=0}^{i-1} \left(1 - \frac{\Gamma(i, \lambda A_1)}{(i-1)!}\right) B_{i,p_{com}}(j) \right) \\ & \cdot \mathbb{P}\left(K_0 = i \mid N_0 \textit{ survives}\right) \frac{d_1\, e^{-\lambda d_1^2 \pi}}{\int_0^r d\, e^{-\lambda d^2 \pi}\,\mathrm{d}d}\,\mathrm{d}d_1\,, \end{aligned} \tag{3.9}$$

where $\mathbb{P}\left(K_0 = i \mid N_0 \textit{ survives}\right)$ is given in Equation (3.4) and p_{com} is given in Lemma 3.1.

Proof. Node N_1 survives the thinning process if $K_1 \geq k$. Since it already has $K_c + 1$ neighbors in A_c (namely, N_0 and the common neighbors), it will survive the thinning if at least $\max(0, k - (K_c + 1))$ further nodes are located within A_1. The random number of such non-common neighbors is denoted by $K_1' \coloneqq K_1 - (K_c + 1)$. Since K_1' is independent of K_0, it follows a Poisson distribution with parameter λA_1. Hence, we have

$$\mathbb{P}(K_1' \geq i) = 1 - \frac{\Gamma(i, \lambda A_1)}{(i-1)!}\,. \tag{3.10}$$

The desired survival probability $\mathbb{P}(N_1 \,\text{survives} \mid N_0 \,\text{survives})$ can be written as

$$\begin{aligned}&\mathbb{P}(K_1' + K_c + 1 \geq k \mid K_0 \geq k) = \\ &\quad = \sum_{i=k}^{\infty} \left(\sum_{j=0}^{i-1} \mathbb{P}(K_1' \geq k - j - 1)\, B_{i,p_{com}}(j) \right) \mathbb{P}\left(K_0 = i \mid N_0 \,\text{survives}\right)\,, \end{aligned} \tag{3.11}$$

where the probabilities in the sum are given by Equations (3.10) and (3.6), respectively. This probability is a function of the node density λ, the thinning parameters k and r, and the distance d_1. In general we do not know the distance d_1 between the two nodes N_0 and N_1. Let the random variable D_1 denote this distance. For a homogeneous Poisson point process, the nearest neighbor distance follows the distribution $f_{D_1}(d_1) = 2\pi\lambda\, d_1\, \mathrm{e}^{-\lambda d_1^2 \pi}$ (see [Cre91]). Since in our case the condition $d_1 \leq r$ applies we have to normalize the pdf yielding $f_{D_1}(d_1 \mid d_1 \leq r) = \frac{f_{D_1}(d_1)}{\int_0^r f_{D_1}(d)\,\mathrm{d}d}$. This leads to the overall survival probability

$$\mathbb{P}(N_1 \,\text{survives} \mid N_0 \,\text{survives}) = \int_0^r \mathbb{P}(K_1' + K_c + 1 \geq k \mid K_0 \geq k)\, f_{D_1}(d_1 \mid d_1 \leq r)\,\mathrm{d}d_1\,. \tag{3.12}$$

□

All calculations above are based on the size of the different areas. The common area is $A_c = 2r^2 \arccos\left(\frac{d_1}{2r}\right) - d_1\sqrt{\frac{r^2-d_1^2}{4}}$. The area A_1 can be computed with $A_1 = r^2\pi - A_c$. The *empty area* A_{ce} is part of A_c; it is given by

$$A_{ce} = \begin{cases} d_1^2\pi & \text{if } d_1 \leq \frac{r}{2} \\ d_1^2 \arccos\left(1 - \frac{r^2}{2d_1^2}\right) + r^2 \arccos\left(\frac{r}{2d_1}\right) - \frac{r}{2}\sqrt{4d_1^2 - r^2} & \text{else.} \end{cases} \tag{3.13}$$

3.1.2.4 Survival of Other Neighbors

Next, we generalize the probability $\mathbb{P}(N_1 \text{ survives} \mid N_0 \text{ survives})$ and derive the survival probability $\mathbb{P}(N_l \text{ survives} \mid N_0 \text{ survives})$ for the l^{th} nearest neighbor N_l with $l = 1, 2, \ldots, k$, i.e., the node with the l^{th} smallest distance to N_0. We again start by deriving the number of common neighbors of N_0 and N_l.

Lemma 3.2. *Let d_l with $l \in \mathbb{N}$ denote the distance between N_0 and N_l, and let the random variable $K_c^{(l)}$ denote the number of common neighbors of these nodes. Then we have*

$$\begin{aligned} &\mathbb{P}(K_c^{(l)} = j \,|\, N_0 \textit{ survives}) = \\ &= \sum_{i=k}^{\infty} \left(\sum_{h=0}^{j} B_{i-l,p_c^{(l)}}(h)\, B_{l-1,p_{ce}^{(l)}}(j-h) \right) \mathbb{P}(K_0 = i \mid N_0 \textit{ survives}), \end{aligned} \tag{3.14}$$

where the probabilities for the binomial distributions are given by

$$p_{ce}^{(l)} = \begin{cases} 1 & \textit{if } d_l \leq \frac{r}{2} \\ \frac{A_{ce}^{(l)}}{d_l^2\pi} & \textit{else,} \end{cases} \tag{3.15}$$

and

$$p_c^{(l)} \coloneqq \frac{A_c^{(l)} - A_{ce}^{(l)}}{(r^2 - d_l^2)\pi}\,. \tag{3.16}$$

The probability $\mathbb{P}(K_0 = i \mid N_0 \textit{ survives})$ is given in Equation (3.4).

Proof. In the proof of Lemma 3.1 it was stated that a circle of radius $d_1 = d(N_0, N_1)$ around N_0 is empty. In general, for $l > 1$ exactly $l-1$ neighbors are located within a circle of radius $d_l \coloneqq d(N_0, N_l)$, namely $N_1, N_2, \ldots, N_{l-1}$. This circle, which is called C_l, can be divided into two parts: $A_{ce}^{(l)}$ containing the common neighbors of N_0 and N_l, and $A_{0e}^{(l)}$ containing nodes that are only neighbors to N_0 (see Figure 3.3(c), in which $l = 4$).

We have to distinguish two cases: If $d_l \leq \frac{r}{2}$ the area $A_{0e}^{(l)}$ equals zero and therefore all $l-1$ nodes in C_l are inside $A_{ce}^{(l)}$, i.e., are common neighbors. Otherwise, the number

of nodes within $A_{ce}^{(l)}$ is binomially distributed according to $B_{l-1,p_{ce}^{(l)}}$. The probability $p_{ce}^{(l)}$ that a given node in C_l is located in $A_{ce}^{(l)}$ is

$$p_{ce}^{(l)} = \begin{cases} 1 & \text{if } d_l \leq \frac{r}{2} \\ \frac{A_{ce}^{(l)}}{d_l^2 \pi} & \text{else.} \end{cases} \tag{3.17}$$

The neighbors of N_0 that are further away than N_l are located outside C_l. The probability that such a node is located within $A_c^{(l)} \setminus A_{ce}^{(l)}$ is

$$p_c^{(l)} \coloneqq \frac{A_c^{(l)} - A_{ce}^{(l)}}{(r^2 - d_l^2)\pi} \,. \tag{3.18}$$

Therefore, the number of nodes within $A_c^{(l)} \setminus A_{ce}^{(l)}$ is binomially distributed according to $B_{K_0-l,p_c^{(l)}}$. If N_0 and N_l have j common neighbors, they are split onto the two areas $A_{ce}^{(l)}$ and $A_c^{(l)} \setminus A_{ce}^{(l)}$. Since the number of nodes within both of these areas is binomially distributed, the number j is a combination of these two binomial distributions, leading to the result (compare with Equation (3.6)). □

Theorem 3.3. *Let N_l denote the l^{th} nearest neighbor of node N_0. Then the survival probability of N_l under the condition that N_0 survives the thinning is given by*

$$\begin{aligned} &\mathbb{P}(N_l \textit{ survives} \,|\, N_0 \textit{ survives}) = \\ &= \int_0^r \sum_{i=k}^{\infty} \left(\sum_{j=0}^{i-1} \left(1 - \frac{\Gamma(k-j-1, \lambda r^2 \pi)}{(k-j-2)!} \right) \sum_{h=0}^{j} B_{i-l,p_c^{(l)}}(h)\, B_{l-1,p_{ce}^{(l)}}(j-h) \right) \\ &\quad \cdot \mathbb{P}(K_0 = i \mid N_0 \textit{ survives}) \, \frac{d_l^{2l-1}\, e^{-\lambda d_l^2 \pi}}{\int_0^r d^{2l-1}\, e^{-\lambda d^2 \pi} \,\mathrm{d}d} \,\mathrm{d}d_l \,, \end{aligned} \tag{3.19}$$

where $p_c^{(l)}$ and $p_{ce}^{(l)}$ are given in Lemma 3.2.

Proof. In order to obtain the survival probability $\mathbb{P}(N_l \,\text{survives} \mid N_0 \,\text{survives})$, we first have to sum $\mathbb{P}(K_c^{(l)} = j \,|\, N_0 \,\text{survives})$ over all possible values for j. Then we integrate the result over all possible distances $0 \leq d_l \leq r$ weighted with the corresponding probabilities. The pdf $f_{D_l}(d)$ of the distance D_l between N_0 and its l^{th} nearest neighbor N_l *before thinning* is [Tho56]

$$f_{D_l}(d) = \frac{2\pi^l \lambda^l d^{2l-1}}{(l-1)!} \, \mathrm{e}^{-\pi\lambda d^2} \,. \tag{3.20}$$

Conditioning this distance with $d_l \leq r$ gives $f_{D_1}(d_1 \mid d_1 \leq r) = \frac{d_l^{2l-1}\, \mathrm{e}^{-\lambda d_l^2 \pi}}{\int_0^r d^{2l-1}\, \mathrm{e}^{-\lambda d^2 \pi} \,\mathrm{d}d}$. Overall, this yields Equation (3.19). □

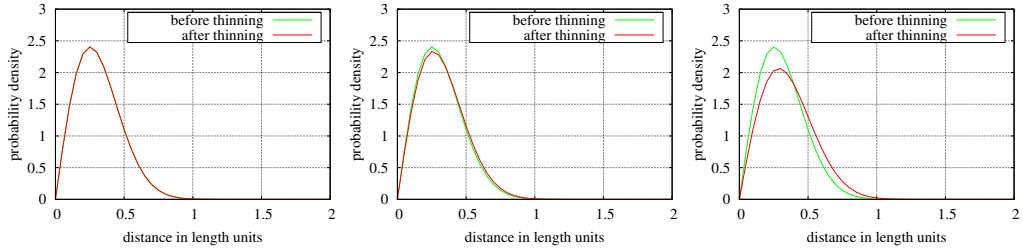

(a) $k = 17$. (b) $k = 27$. (c) $k = 37$.

Figure 3.4: Pdfs of the nearest neighbor distance before and after the thinning process.

3.1.2.5 Nearest Neighbor Distance

Next, we derive the pdf of the distance between a node and its nearest neighbor in $\mathcal{T}$. Let again N_0 be a node that survives the thinning process.

Theorem 3.4. *The pdf of the distance between a surviving node N_0 and its nearest neighbor is given by*

$$f_{D_1'}(d) = \sum_{l=1}^{\infty} f_{D_l}(d)\, \mathbb{P}(N_l \text{ survives} \mid N_0 \text{ survives}) \cdot \prod_{j=1}^{l-1} (1 - \mathbb{P}(N_j \text{ survives} \mid N_0 \text{ survives}))\,. \tag{3.21}$$

Proof. If the nearest neighbor N_1 of a surviving node N_0 also survives the thinning process, the nearest neighbor distance stays unchanged. If N_1 does not survive, there are two options: node N_2 survives or it is removed. If it survives, it is the new nearest neighbor after thinning; therefore, the nearest neighbor distance corresponds to $f_{D_2}(d)$. This principle can be further applied for larger l. Hence, we can obtain the pdf of the nearest neighbor distance *after thinning* by summing over all possible new nearest neighbors with respect to their probabilities. □

Since the infinite sum in Equation (3.21) is hard to compute, we provide an approximation by using the fact that the product $\prod_{j=1}^{l-1} 1 - \mathbb{P}(N_j \text{ survives} \mid N_0 \text{ survives})$ gets smaller for larger l. This approximation is achieved by stopping the summation at a certain index $l = l_{\max}$ (e.g., where the product is below a certain threshold value

ϵ), yielding

$$\begin{aligned} f_{D_1'}(d) &\approx f_{D_{l_{\max}}}(d) \prod_{j=1}^{l_{\max}-1} (1 - \mathbb{P}(N_j \text{ survives} \mid N_0 \text{ survives})) \\ &\quad + \sum_{l=1}^{l_{\max}-1} f_{D_l}(d)\, \mathbb{P}(N_l \text{ survives} \mid N_0 \text{ survives}) \\ &\qquad \cdot \prod_{j=1}^{l-1} (1 - \mathbb{P}(N_j \text{ survives} \mid N_0 \text{ survives})). \end{aligned} \tag{3.22}$$

Comprehensive simulations have shown that this approximation is sufficiently accurate for reasonably chosen ϵ.

Example 3.3. Figure 3.4 depicts the pdf of the nearest neighbor distance before and after thinning. We apply $r = 2$, $\lambda = 2.5$, and three different values for k. For $k = 17$, more than 99% of the initial nodes survive. Thus, there is almost no change in the pdf. As k increases, the number of nodes surviving decreases and therefore the nearest neighbor distance increases. For $k = 27$ there are about 80% of the nodes remaining, and at $k = 37$ only 10% of the nodes survive the thinning process.

A comprehensive comparison between the results derived in this section and simulations is presented in Appendix A.

3.1.2.6 Distance to Other Neighbors

In the following we generalize the results of the previous section to obtain the pdf of the distance to the k^{th} nearest neighbor in $\mathcal{T}$.

Theorem 3.5. *The pdf of the distance between N_0 and its k^{th} nearest neighbor is the weighted sum over the pdfs of all possible nodes, yielding*

$$\begin{aligned} f_{D_k'}(d) &= \sum_{l=1}^{\infty} f_{D_1'}(d)\, \mathbb{P}(N_l \textit{ survives} \mid N_0 \textit{ survives}) \\ &\quad \cdot \sum_{v \in V(k-1)} \prod_{j=1}^{l-1} (v_j + (-1)^{v_j}\, \mathbb{P}(N_j \textit{ survives} \mid N_0 \textit{ survives})) \ . \end{aligned} \tag{3.23}$$

Proof. Let N_0 be a node that survives the thinning process and N_l denote the l^{th} nearest neighbor before thinning. Further, let $v \in \{0,1\}^{l-1}$ be the vector for which $v_i = 0$ if N_i survives the thinning and $v_i = 1$ otherwise for all $i = 1, \ldots, j$. Let $V(k-1)$ denote the set of all vectors v with $\sum_{i=1}^{l-1} v_i = k - 1$.

Then, N_l is the new k^{th} nearest neighbor if N_l survives and $v \in V(k-1)$. Hence, the probability that N_l is the new k^{th} nearest neighbor is given by

$$\mathbb{P}(N_l \text{ new } k^{\text{th}} \text{ nearest neighbor} \mid N_0 \text{ survives}) = \mathbb{P}(N_l \text{ survives} \mid N_0 \text{ survives}) \cdot \sum_{v \in V(k-1)} \prod_{j=1}^{l-1} (v_j + (-1)^{v_j} \, \mathbb{P}(N_j \text{ survives} \mid N_0 \text{ survives})) \ . \tag{3.24}$$

By summing up the pdfs of the distances to the k^{th} nearest neighbor over all k weighted with the probabilities given above we can obtain the result. □

This infinite sum can again be simplified by stopping the summation at a certain index $l = l_{max}$ similar to Equation (3.22), yielding

$$\begin{aligned} f_{D_k'}(d) \ \approx \ & f_{D_{l_{max}}}(d) \sum_{v \in V(k-1)} \prod_{j=1}^{l_{max}-1} (v_j + (-1)^{v_j} \, \mathbb{P}(N_j \text{ survives} \mid N_0 \text{ survives})) \\ & + \sum_{l=1}^{l_{max}-1} f_{D_1'}(d) \, \mathbb{P}(N_l \text{ survives} \mid N_0 \text{ survives}) \\ & \cdot \sum_{v \in V(k-1)} \prod_{j=1}^{l-1} (v_j + (-1)^{v_j} \, \mathbb{P}(N_j \text{ survives} \mid N_0 \text{ survives})) \ . \end{aligned} \tag{3.25}$$

3.1.3 Visualization for Different Parameters

This section shows, by example, what typical spatial distributions $\mathcal{T}$ look like and how the input parameters impact its shape. We base the simulations on a uniform

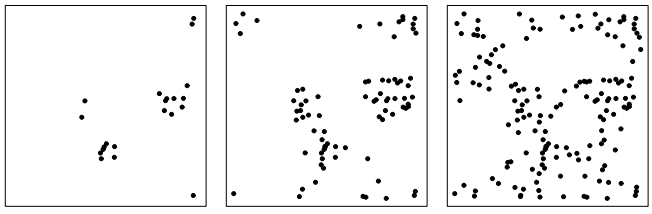

(a) $k = 10$.

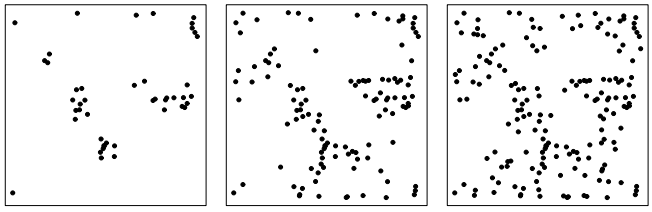

(b) $k = 6$.

Figure 3.5: Simulations with fixed k and increasing r.

random distribution of $n = 200$ nodes on an $a \times a$ square with $a = 5$. The original node density of a corresponding Poisson process is $\lambda = \frac{n}{a^2} = 8$. Thinning is applied without border effects.

Example 3.4. In a first series of experiments thinning is performed with a varying neighborhood radius r. For $k = 10$, Figure 3.5(a) shows how the node distribution changes if we increase r from 0.5 (left) over 0.6 (middle) to 0.7 (right). Figure 3.5(b) depicts the same experiment with $k = 6$ and $r = 0.4$ to 0.6 (again left to right).

Example 3.5. In a second series of experiments, the neighborhood radius is kept constant at $r = 0.5$, while k is increased stepwise. Figure 3.6 presents example distributions with stepwise increment of k from $k = 3$ (top left) to 10 (bottom right). As can be seen, the number of nodes decreases for higher k while the remaining nodes get more clustered.

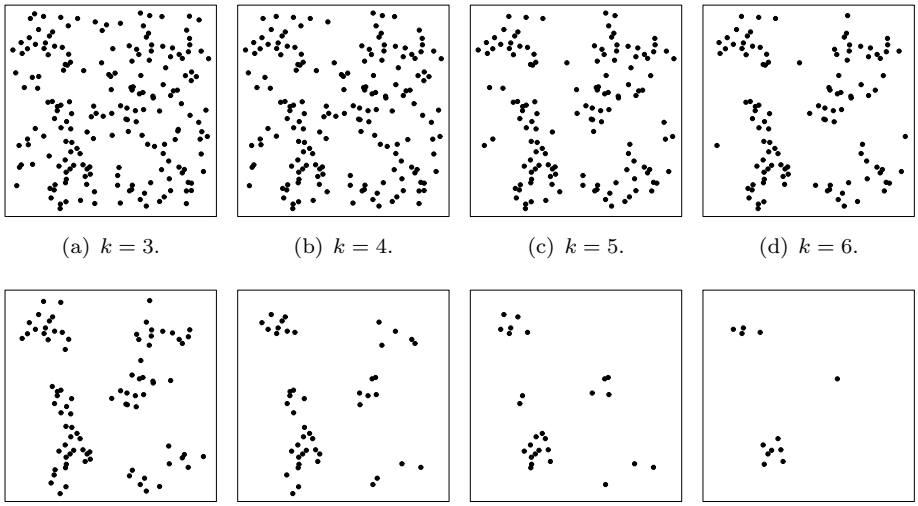

(a) $k = 3$. (b) $k = 4$. (c) $k = 5$. (d) $k = 6$.

(e) $k = 7$. (f) $k = 8$. (g) $k = 9$. (h) $k = 10$.

Figure 3.6: Simulations with fixed r and increasing k.

Example 3.6. In a third series, thinning is done with correlated values of r and k. For given r, the *required* number of neighbors is always chosen to be the *expected* number of neighbors, i.e., $k = \lfloor \mu \rfloor = \left\lfloor \frac{n\pi}{a^2} r^2 \right\rfloor$. Figure 3.7 depicts three example distributions $\mathcal{T}$ after thinning. Many small clusters result from a thinning with small r and small k, while the number of clusters decreases with increasing r and k. The expected number of nodes remaining for the given parameters are $\mathbb{E}(n') = 125$, 112, and 107, respectively. The actual numbers of nodes remaining are $n' = 117$, 114, and 118.

Thinning can be performed several times on the same set of nodes. It is possible (but not necessary) that each iteration removes nodes, since the number of their neighbors has been reduced in previous iterations. After some number of iterations, such *multiple thinning* converges, either because all nodes are removed or the remaining nodes are located very close together.

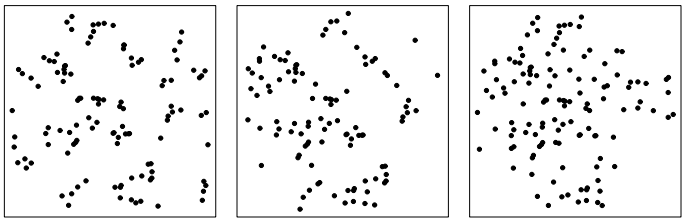

(a) $r = 0.29$, $k = 2$. (b) $r = 0.49$, $k = 6$. (c) $r = 1$, $k = 25$.

Figure 3.7: Simulations with increasing r and k.

Example 3.7. The effect of multiple thinning is depicted in Figure 3.8 (same parameters as above and $k = 6$) with convergence after 6 iterations ($n' = 23$). After the first thinning iteration the clusters are still blurred; after a few iterations they become clearer; finally, each node has at least k nodes in its neighborhood, and there are no standalone nodes left. Each step but the final one removes nodes that are *important* to the remaining nodes, i.e., that are essential for the surviving of nodes.

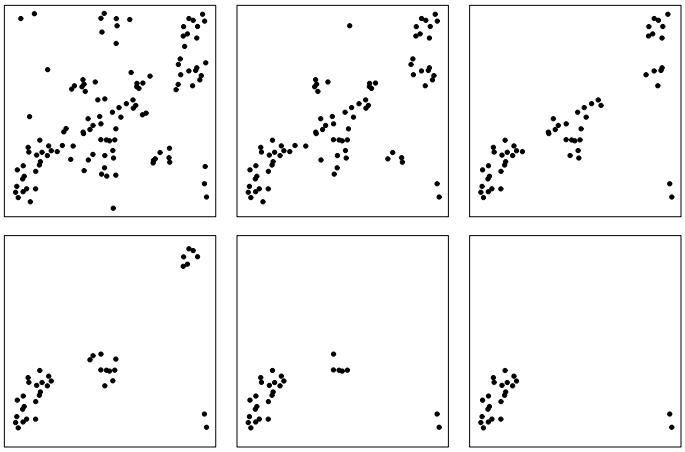

Figure 3.8: Multiple thinning.

3.2 Measuring Inhomogeneity

When applying the inhomogeneous node distribution model presented in Chapter 3.1, it is possible to synthesize more realistic node distributions that have a similar inhomogeneity than a given real distribution. An open problem at this point is how to compare the inhomogeneity of different distributions. Since manual comparison by humans is a huge effort and is affected by the subjective perception of each individual, we are in need for a objective measure of inhomogeneity of a given node distribution.

Hence, in the following we introduce a measure for the inhomogeneity of a given node distribution (see [2]). With this measure in hand, it is possible to generate node

distributions with all meaningful inhomogeneity values in a given scenario as well as assessing the data of a real-world node distribution and then synthesize artificial node distributions with a similar inhomogeneity. We also compare the inhomogeneity measure with human perception via a web survey participated by researchers and students in Austria and South Korea. As the results show the inhomogeneity measure matches quite well the judgment of the participants of the survey.

Before introducing the inhomogeneity measure, we define which general requirements we expect of such a measure. An inhomogeneity measure should possess the following three properties:

1. The measure is bounded between 0 and 1, with 0 indicating a perfectly uniform, and 1 indicating an extremely non-uniform distribution. Later we will see what the terms perfectly uniform and extremely non-uniform mean. This property is mainly for an easy usage of the measure.

2. The measure is independent of the number of nodes within the area, i.e. more nodes should not result in higher inhomogeneity values. As no reference measure for inhomogeneity exists it is impossible to create different distributions with various numbers of nodes but the same inhomogeneity to verify this property. Further, it should not depend on the size of the area in which the nodes are distributed.

3. The measure is independent of linear operations (e.g. moving, scaling, mirroring, rotating), as such transformations do not have any influence on the degree of inhomogeneity of a distribution. Furthermore, the measure supports wrap-around distance metrics to avoid border effects (see, e.g. [1]).

3.2.1 A Grid-Based Inhomogeneity Measure

In the following we are going to introduce our inhomogeneity measure. Afterwards, some properties of the measure are proven. Finally, some sample distributions together with their inhomogeneity values are presented.

3.2.1.1 Definitions

Let A denote a rectangular area with side lengths a and b. Then,a subdivision of both edges of A into z parts of same length is called a *z-segmentation* of the area A. In other words, the area is subdivided into a grid with z^2 rectangular subareas of same size. These subareas are denoted by A_i with $i = 1, 2, \ldots, z^2$. Let n_i denote the number of nodes located in the subarea A_i.

An *offset* $(x_o, y_o) \in [0, \frac{a}{z}) \times [0, \frac{b}{z})$ of a z-segmentation is defined as follows: In the horizontal direction, the entire grid is moved to the right by x_o; the parts of the segmentation that leave A at the right border are assumed to be inserted at the left border of A. The value y_o plays the same role for the vertical direction. The

upper bounds for x_o and y_o are due to symmetry. For a particular offset (x_o, y_o), the number of nodes in a subarea A_i is called $n_{i,(x_o,y_o)}$. A z'-segmentation is called a *refinement* of a z-segmentation if and only if $z' > z$.

3.2.1.2 Derivation of the Inhomogeneity Measure

Let n nodes be uniformly randomly distributed on an area A. The expected number of nodes in each subarea A_i is

$$\bar{n}(z) \coloneqq \bar{n}_i(z) = \frac{n}{z^2} \ \forall i \ . \tag{3.26}$$

The deviation of the actual number of nodes n_i in an area A_i from the expected value $\bar{n}(z)$ is an indicator for the local inhomogeneity of the spatial distribution. Hence, we define the *inhomogeneity* of a z-segmentation with offset (x_o, y_o) as

$$\psi_{(x_o,y_o)}(z) \coloneqq \frac{1}{2n} \sum_{i=1}^{z^2} \left| n_{i,(x_o,y_o)} - \bar{n}(z) \right| , \tag{3.27}$$

with the normalization factor $\frac{1}{2n}$ (see Lemma 3.4 below).

As illustrated in Figure 3.9, the value of $\psi_{(x_o,y_o)}(z)$ depends on the offset. Figure 3.9(a) depicts a node cluster that is centered; Figure 3.9(b) shows the same cluster moved to the upper left corner. Both figures contain a 2-segmentation of the area. If the cluster is centered, all four subareas contain approximately the same number of nodes. This would give the impression that there is a homogeneous distribution. This effect must be avoided, as a good inhomogeneity measure is *independent of linear operations* of the entire set of nodes. To achieve this independence, an offset must be chosen that maximizes the inhomogeneity value for a given z-segmentation (as in Figure 3.9(b)). Thus, we define the *inhomogeneity* of a z-segmentation as

$$\psi(z) \coloneqq \max_{(x_o,y_o)} h_{(x_o,y_o)}(z). \tag{3.28}$$

The inhomogeneity $\psi(z)$ can be interpreted as a measure with an adjustable locality. If the z-segmentation is being refined, more local deviations to an idealized

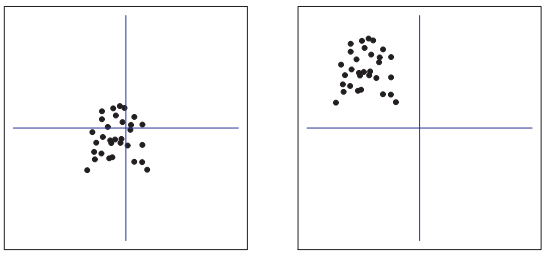

(a) Centered Cluster. (b) Moved Cluster.

Figure 3.9: Different inhomogeneity values for a moved cluster.

homogeneous distribution are taken into account. At some point when the segmentation is sufficiently refined, even for a homogeneous distribution, the value is increasing due to local variations. For inhomogeneous distributions these deviations can be recognized by this measure with a much less refined segmentation, e.g. if all nodes are in the upper left quarter of A, even a 2-segmentation indicates complete inhomogeneity. Thus, high values of $\psi(z)$ for rough z-segmentations indicate an inhomogeneous distribution, whereas small values indicate a homogeneous distribution. For more refined z-segmentations the difference between these two situations is decreasing. At a certain point (e.g. if there is no subarea containing more than one node) there is no difference between a homogeneous and an inhomogeneous distribution.

Next, we present the definition of an inhomogeneity measure that is independent of the area segmentation z. For this purpose, we generate area segmentations with $z = 2, 4, 8, \ldots, 2^{z_{\max}}$ ($z_{\max} \in \mathbb{N}$) until we have reached a certain segmentation in which each subarea contains at most one node. For each segmentation, we compute $\psi(z)$ and build a weighted sum in which a more refined segmentation (with high z) gets a lower weight. The *inhomogeneity* ψ of a node distribution is thus defined as

$$\begin{aligned} \psi &:= \sum_{j=1}^{r} w^{1-j}\, \psi(2^j) \\ &= \frac{1}{2n} \sum_{j=1}^{z_{\max}} w^{1-j} \max_{(x_o,y_o)} \sum_{i=1}^{2^{2j}} \left| n_{i,(x_o,y_o)} - \frac{n}{2^{2j}} \right| . \end{aligned} \tag{3.29}$$

The constant w is selected in a way to achieve $\psi \leq 1$ (see Section 3.2.1.4: $w \approx 4.79129$). The upper bound $z_{\max}$ in the sum is chosen in a way that each subarea in a $2^{z_{\max}}$-segmentation contains at most one node. If two or more nodes have exactly the same position, the sum goes to infinity. This infinite sum converges for all $w > 1$.

3.2.1.3 Basic Properties of $\psi(z)$

In the following we prove some basic properties of the inhomogeneity measure $\psi(z)$.

Lemma 3.3. *The inhomogeneity $\psi_{(x_o,y_o)}(z)$ never decreases for a refinement of the segmentation, i.e.,*

$$\psi_{(x_o,y_o)}(z') \geq \psi_{(x_o,y_o)}(z) \quad \forall\, z \text{ dividing } z' . \tag{3.30}$$

Proof. If z divides z' there exists a set of subareas A'_j with $j = 1, \ldots, t$ of the z'-segmentation for each A_i being a subarea of the z-segmentation such that $\bigcup_{j=1}^{t} A'_j = A_i$. Let $n'_{j,(x,y)}$ be the number of nodes located in A'_j. For a given A_i we get

$$|n_{i,(x_o,y_o)} - \bar{n}(z)| = \left| \sum_{j=1}^{t} n'_{j,(x,y)} - t\,\bar{n}(z) \right| \leq \sum_{j=1}^{t} |n'_{j,(x,y)} - \bar{n}(z)| \tag{3.31}$$

due to the triangle inequality. □

Lemma 3.4. *Consider a distribution of n nodes. If we refine a segmentation to infinitely small subareas, the inhomogeneity $\psi(z)$ converges to 1, i.e., $\lim_{z\to\infty} \psi(z) = 1$.*

Proof. There exists a z such that in no subarea of the corresponding z-segmentation two nodes with different positions are located. In other words, if there are two or more nodes in the same subarea, they have exactly the same position. Let m_i with $i = 0, \ldots, n$ denote the number of subareas containing i nodes. Then we have

$$\psi(z) = \frac{1}{2n} \left(\sum_{i=1}^{n} m_i \left| \frac{n}{z^2} - i \right| + m_0 \left| \frac{n}{z^2} - 0 \right| \right) . \tag{3.32}$$

We use the fact that $m_0 = z^2 - \sum_{i=1}^{n} m_i$, let $z \to \infty$, and get

$$\lim_{z\to\infty} \psi(z') = \frac{1}{2n} \left(\underbrace{\sum_{i=0}^{n} | - m_i\, i|}_{=n} + n \right) = 1 . \tag{3.33}$$

□

This property shows that the inhomogeneity $\psi(z)$ converges to a fixed value for a sufficiently fine segmentation of the area. This convergence holds independently of the distribution. The speed of convergence depends, however, on the distribution. The inhomogeneity ψ, which is independent of the segmentation, is higher for inhomogeneous distributions. This is due to the larger weights of the first summands.

3.2.1.4 Minimum and Maximum of ψ

In this section, we investigate which distributions minimize and maximize the inhomogeneity measure ψ. This insight is important to interpret a given inhomogeneity value. Obviously, $\psi(z) \geq 0$ holds for all distributions and all z-segmentations.

The inhomogeneity measure should be small for node distributions in which the nodes are *equally scattered* over the entire area. Let us consider the extreme case, which is a grid distribution.

Definition 3.1. A spatial distribution of n nodes is called a *grid distribution* if each subarea of the $\sqrt{n}$-segmentation contains exactly one node. (We require $\sqrt{n} \in \mathbb{N}$.)

In the following we show that a grid distribution leads to the minimum inhomogeneity value, which is 0.

Theorem 3.6. *A grid distribution of 2^i nodes, i even, yields an inhomogeneity $\psi = 0$.*

Proof. We examine a 2^j-segmentation of the area A for $j = 1, 2, \ldots, \frac{i}{2}$. Since each subarea of the $2^{\frac{i}{2}}$-segmentation contains exactly one node and $\bar{n}(2^{\frac{i}{2}}) = 1$, $\psi(2^{\frac{i}{2}}) = 0$.

For the $2^{\frac{i}{2}-1}$-segmentation each subarea therefore contains 4 nodes and the expected number of nodes per subarea is 4. Thus we have again $\psi(2^{\frac{i}{2}-1}) = 0$. If we apply this idea recursively to all $j = \frac{i}{2} - 2, \ldots, 1$ we get $\psi(2^j) = 0$ for all $j = 1, 2, \ldots, \frac{i}{2}$. □

The inhomogeneity value should be large for node distributions in which the nodes are densely located within one subarea, and the remaining subareas are empty. In the extreme case, all nodes are located at the same position.

Theorem 3.7. *If all nodes are located at the same position, the inhomogeneity ψ reaches its maximum.*

Proof. The sum $\sum_{j=1}^{r} w^{1-j}\, \psi(2^j)$ reaches its maximum if and only if all summands are maximized. Therefore, we find the maximum of $\psi(2^j)$ for $j = 1, \ldots, t$. This value is maximal if all n nodes are located inside one common subarea. Since this assumption must hold for arbitrary fine segmentations, the distribution giving the maximum ψ has all n nodes located at the same position. □

Next, we derive the maximum value of ψ. If all n nodes are located in a single subarea, we obtain from Equations (3.26) and (3.27) the inhomogeneity

$$\psi(z) = \frac{1}{2n}\left(\left|n - \frac{n}{z^2}\right| + (z^2 - 1)\left|0 - \frac{n}{z^2}\right|\right) = 1 - \frac{1}{s^2}. \tag{3.34}$$

Substituting Equation (3.34) with $z = 2^j$ into Equation (3.29) yields

$$\psi = \sum_{j=1}^{\infty} w^{1-j}\left(1 - \frac{1}{2^{2j}}\right). \tag{3.35}$$

Since the two series $\sum_{j=1}^{\infty} w^{1-j}$ and $\sum_{j=1}^{\infty} \frac{w^{1-j}}{2^{2j}}$ converge, we may compute their limits separately and get

$$\begin{aligned} \psi &= \sum_{j=1}^{\infty} w^{1-j} - \sum_{j=1}^{\infty} \frac{w^{1-j}}{2^{2j}} \\ &= \frac{w}{w-1} - \frac{w}{4w-1} \\ &= \frac{3w^2}{(w-1)(4w-1)}. \end{aligned} \tag{3.36}$$

To achieve normalized values for ψ, we select the weight w as stipulated by Property 1 in Section 3.2 such that we get

$$0 \le \psi \le 1. \tag{3.37}$$

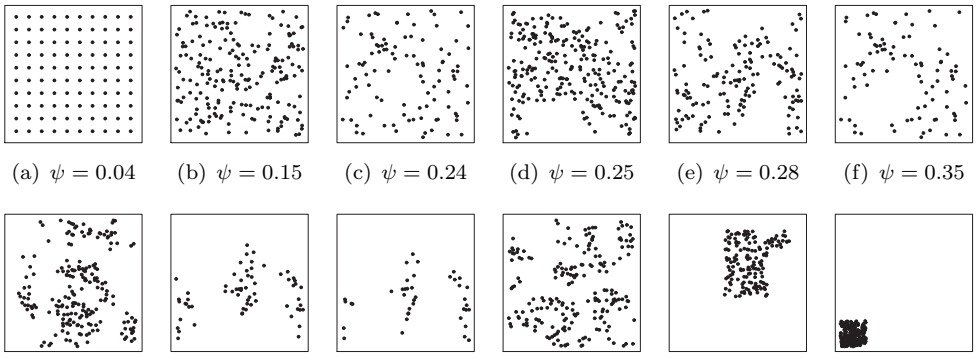

(a) $\psi = 0.04$ (b) $\psi = 0.15$ (c) $\psi = 0.24$ (d) $\psi = 0.25$ (e) $\psi = 0.28$ (f) $\psi = 0.35$

(g) $\psi = 0.35$ (h) $\psi = 0.54$ (i) $\psi = 0.58$ (j) $\psi = 0.63$ (k) $\psi = 0.91$ (l) $\psi = 0.99$

Figure 3.10: Inhomogeneity values for different distributions.

Thus, we set Equation (3.36) equal to 1 and obtain

$$w = \frac{5 + \sqrt{21}}{2} \approx 4.79129\,. \tag{3.38}$$

Note that there is a second solution for w that cannot be used as the sum in Equation (3.35) would diverge.

3.2.1.5 Visualization

Figure 3.10 depicts different distributions and their corresponding inhomogeneity values ψ. Distribution 3.10(a) represents a grid distribution yielding a very low value of $\psi = 0.04$. A random uniform distribution 3.10(b) also gets a low inhomogeneity value of $\psi = 0.15$. By removing some nodes from a uniform distribution as in distributions 3.10(c)–3.10(g) some holes appear, and the inhomogeneity value increases. With even more compacted node clouds as in distributions 3.10(h)–3.10(k) the value of the inhomogeneity becomes even higher. Finally, with a very dense distribution 3.10(l) the inhomogeneity value $\psi = 0.99$ almost reaches its theoretic maximum of $\psi = 1$.

3.2.2 Comparison Between the Measure and Human Perception of Inhomogeneity

We are now interested in the question whether the measure ψ is in line with human's intuition regarding the level of inhomogeneity in a distribution. To investigate this issue, we conducted an online survey, asking researchers and students in Austria and South Korea to compare a set of 100 tuples of distributions with respect to their inhomogeneity. The system presents two pseudo-random distributions and asks the user to select the distribution which he or she finds more uniform, or to choose *similar* if she or he cannot decide. For both distributions the corresponding inhomogeneity measures ψ_1 and ψ_2 are also calculated. The computer bases its *uniformity decision*

on these values. At the end of each survey, the choices of the computer and the user are compared.

3.2.2.1 General Results

The results of a survey with 79 users are as follows. A fraction of 70 % of the tuples are answered *correctly*, i.e., the users classify the distributions in the same manner as the computer. In 18 % of the tuples the users cannot decide although the distributions are different (*undecided*). In the remaining 12 %, the users' classification differs from that of the computer (*incorrect*).

Table 3.1: Answers in the online survey.

Class	0.10	0.20	0.30	0.40	0.50	0.60	0.70
Correct	42%	69%	90%	94%	95%	94%	93%
Undecided	34%	23%	7%	3%	2%	2%	5%
Incorrect	24%	8%	3%	3%	3%	4%	2%

Table 3.1 lists a classification of all answers. The horizontal classes refer to the absolute difference $\psi_\Delta = |\psi_1 - \psi_2|$. The numbers represent the percentage of correct, undecided, and incorrect answers in each class. The values for $\psi_\Delta < 0.1$ show that the decision is difficult for distributions with almost similar inhomogeneity. For $\psi_\Delta > 0.1$, however, the computer's objective decision well matches the human's subjective perception. In fact, 72 % (77 %) of all incorrect (undecided) answers are given to tuples with $\psi_\Delta < 0.1$. In conclusion, the inhomogeneity measure ψ fits well the human perception of inhomogeneity.

3.2.2.2 Perception of Linear Operations

Another goal of the survey is to determine how human perception can cope with wrap-around distance and linear operations applied to distributions. For this purpose, two distributions that are identical but with linear operations applied are presented to the user several times during the survey.

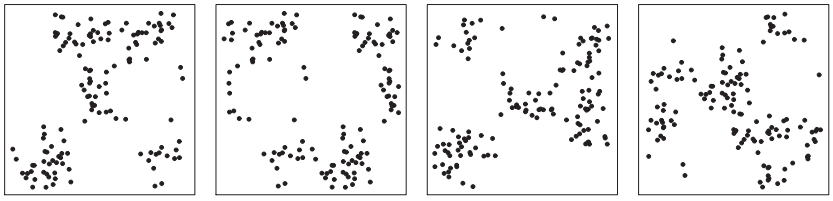

(a) Original (b) Moved (c) Transposed (d) Centered

Figure 3.11: Effect of linear operations on human perception.

An example is given in Figure 3.11. All figures depict the same distribution with $\psi = 0.42$ but with different linear operations applied. Considering the first, left-most distribution as the original, the second one is moved by half the side length

horizontally, the third one is transposed, and the fourth one is moved in such a way that the node with the most dense neighborhood is in the center. These distributions may look different to a human but the distribution is in fact the same, resulting in the same inhomogeneity value.

Table 3.2: Effect of linear operations in online survey.

Linear Operation	Similar Answers (%)
Similar	94%
Exchanged	91%
Mirrored	84%
Moved	81%
Transposed	83%
Centered	80%

Table 3.2 lists the percentage of similarly answered tuples after the linear operation was applied. Results show that presenting the same distributions again and exchanging the left and right image does have some impact on the users' decision (*exchanged*) which can be explained by inattentive users. Applying linear operations, however, results in more distinct differences.

3.3 Related Work for Inhomogeneous Node Distributions

3.3.1 Models for Inhomogeneous Node Distribution

Avidor and Mukherjee [AM01] introduce a model in which *clump centers* are distributed with a homogeneous Poisson process. For each center, a random number of nodes is chosen, and they are distributed uniformly over a disk of a certain radius. This model is also used in [MA05] to study coverage and outage probabilities in hybrid ad hoc networks. A similar approach is employed by Vilzmann *et al.* in [VWAH06] with Gaussian distributed nodes around the clump centers.

Basu and Redi use a similar method to investigate the *energy efficiency* of packet overhearing in sensor networks in [BR04]. Such type of models can be classified as *Poisson cluster processes* [Cre91]. One of their disadvantages is that the stochastic properties are difficult to compute, because the clusters can randomly overlap. In contrast to our model, it is impossible that isolated nodes, i.e., nodes with no neighbors occur in the resulting distribution.

Two alternative models are presented by Liu *et al.* in [LH06]: the first model uses a Gaussian deviation from ideal *grid points*; the second model retrieves a subset of nodes from a Poisson process, selecting those nodes that are closest to grid points. The resulting distributions reflect, however, still the regular shape of the grid points.

Thompson has derived the probability density function of the *distance* to the k^{th} nearest neighbor of a homogeneous Poisson point process in [Tho56]. Haenggi has

derived similar results in [Hae05]. We generalized these results to derive the nearest neighbor distance distribution of our model.

In [BL02] Borschbach *et al.* introduce a *graph theoretical model* for networks based on planar graphs. This model is then used to characterize the connectivity on homogeneous networks. Further, they give a characterization of inhomogeneity based on their model. These graph theoretic models are, however, not well suited when analyzing interference. The reason is that the channel between all pairs of nodes is of interest, no matter if they are connected or not.

Note that in contrast to our work the books [Cre91, SKM95] mainly use the term *thinning* to remove nodes *independently* from other nodes; the resulting node locations are again *uniformly* distributed. An alternative to thinning is the class of doubly stochastic processes — called Cox processes [Cre91, Cox55]. It basically randomizes the intensity λ of a Poisson point process, hence being a generalization of a Poisson point process. In [LS79] Lewis *et al.* apply thinning to simulate inhomogeneous node distributions. The authors also provide a subroutine package that allows the generation and handling of inhomogeneous node distributions, which is, however, not state of the art today.

Further papers address the *impact of the node distribution* on the performance of wireless systems. Baier and Bandelow show in [BB97] that theoretical computations of the capacity based on uniform distributions overestimate the capacity in a real-world scenario. Adrian *et al.* [AHP99] analyze the effects of different non-uniform distributions on CDMA systems. These works show the importance of having inhomogeneous node distribution models at hand when analyzing the performance of communications protocols.

Alfano *et al.* anlayze the *capacity in wireless networks* with inhomogeneously distributed nodes. They derive upper [AGL09b] and lower [AGL09a, AGLM10] bounds for the network capacity with nodes distributed according to a Cox process. The major disadvantage of Cox processes when creating node distributions is that it is necessary to defined a *map* of intensities over the whole area of interest before applying them. When applying our approach it suffices to define the two numbers r and k to prearrange the inhomogeneity of the resulting node distribution.

3.3.2 Measuring Inhomogeneity

Classical approaches in statistics use multiple *hypothesis testing* against a given distribution — e.g. the uniform distribution — to derive statements about the homogeneity or inhomogeneity of given node locations (see, e.g. [Vit74]; [Bak41]). Such hypothesis tests are, e.g. the chi-squared test and the Kolmogorov-Smirnov test. Since the output of a test can only be *yes* or *no*, it does not provide any measure of the inhomogeneity in the sense of a real value between zero and one. Note, that the p-value of the test is inadequate for such purposes.

Johansson describes in [Joh00] how *kurtosis* can be used to measure the homogeneity of any property (e.g. the location of nodes) on a given area. This approach

is, however, not applicable to our scenario as it assumes some knowledge of the given distribution (e.g. the probability density function), which in general we do not know.

Spatial inhomogeneity measures are also needed and applied in *chemistry and physics*. An overview of an aspect of work in that area is given by Piasecki in [Pia08]. For example, Zwicky uses in [Zwi57] an approach similar to Equation (3.27) of our model to measure the inhomogeneity of the distribution of galaxies and star clusters on the night sky. The measure does, however, not consider the offsets introduced in this work and is thus variant to linear operations.

In complex networks, inhomogeneity is sometimes measured by the *clusterization* of the graph, as e.g. by Muff *et al.* in [MRC05]. They define a measure for assessing the quality of the clusterization of a given network. This approach can easily be applied to communication networks, if the connectivity of a pair of nodes is clearly defined. It is, however, not applicable if we want to measure the inhomogeneity of a node set of which no information on connectivity is known.

3.3.3 Mobility Models

The analysis of the spatial node distribution is also of importance if we consider mobile nodes. In particular, the question arises whether a certain mobility model *retains a uniform random node distribution* or not, or whether it changes the distribution. This issue is investigated by Bettstetter *et al.* in [Bet01], where two frequently used random mobility models, namely the random waypoint model [JM96], and the random direction model [Bet01] are analyzed. It is shown that nodes following the random waypoint model are not uniformly distributed but have a higher density in the middle of the simulation area and almost zero density near the borders. Independent of this work, Santi *et al.* come to the same conclusion in [BRS02, RS02]. In summary, these papers show the need for a mobility model that is able to maintain a certain inhomogeneity of nodes over time.

In the article [HLV06], Hyytia *et al.* present a *modified RWP model*. Instead of a uniform distribution of the waypoints over the simulation area, the authors use a two-dimensional probability density. For a given inhomogeneity it is, however, difficult to derive such a density. Furthermore, with this model the cluster positions and shapes are to some extend predetermined. A similar approach is presented by Hsu *et al.* in [HMS+05]. In their approach the destination location depends on the current location and time, which leads to the same drawbacks.

In [GSN05] Gloss *et al.* propose a variation of the RD model, called *RD with Location Dependent Parametrization*. In this model the new direction of each node depends on its current position. The parametrization of the model can be obtained from existing mobility patterns by applying the conversion model, which is also discussed in the paper. Due to the fact that this parametrization is determined before the simulation starts and is not changed afterwards, the cluster positions and shapes are fixed, which can be considered a drawback compared to our model.

In practice entities often visit some locations on a regular basis. To reflect this fact in a mobility model, a time-variant mobility model with *location visiting preferences and periodical re-appearance of nodes* at certain locations is described by Hsu *et al.* in [HSPH07]. Again, the places of periodical re-appearance are predetermined and will not change in the course of the simulation.

A different approach is taken by Siomina in [Sio05], where known mobility models are applied on *inhomogeneous areas*. These areas consist of regions that attract nodes with different strength, leading to areas with higher densities and clusters. The disadvantage of this mobility model is, however, that this *attraction map* is rather static and hence allows no group mobility.

A mobility model to *control the degree of inhomogeneity* is presented by Lim *et al.* in [LYD06]. Here, nodes are distributed on the simulation area in a way that nodes are more likely to be placed into regions that already contain more nodes. During simulation, nodes again tend to move to subareas that are higher populated than to others. The major disadvantage of this approach is that the degree of inhomogeneity cannot be exactly predefined.

Inhomogeneous node distributions are of special interest when modeling *delay tolerant networks*. Here, the network is not always connected, but consists of several disjoint clusters. Some few mobile nodes (so called *message ferries*) store messages and forward them to other clusters. Tan *et al.* in [TBA08] propose a mobility model that reproduces this behavior of nodes. An overview of different types of Markovian mobility models for delay tolerant networks is presented by Dang *et al.* in [DW09]. In contrast to these mobility models, the model presented by Gyarmati *et al.* in [3] explicitly considers the inhomogeneity of the resulting node distribution. This allows to specify a certain target inhomogeneity value that should be roughly kept during the movement of the nodes.

A *comparison of different mobility models* is presented in [MNdM04]. Here, the authors especially regard to border effects and countermeasures therefore, which could by torus areas and bouncing borders. They evaluate mobility models by their similarity to real traces. An overview of different mobility models in sparse ad-hoc networks is presented by Huan *et al.* in [HHL08]. Additionally, a mobility model is proposed in which nodes move as a chain. In [GH09b] Gu and Hong propose a method to classify the mobility of nodes without measuring location nor velocity. Instead, the method relies only on information about the current neighbors of a node and the rate at which they change. The disadvantage of such an approach is that mobility and connectivity are no longer independent of each other.

Chapter 4

Temporal Correlation of Interference

Wireless communication networks usually implement techniques to guarantee or at least increase the likelihood of the delivery of a packet. Such a technique could in the simplest case be a retransmission protocol that sends a packet a second time if the destination does not respond with an acknowledgment packet. In a more sophisticated case, it could be a recent method that exploits temporal and/or spatial diversity as, e.g., cooperative relaying protocols. In this thesis we give an overview of these transmission methods in Section 2.8.

All these methods have one assumption in common: They assume that the channel conditions at the retransmission (or relay transmission in the case of cooperative relaying) are uncorrelated to the channel conditions at the original transmission. If this assumption holds, the success of each transmission is independent of the success of all others. Therefore, the overall transmission success probability is increased. If, however, this assumption does not hold, the gain in performance achieved by these methods is degraded.

The correlation of the channel conditions of two separate transmissions can mainly have two sources: First, the channel state itself can be correlated, which is determined by the channel coherence time (in the case of time diversity) and the spatial divergence of the transmission paths (in the case of spatial diversity) or a combination of them. Most transmission methods are designed to avoid this source of correlation. For example, in MIMO systems, where each device has two or more antennas, the distance between these antennas is chosen to be larger than half the wavelength of the transmitted signal. This guarantees that the channels between all pairs of antennas are uncorrelated, leading to a performance improvement due to the diversity gain.

Second, the interference present at the destination node during both transmissions can be correlated. This source of correlation is often neglected in the design of transmission methods, although it has, depending on the communication

scenario, a huge influence on the overall performance of the network. Only recently fellow researchers started investigating both the temporal and the spatial correlation of interference and its impact on the outage probability of a transmission [GH09a, Hae09, HG09]. In the following we contribute to this research by formally deriving the temporal correlation of the interference, which is the basis for analyzing the performance of state-of-the-art transmission methods from a networking perspective. We thereby extend the work of Haenggi et al. [GH09a] by considering additional sources of the temporal correlation of interference.

Preliminary results have been obtained in cooperation with G. Brandner and C. Bettstetter. They are currently under review in [10].

4.1 Correlation between Interference of Disjoint Node Sets

In this section we derive the correlation between the overall interference caused by two disjoint sets of nodes. This value is needed for the analysis of temporal correlation of interference later. Correlation is measured in terms of Pearson's correlation coefficient

$$\rho(X,Y) := \frac{\operatorname{cov}(X,Y)}{\sqrt{\operatorname{var}(X)}\sqrt{\operatorname{var}(Y)}} \tag{4.1}$$

for arbitrary random variables X and Y.

Let $\mathcal{N}$ be a fixed realization of a Poisson point process with intensity λ and n_1 and n_2 be two probabilities with $n_1 + n_2 \leq 1$. Note that in the following analysis this realization $\mathcal{N}$ is considered to be fixed, i.e. not random. We randomly sample nodes of $\mathcal{N}$ with probability n_1 yielding a set of nodes $\mathcal{N}_1$ with density λn_1. From the set of non-sampled nodes $\mathcal{N} \setminus \mathcal{N}_1$ we randomly sample nodes with probability $\frac{n_2}{1-n_1}$, which we denote by $\mathcal{N}_2$. Let $\mathcal{N}_0$ denote all nodes that have not been sampled, i.e., $\mathcal{N}_0 := \mathcal{N} \setminus (\mathcal{N}_1 \cup \mathcal{N}_2)$. Then, the expected fraction of nodes in $\mathcal{N}_1$ is n_1, in $\mathcal{N}_2$ it is n_2, and in $\mathcal{N}_0$ it is $1 - n_1 - n_2$.

The sets $\mathcal{N}_0$, $\mathcal{N}_1$, and $\mathcal{N}_2$ form a partitioning of $\mathcal{N}$. The following theorems give the correlation between the interference $I(\mathcal{N}_1)$ caused by $\mathcal{N}_1$ and $I(\mathcal{N}_2)$ caused by $\mathcal{N}_2$ as a function of n_1 and n_2. We start with the case for which no fading is present.

Theorem 4.1. *Let $\mathcal{N}$ denote a fixed set of nodes resulting from a Poisson point process with intensity λ. We partition $\mathcal{N}$ into three sets $\mathcal{N}_1$, $\mathcal{N}_2$, and $\mathcal{N}_0$ with densities $n_1\lambda$, $n_2\lambda$, and $(1 - n_1 - n_2)\lambda$, respectively. The correlation coefficient between the interference values $I(\mathcal{N}_1)$ and $I(\mathcal{N}_2)$ under the condition $\mathcal{N}$ without fading is*

$$\rho\left(I(\mathcal{N}_1), I(\mathcal{N}_2) \mid \mathcal{N}\right) = -\sqrt{\frac{n_1 n_2}{(1-n_1)(1-n_2)}}\,. \tag{4.2}$$

Proof. An indicator variable $T_x(\mathcal{N}_\cdot)$ denotes whether a node x is contained in the set $\mathcal{N}_\cdot$ or not, i.e.,

$$T_x(\mathcal{N}_\cdot) \coloneqq \begin{cases} 1 & x \in \mathcal{N}_\cdot \\ 0 & \text{else}\,. \end{cases} \tag{4.3}$$

In the following we use two indicator variables: $T_x \coloneqq T_x(\mathcal{N}_1)$ and $T'_y \coloneqq T_y(\mathcal{N}_2)$. These variables are Bernoulli distributed with variance $n_\cdot(1-n_\cdot)$. The covariance of the two indicator variables is given by

$$\operatorname{cov}(T_x, T'_y) = \begin{cases} \mathbb{E}\left(T_x T'_y\right) - \mathbb{E}\left(T_x\right)\,\mathbb{E}\left(T'_y\right) = 0 - n_1 n_2 & \text{for } x = y, \\ 0 & \text{else.} \end{cases} \tag{4.4}$$

The covariance for given node locations can be expressed as

$$\begin{aligned} \operatorname{cov}\left(I(\mathcal{N}_1), I(\mathcal{N}_2) \,|\, \mathcal{N}\right) &= \operatorname{cov}\left(\sum_{x\in\mathcal{N}} p_t\, l(\|x\|)\, T_x,\, \sum_{y\in\mathcal{N}} p_t\, l(\|y\|)\, T'_y \,\middle|\, \mathcal{N} \right) \\ &= p_t^2 \sum_{x,y\in\mathcal{N}} l(\|x\|)\, l(\|y\|) \operatorname{cov}(T_x, T'_y) \qquad (4.5) \\ &\overset{(4.4)}{=} -p_t^2\, n_1 n_2 \sum_{x\in\mathcal{N}} l^2(\|x\|)\,. \qquad (4.6) \end{aligned}$$

The variance of $I(\mathcal{N}_1)$ is given by

$$\begin{aligned} \operatorname{var}(I(\mathcal{N}_1) \,|\, \mathcal{N}) &= \operatorname{var}\left(\sum_{x\in\mathcal{N}} p_t\, l(\|x\|)\, T_x \,\middle|\, \mathcal{N} \right) \\ &= p_t^2 \sum_{x\in\mathcal{N}} l^2(\|x\|) \operatorname{var}(T_x) \\ &= p_t^2\, n_1(1-n_1) \sum_{x\in\mathcal{N}} l^2(\|x\|) \qquad (4.7) \end{aligned}$$

and similar for $\operatorname{var}(I(\mathcal{N}_2) \,|\, \mathcal{N})$. Therefore, the correlation coefficient can be obtained by dividing Equation (4.6) by the square roots of the variances derived in Equation (4.7) yielding

$$\begin{aligned} \rho\left(I(\mathcal{N}_1), I(\mathcal{N}_2) \,|\, \mathcal{N}\right) &= \frac{-p_t^2\, n_1 n_2 \,\sum_{x\in\mathcal{N}} l^2(\|x\|)}{\sqrt{n_1(1-n_1)}\sqrt{n_2(1-n_2)}\, p_t^2 \,\sum_{x\in\mathcal{N}} l^2(\|x\|)} \\ &= -\sqrt{\frac{n_1 n_2}{(1-n_1)(1-n_2)}}\,, \qquad (4.8) \end{aligned}$$

which is the correlation coefficient conditioned by the set of nodes $\mathcal{N}$. The second equation holds if the sum over all path loss values converges. □

Note that the result of Theorem 4.1 also holds for any fixed, non-empty set of nodes $\mathcal{N}$, which not necessarily has to be the realization of a point process.

The following theorem gives the correlation between the interference values caused by $\mathcal{N}_1$ and $\mathcal{N}_2$ as a function of n_1 and n_2 under the additional assumption that all links are independently affected by Rayleigh fading.

Theorem 4.2. *Let again $\mathcal{N}$ denote a fixed realization of a Poisson point process with intensity λ. We partition $\mathcal{N}$ into the disjoint sets $\mathcal{N}_0$, $\mathcal{N}_1$, and $\mathcal{N}_2$ as defined in Theorem 4.1. If each node experiences Rayleigh fading independent from all other nodes, fading has no influence on the covariance* $\operatorname{cov}(I(\mathcal{N}_1), I(\mathcal{N}_2))$*. It is hence equal to the covariance given in Equation* (4.6)*.*

Proof. We use the same indicator variables T_x and T'_y as defined above. Further, let h_x^2 denote the channel state of node x. Then, the covariance of the indicator variables and channel states is

$$\begin{aligned} \operatorname{cov}(T_x h_x^2, T'_y h_y^2) &= \mathbb{E}(T_x T'_y h_x^2 h_y^2) - \mathbb{E}(T_x h_x^2)\,\mathbb{E}(T'_y h_y^2) \\ &= \begin{cases} \mathbb{E}(T_x T'_x h_x^4) - n_1 n_2 = -n_1 n & \text{for } x = y \\ 0 & \text{else.} \end{cases} \end{aligned} \tag{4.9}$$

Note that the result of this equation is equal to that in Equation (4.4). Hence, substituting Equation (4.9) into Equation (4.5) gives

$$\operatorname{cov}\left(I(\mathcal{N}_1), I(\mathcal{N}_2) \,|\, \mathcal{N}\right) = -p_t^2\, n_1 n_2 \sum_{x \in \mathcal{N}} l^2(\|x\|)\,, \tag{4.10}$$

which proves the theorem. □

Note that, although the covariance is not influenced by fading, the variance in general increases, leading to a smaller correlation coefficient.

4.2 Temporal Correlation of Interference

For a given node, the interference values within two consecutive time slots are, in general, correlated. We consider three causes for this temporal correlation: the nodes' locations, the channel state, and the traffic. For each of these reasons, we distinguish three extremal cases (cf. [Hae09]): the value is *0. fixed* (not random), *1. random and independent*, or *2. random and fully dependent*.

- *The locations of the nodes:* Since the interferers are a subset of a predefined set of nodes, a temporal dependency arises from their fixed locations.

  0. Fixed: The distribution of the nodes is fixed. This implies that the node locations are a condition under which all analysis is performed and does not cause any correlation of the interference at all.

1. *Random and independent:* The positions of the nodes are independently distributed in each time slot and are hence uncorrelated between each pair of slots.
2. *Random and fully dependent:* The node locations are the same for all time slots, but they are not considered as a condition. Hence they are causing a correlation of the interference.

- *The channel state:* The channel state can be independent or dependent in consecutive time slots, depending on the channel coherence time c in relation to the message length s.

  0. *Fixed:* No fading is employed.
  1. *Random and independent:* Rayleigh fading with a channel coherence time equal to the length of 1 time slot is used, i.e. the channel state is independent for each slot.
  2. *Random and fully dependent:* The channel coherence time is $c \geq 2$ time slots, for which the channel state is considered to be the same.

- *The traffic model:* The dependence of the traffic can also introduce a temporal dependence of interference.

  0. *Fixed:* A fixed traffic pattern is used, i.e. in all time slots the set of senders $\mathcal{S}$ stays the same.
  1. *Random and independent:* In each time slot an expected fraction of p nodes is selected to start a new transmission. The length of each transmission is chosen to fit into one slot.
  2. *Random and fully dependent:* Again, in each time slot an expected fraction of p nodes is selected to start a new transmission. The length of each transmission is, however, $s \geq 2$. This approach can be used, e.g. for modeling time diversity, if $s = 2$. Here, in each time slot the expected fraction of senders is ps.

In the following we perform a comprehensive analysis of the temporal correlation of interference, which addresses all possible combinations of the extremal cases described above. Each of the $3^3 = 27$ cases is denoted by a triple of numbers $(i, j, k) \in \{0, 1, 2\}^3$, where i determines the node distribution, j indicates the fading employed, and k determines the traffic pattern. The correlation coefficients $\rho(i, j, k)$ with $(i, j, k) \in \{0, 1, 2\}^3$ are measures of correlation between two consecutive time slots $t - 1$ and t.

In many cases it is useful to subdivide the senders $\mathcal{S}$ of a given pair of slots into three subsets: Nodes sending in both time slots are denoted with $\mathcal{S}_{11}$. Nodes transmitting either only in slot $t - 1$ or only in slot t are denoted with $\mathcal{S}_{10}$ and $\mathcal{S}_{01}$, respectively. The set of nodes $\mathcal{S}_{11}$ can be further subdivided into the set $\mathcal{S}_{11}^*$ containing nodes for which the same transmission is taking place in $t - 1$ and t, and

Table 4.1: Correlation of interference – summary of results.

Locations	Channel	Traffic	Interference	
i	j	k	ρ	Eq.
0	0	0	undefined	
0	0	1	0	(4.11)
0	0	2	$\frac{(s-1)(sp-1)}{s(p(s-1)-1)}$	(4.29)
0	1	0	0	(4.11)
0	1	1	0	(4.11)
0	1	2	$\frac{(s-1)(sp-1)^2}{s(p(s-1)-1)(sp-2)}$	(4.32)
0	2	0	$\frac{c-1}{c}$	(4.40)
0	2	1	$\frac{p(1+p(c-2))}{(2-p)(1+p(c-1))}$	(4.56)
0	2	2	-	(4.69)
1	0, 1, or 2	0, 1, or 2	0	(4.12)
2	0	0	1	(4.15)
2	0	1	p	(4.13)
2	1	0	$1/2$	(4.16)
2	1	1	$p/2$	(4.14)
2	0, 1	2	$\frac{s-1+p/(1-p(s-1))}{\mathbb{E}(h^4)s}$	(4.39)
2	2	0	$\frac{2c-1}{2c}$	(4.41)
2	2	1	$\frac{p}{2}\left(2-\frac{p}{1+p(c-1)}\right)$	(4.44)
2	2	2	-	(4.71)

$\mathcal{S}_{11}^{**}$ containing nodes that finish a transmission in slot $t-1$ and start a new one in slot t. Clearly we have $\mathcal{S}_{11} = \mathcal{S}_{11}^{*} \cup \mathcal{S}_{11}^{**}$. Similarly, the set $\mathcal{S}_{11}$ can be subdivided into the set $\mathcal{S}_{11}'$ containing nodes that have the same channel state in both time slots and the set $\mathcal{S}_{11}''$ containing nodes that have different channel states in the two slots. Let S_{11} denote the fraction of nodes within the set $\mathcal{S}_{11}$ and similar for the other sets. Furthermore, let $I_{11} \coloneqq I(\mathcal{S}_{11})$ denote the interference caused by the nodes in $\mathcal{S}_{11}$ and similar for all other sets.

An overview of all results obtained in the following analysis is presented in Table 4.1. These results have been backed up by simulations, but the results of them are only shown for case $(0, 0, 2)$, Figure 4.1. For all other cases the simulation results are not shown as they would not provide any additional information.

4.2.1 The Non-Random Case $(0, 0, 0)$.

The only case, where no random factor is present is $(0, 0, 0)$. Here, the variance of the interference equals zero since the interference value stays constant over all time slots. Hence, the correlation coefficient $\rho(0, 0, 0)$ is not defined.

4.2.2 The Cases Without Correlation; Cases $(0, 0, 1)$, $(0, 1, 0)$, and $(0, 1, 1)$.

If the node distribution is fixed, correlation can only arise from fading or traffic models. Hence, if $j, k \in \{0, 1\}$ with $j + k > 0$ no source of correlation is present and we have

$$\rho(0, j, k) = 0 \qquad \forall j, k \in \{0, 1\},\ j + k > 0\,. \tag{4.11}$$

4.2.3 The Correlation for Independent Node Distributions; Cases $(1, j, k)$.

All scenarios in which the node distribution of each slot is statistically independent can be jointly analyzed. Here, even if dependencies are present in traffic and fading, due to the new random position of all nodes these dependencies show no effect. Hence, the correlation for all of these cases is 0, i.e.

$$\rho(1, j, k) = 0 \qquad \forall j, k \in \{0, 1, 2\}\,. \tag{4.12}$$

4.2.4 The Correlation Caused by the Node Distribution; Cases $(2, j, k)$ with $j, k \in \{0, 1\}$.

The implications of a correlated node distribution on interference is investigated by Haenggi and Ganti ([GH09a, HG09]), which corresponds to cases $(2, 0, 1)$ and $(2, 1, 1)$ in our notation. Results (Corollary 2 in [GH09a]) state that

$$\rho(2, 0, 1) = p \quad \text{and} \tag{4.13}$$

$$\rho(2, 1, 1) = \frac{p}{2}\,. \tag{4.14}$$

These results can be further applied to the following cases: In case $(2, 0, 0)$ in each time slot the same nodes transmit. Therefore, we can neglect all other nodes that never transmit, leading to the same situation as in case $(2, 0, 1)$ with sending probability $p = 1$, i.e.

$$\rho(2, 0, 0) = 1\,. \tag{4.15}$$

Similarly, case $(2, 1, 0)$ can be derived from $(2, 1, 1)$ by setting $p = 1$, leading to

$$\rho(2, 1, 0) = \frac{1}{2}\,. \tag{4.16}$$

4.2.5 The Correlation Caused by the Traffic; Cases $(0, 0, 2)$ and $(0, 1, 2)$.

In the following we analyze the correlation of interference caused by transmissions that are longer than one slot. We start by calculating the fractions of nodes that are in the sets $\mathcal{S}_{10}$, $\mathcal{S}_{01}$, and $\mathcal{S}_{11}$ as introduced in the beginning of this section.

Lemma 4.1. *The expected fraction of nodes in $\mathcal{S}_{11}$ is given by*

$$\mathbb{E}\left(S_{11}\right) = p(s-1) + \frac{p^2}{1-p(s-1)}\,, \tag{4.17}$$

and the expected fraction of nodes in the other two sets is

$$\mathbb{E}\left(S_{10}\right) = \mathbb{E}\left(S_{01}\right) = p - \frac{p^2}{1-p(s-1)}\,. \tag{4.18}$$

Proof. The set $\mathcal{S}_{11}$ can be further subdivided into the sets $\mathcal{S}_{11}^{*}$ and $\mathcal{S}_{11}^{**}$. The nodes in $\mathcal{S}_{11}^{*}$ start a transmission in one of the slots $t-1$, $t-2$,..., $t-(s-1)$. Hence we have $\mathbb{E}(S_{11}^{*}) = p(t-1)$. The nodes in $\mathcal{S}_{11}^{**}$ start a transmission in slot $t-s$. These transmission ends in slot $t-1$. In slot t a fraction p of all nodes is starting a new transmission. Since a fraction of $(s-1)p$ nodes is already transmitting, the nodes starting a new transmission are selected from the other nodes. Thus, each of them is starting a new transmission in slot t with probability $\frac{p}{1-p(s-1)}$. Therefore, we have $\mathbb{E}(S_{11}^{**}) = \frac{p^2}{1-p(s-1)}$. The sum $\mathbb{E}(S_{11}^{*}) + \mathbb{E}(S_{11}^{**})$ gives the first result.

In each time slot a fraction of p is starting a transmission. To calculate $\mathbb{E}(S_{01})$ we have to subtract all nodes that have also sent in $t-1$, which are $\mathbb{E}(S_{11}^{**})$, from p leading to the second result. □

4.2.5.1 Fixed Channel

In case $(0, 0, 2)$ the state of the channel is fixed, i.e., no fading is applied. When computing the correlation coefficient we first have to determine the corresponding covariance and variances.

Lemma 4.2. *The expected value of the variance parameterized by the nodes' locations is given by*

$$\mathbb{E}\big(\mathrm{var}(I(\mathcal{S}) \mid \mathcal{N})\big) = p_t^2\, \mathbb{E}\left(\sum_{x \in \mathcal{N}} l^2(\|x\|)\right)\, sp(1-sp)\,. \tag{4.19}$$

Proof. Let $T_x(\mathcal{S})$ denote the indicator variable that node $x \in \mathcal{S}$. Hence, $T_x(\mathcal{S})$ is Bernoulli distributed and its variance is $\mathrm{var}(T_x) = \mathbb{E}(S)(1-\mathbb{E}(S))$. The expected

variance of $I(\mathcal{S})$ for fixed node locations $\mathcal{N}$ is given by

$$\begin{aligned}
\mathbb{E}\big(\mathrm{var}(I(\mathcal{S}) \,|\, \mathcal{N})\big) &= \mathbb{E}\left(\mathrm{var}\left(\sum_{x\in\mathcal{N}} p_t\, l(\|x\|)\, T_x(\mathcal{S})\right)\right) \\
&= p_t^2\, \mathbb{E}\left(\sum_{x\in\mathcal{N}} l^2(\|x\|)\, \mathrm{var}\big(T_x(\mathcal{S})\big)\right) \qquad (4.20) \\
&= p_t^2\, \mathbb{E}\left(\sum_{x\in\mathcal{N}} l^2(\|x\|)\, \mathbb{E}(S)(1-\mathbb{E}(S))\right) \\
&= p_t^2\, \mathbb{E}\left(\sum_{x\in\mathcal{N}} l^2(\|x\|)\right) sp(1-sp)\,. \qquad (4.21)
\end{aligned}$$

Note that the second equality holds since p_t and $l(\|x\|)$ are constants regarding the variance operator. □

Lemma 4.3. *The expected value of the covariance parameterized by the nodes' locations is given by*

$$\mathbb{E}\big(\mathrm{cov}(I_{11}+I_{10}, I_{11}+I_{01} \,|\, \mathcal{N})\big) = p_t^2\, \mathbb{E}\left(\sum_{x\in\mathcal{N}} l^2(\|x\|)\right) \frac{p(s-1)(1-sp)^2}{1-p(s-1)}\,. \qquad (4.22)$$

Proof. The covariance can be decomposed by

$$\begin{aligned}
\mathbb{E}\left(\mathrm{cov}(I_{11}+I_{10}, I_{11}+I_{01} \,|\, \mathcal{N})\right) &= \mathbb{E}\left(\mathrm{var}(I_{11} \,|\, \mathcal{N})\right) + 2\,\mathbb{E}\left(\mathrm{cov}(I_{11}, I_{10} \,|\, \mathcal{N})\right) \\
&\quad + \mathbb{E}\left(\mathrm{cov}(I_{10}, I_{01} \,|\, \mathcal{N})\right)\,. \qquad (4.23)
\end{aligned}$$

The covariances in this expression can be computed by rearranging Equation (4.1) to

$$\mathbb{E}\left(\mathrm{cov}(I_{10}, I_{01} \,|\, \mathcal{N})\right) = \rho(I_{10}, I_{01} \,|\, \mathcal{N}) \sqrt{\mathbb{E}\left(\mathrm{var}(I_{10} \,|\, \mathcal{N})\right)} \sqrt{\mathbb{E}\left(\mathrm{var}(I_{01} \,|\, \mathcal{N})\right)} \qquad (4.24)$$

and similar for $\mathbb{E}\left(\mathrm{cov}(I_{11}, I_{10} \,|\, \mathcal{N})\right)$.

Next, we compute all variances and correlations needed in the expressions above. We apply Theorem 4.1 to determine the correlation coefficients

$$\rho(I_{10}, I_{01} \,|\, \mathcal{N}) = -\frac{p(sp-1)}{sp(p-1)+1}\,, \qquad (4.25)$$

$$\rho(I_{10}, I_{11} \,|\, \mathcal{N}) = -\sqrt{\frac{p^2(1-s+ps(s-2))}{(p(s-2)-1)(ps(p-1)+1)}}\,. \qquad (4.26)$$

The variances can be computed by substituting the fraction of nodes derived in Lemma 4.1 into Equation (4.20) yielding

$$\mathbb{E}\big(\mathrm{var}\left(I_{11} \,|\, \mathcal{N}\right)\big) = p_t^2\, \mathbb{E}\left(\sum_{x\in\mathcal{N}} l^2(\|x\|)\right) \frac{p(sp-1)(sp-2p-1)(s^2p-2sp-s+1)}{(p(s-1)-1)^2}\,, \qquad (4.27)$$

$$\mathbb{E}\big(\mathrm{var}\left(I_{10} \mid \mathcal{N}\right)\big) = p_t^2\, \mathbb{E}\left(\sum_{x\in\mathcal{N}} l^2(\|x\|)\right) \frac{p(sp-1)(sp^2-sp+1)}{(p(s-1)-1)^2} \tag{4.28}$$

and equal for $\mathbb{E}\big(\mathrm{var}(I(\mathcal{S}_{10}) \mid \mathcal{N})\big)$. Substituting Equations (4.25), (4.26), (4.27), and (4.28) into Equation (4.24) and further into Equation (4.23) yields the result. □

Theorem 4.3. *The correlation coefficient for case* $(0,0,2)$ *is given by*

$$\rho(0,0,2) = \frac{(s-1)(1-sp)}{s\,(1-p(s-1))}\,. \tag{4.29}$$

Proof. By dividing Equation (4.22) by Equation (4.19) we get the result. □

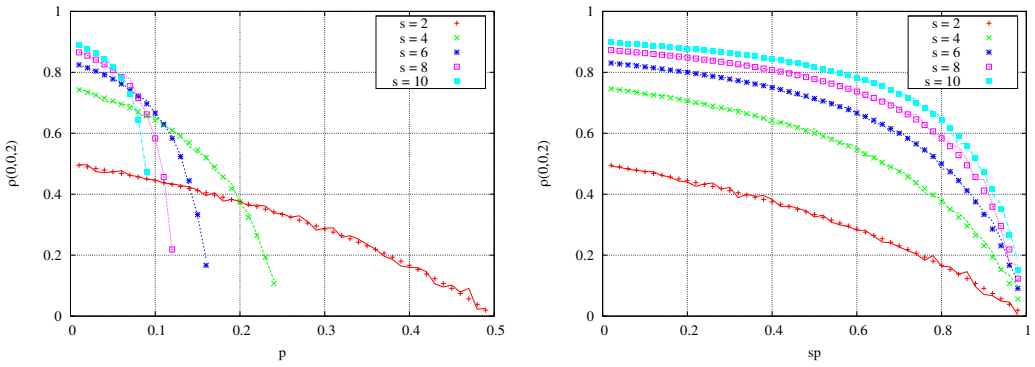

(a) Plot of $\rho(0,0,2)$ over p.

(b) Plot of $\rho(0,0,2)$ over sp.

Figure 4.1: Interference correlation in case $(0,0,2)$.

A plot of $\rho(0,0,2)$ for different values of p and s is presented in Figure 4.1. For the simulation results we applied $\alpha = 3$, $\lambda = 10^{-4}$, and $p_t = 1$ mW. For a fixed message length the correlation coefficient is decreasing with an increasing number of concurrent transmissions. As can be seen in Figure 4.1(a), this effect is stronger for larger values of s since a higher percentage of nodes is transmitting. This is due to the fact that for high values of p almost all nodes are transmitting. Therefore, each node is either inside $\mathcal{S}_{10}$ or inside $\mathcal{S}_{11}$, while nodes are interchanging between these sets. This causes a high anti-correlation $\rho(\mathcal{S}_{10}, \mathcal{S}_{11})$ and hence an overall correlation coefficient $\rho(0,0,2)$ that decreases with p. Note that the curves end at $ps = 1$. Figure 4.1(b) shows the correlation coefficient $\rho(0,0,2)$ over the expected fraction of nodes transmitting in each slot ps. For fixed p the correlation increases with s. This behavior is due to the fact that s is an indicator for the fraction of nodes sending in both time slots $t-1$ and t, which are the cause of the correlation. For large values of s the correlation coefficient increases further and approaches one in the limit, i.e., $\lim_{s\to\infty} \rho(0,0,2) = 1$. Note that while computing the limit we have to keep sp constant. The special case $s = 1$ is similar to case $(0,0,1)$ for which the correlation coefficient is equal to zero.

4.2.5.2 Random Independent Channel

In case $(0, 1, 2)$ independent Rayleigh fading is applied. From Theorem 4.2 it follows that the covariance $\mathrm{cov}(I_{11}+I_{10}, I_{11}+I_{01})$ stays unchanged compared to case $(0, 0, 2)$. Thus, we only have to derive the overall variance of interference $\mathrm{var}(I(\mathcal{N}_s))$.

Lemma 4.4. *The expected value of the variance parameterized by the nodes' locations is given by*

$$\mathbb{E}\big(\mathrm{var}(I(\mathcal{S}) \mid \mathcal{N})\big) = p_t^2\, \mathbb{E}\left(\sum_{x\in\mathcal{N}} l^2(\|x\|)\right) sp(2-sp)\,. \tag{4.30}$$

Proof. The variance of the Bernoulli variable $T_x(\mathcal{S})$ together with the channel state h_x^2 is

$$\begin{aligned} \mathrm{var}\big(h_x^2 T_x(\mathcal{S})\big) &= \mathbb{E}\big(h_x^4 T_x^2(\mathcal{S})\big) - \mathbb{E}\big(h_x^2 T_x(\mathcal{S})\big)^2 \\ &= 2sp - (sp)^2 \end{aligned} \tag{4.31}$$

for a node $x \in \mathcal{N}$. By substituting this variance into Equation (4.20) we get the result. □

Theorem 4.4. *The correlation coefficient for case* $(0, 1, 2)$ *is given by*

$$\rho(0,1,2) = \frac{(s-1)(1-sp)^2}{s\,(1-p(s-1))\,(2-sp)}\,. \tag{4.32}$$

Proof. By dividing Equation (4.22) by Equation (4.30) we get the result. □

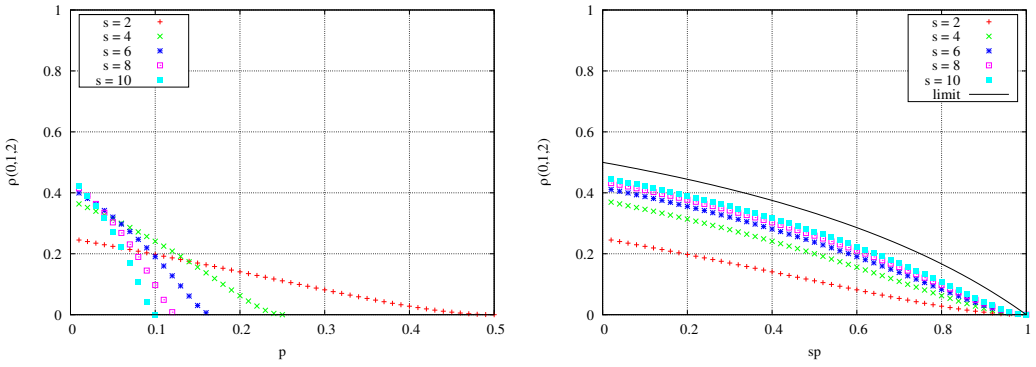

(a) Plot of $\rho(0, 1, 2)$ over p.

(b) Plot of $\rho(0, 1, 2)$ over sp.

Figure 4.2: Interference correlation in case $(0, 1, 2)$.

A plot of the correlation coefficient $\rho(0, 1, 2)$ can be found in Figure 4.2. The trends in this plot are similar to the trends in Figure 4.1. The variance is approximately doubled and hence the correlation is approximately halved compared to case

$(0,0,2)$. The discrepancies between $\rho(0,1,2)$ and $\frac{\rho(0,0,2)}{2}$ are due to the fact that fading does not exactly double the variance, as can be observed when comparing Equations (4.19) and (4.30). Figure 4.2(b) shows the correlation coefficient $\rho(0,1,2)$ over *sp*. Similar to Figure 4.1(b) we can see that the correlation is in general higher for higher values of s when maintaining the fraction of sending nodes *sp* constant. When considering the extremal case we have a similar situation as for case $(0,0,2)$. For $s = 1$ we have the same situation as in case $(0,1,1)$ and hence no correlation. If we consider very large values of s the correlation increases further and in the limit approaches $\lim_{s\to\infty} \rho(0,1,2) = \frac{p-1}{p-2}$. This limiting function is also depicted in Figure 4.2(b). Note that when computing the limit we leave *sp* constant which implies that p approaches zero.

4.2.6 The Correlation Caused by Node Distribution and Traffic; Cases $(2,j,2)$, $j = 0,1$

First, we partition the sending nodes of each slot into the sets $\mathcal{S}_{11}$, $\mathcal{S}_{10}$, and $\mathcal{S}_{01}$ as introduced at the beginning of Section 4.2. The expected fractions of nodes inside these sets are the same as in cases $(0,0,2)$ and $(0,1,2)$ and have already been derived in Lemma 4.1.

Lemma 4.5. *The variance of interference is given by*

$$\operatorname{var}(I(\mathcal{S})) = \mathbb{E}\left(h^4\right)\, p_t^2\, sp\lambda \int_{\mathbb{R}^2} l^2(\|x\|)\,\mathrm{d}x\,, \tag{4.33}$$

with $\mathbb{E}(h^4) = 2$ *for Rayleigh fading and* $\mathbb{E}(h^4) = 1$ *if no fading is present.*

Proof. The following derivation is similar to that in [GH09a]. We start with deriving the second moment $\mathbb{E}(I^2(\mathcal{S}))$ of the interference by

$$\begin{aligned}
\mathbb{E}\left(I^2(\mathcal{S})\right) &= \mathbb{E}\left(\left(\sum_{x\in\mathcal{S}} p_t\, l(\|x\|)\, h_x^2\right)^2\right) \\
&= \mathbb{E}\left(\sum_{x\in\mathcal{S}} p_t^2\, l^2(\|x\|)\, h_x^4\right) + \mathbb{E}\left(\sum_{\substack{x,y\in\mathcal{S}\\ x\neq y}} p_t^2\, l(\|x\|)\, l(\|y\|)\, h_x^2 h_y^2\right) \\
&= \mathbb{E}\left(h^4\right)\, p_t^2\, sp\lambda \int_{\mathbb{R}^2} l^2(\|x\|)\,\mathrm{d}x + \left(p_t\, sp\lambda \int_{\mathbb{R}^2} l(\|x\|)\,\mathrm{d}x\right)^2 . \qquad (4.34)
\end{aligned}$$

Note that the last equality holds due to Campbell's theorem (see Chapter 10.2 in [PP02] or Chapter 6 in [DVJ03]). Using the theorem of Steiner, the variance is

$$\begin{aligned}
\operatorname{var}\big(I(\mathcal{S})\big) &= \mathbb{E}\left(I^2(\mathcal{S})\right) - \left(\mathbb{E}\left(I(\mathcal{S})\right)\right)^2 \\
&= \mathbb{E}\left(h^4\right)\, p_t^2\, sp\lambda \int_{\mathbb{R}^2} l^2(\|x\|)\,\mathrm{d}x\,. \qquad (4.35)
\end{aligned}$$

Note that $\mathbb{E}(h^4) = 2$ for Rayleigh fading and $\mathbb{E}(h^4) = 1$ if no fading is present. □

Next, we derive the covariance of the interferences in the time slots $t-1$ and t.

Lemma 4.6. *The covariance of interference is given by*

$$\operatorname{cov}\left(I_{11}+I_{10}, I_{11}+I_{01}\right) = p_t^2\left((s-1)p + \frac{p^2}{1-(s-1)p}\right)\lambda\int_{\mathbb{R}^2} l^2(\|x\|)\,\mathrm{d}x\,. \quad (4.36)$$

Proof. The second moment of the interference values in the time slots $(t-1)$ and t is

$$\begin{aligned}
&\mathbb{E}\big(\,(I_{11}+I_{10})\,(I_{11}+I_{01})\,\big) = \\
&= \mathbb{E}\Bigg(\sum_{x\in\mathcal{S}_{11}\cup\mathcal{S}_{10}} p_t\, l(\|x\|)\, h_x^2 \sum_{y\in\mathcal{S}_{11}\cup\mathcal{S}_{01}} p_t\, l(\|y\|)\, h_y^2\Bigg) \\
&= \mathbb{E}\Bigg(\sum_{x\in\mathcal{S}_{11}} p_t^2\, l^2(\|x\|)\, h_x^4\Bigg) + \mathbb{E}\Bigg(\sum_{\substack{x\in\mathcal{S}_{11}\cup\mathcal{S}_{10}\\ y\in\mathcal{S}_{11}\cup\mathcal{S}_{01}\\ x\neq y}} p_t^2\, l(\|x\|)\, l(\|y\|)\, h_x^2 h_y^2\Bigg) \\
&= p_t^2\left(p(s-1) + \frac{p^2}{1-p(s-1)}\right)\lambda\int_{\mathbb{R}^2} l^2(\|x\|)\,\mathrm{d}x \\
&\quad + \left(p_t s\, p\lambda\int_{\mathbb{R}^2} l(\|x\|)\,\mathrm{d}x\right)^2 . \qquad (4.37)
\end{aligned}$$

Furthermore, it follows from Equation (2.41) that

$$\mathbb{E}\big(I_{11}+I_{10}\big) = \mathbb{E}\big(I_{11}+I_{01}\big) = p_t sp\lambda\int_{\mathbb{R}^2} l(\|x\|)\,\mathrm{d}x\,. \quad (4.38)$$

Combining these two expressions yields the result. □

Theorem 4.5. *The correlation coefficient for cases* $(2,j,2)$ *with* $j=0,1$ *is given by*

$$\rho(2,j,2) = \frac{s-1+\frac{p}{1-p(s-1)}}{s\,\mathbb{E}(h^4)} \quad \text{for } j=0,1 \quad (4.39)$$

with $\mathbb{E}(h^4)=1$ *for nonfading channels* ($j=0$) *and* $\mathbb{E}(h^4)=2$ *for Rayleigh fading* ($j=1$).

Proof. Dividing Equation (4.36) by Equation (4.33) yields the result. □

A plot of the correlation coefficient $\rho(2,0,2)$ can be found in Figure 4.3. As can be seen, the correlation coefficient is higher for larger values of p and s. The curves can be roughly interpreted as a blend of cases $(0,0,2)$ and $(2,0,1)$ in the following way: The values of the correlation for p being almost zero are similar to case $(0,0,2)$, since $\rho(2,0,1)$ is equal to the fraction of sending nodes, i.e. equal to sp, and hence almost zero. When increasing the value of p the correlation caused by the traffic is decreasing but the correlation caused by the node positions is increasing linearly with sp. Ultimately, when sp approaches one the curves in Figure 4.3 are approximating

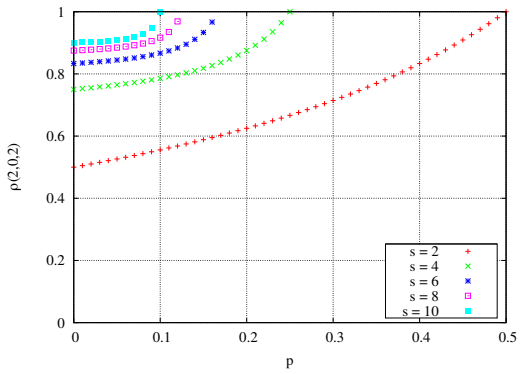

Figure 4.3: Interference correlation in case $(2, 0, 2)$.

the linear function sp. In the limiting case when s gets very high and for constant sp, the correlation coefficient approaches one, i.e. $\lim_{s\to\infty} \rho(2, 0, 2) = 1$.

When Rayleigh fading is considered, the variance is doubled as can be observed in Equation (4.33). Hence, the correlation coefficient is halved, i.e. $\rho(2, 1, 2) = \frac{\rho(2,0,2)}{2}$. The limit for $s \to \infty$ is also halved, i.e. $\lim_{s\to\infty} \rho(2, 1, 2) = \frac{1}{2}$. Therefore, a plot of $\rho(2, 1, 2)$ is omitted.

4.2.7 The Correlation Caused by Fading; Cases $(0, 2, 0)$, $(2, 2, 0)$.

In case $(0, 2, 0)$ the sending nodes are preselected and do not change. Therefore, the channel states of each node change after c slots. These changes are independent for each node, i.e., not synchronized.

Theorem 4.6. *The correlation coefficient for case* $(0, 2, 0)$ *is given by*

$$\rho(0, 2, 0) = \frac{c - 1}{c} \,. \tag{4.40}$$

Proof. In case $(0, 2, 0)$, the sending nodes are preselected and do not change. In each pair of slots, the expected fraction of nodes changing their channel state is $\frac{1}{c}$. The interference of these nodes is uncorrelated. The interference correlation of all other nodes, which perceive the same channel state in both slots, is 1. Hence, the overall correlation is $1 - \frac{1}{c}$. □

In case $(2, 2, 0)$ the correlation caused by the nodes' locations is also considered.

Theorem 4.7. *The correlation coefficient for case* $(2, 2, 0)$ *is given by*

$$\rho(2, 2, 0) = \frac{2c - 1}{2c} \,. \tag{4.41}$$

Proof. In each pair of slots, the expected fraction of nodes changing their channel state is $\frac{1}{c}$. The interference correlation of these senders is $\frac{1}{2}$, similar to case $(2,1,0)$. The interference correlation of nodes with the same channel state is 1, as derived for case $(2,0,0)$. Thus, the overall interference correlation is a weighted sum of these two cases leading to $\frac{1}{2c} + (1 - \frac{1}{c})$. □

4.2.8 The Correlation Caused by Fading Under Random Traffic; Cases $(2,2,1)$, $(0,2,1)$.

In the following we analyze the effect of fading on the interference correlation under the assumption of random traffic. We subdivide the nodes $\mathcal{S}_{11}$ transmitting in both subsequent time slots into two sets: the set $\mathcal{S}'_{11}$ contains all nodes having the same channel conditions in both slots whereas the set $\mathcal{S}''_{11}$ contains all nodes have different channel conditions. Let p_c denote the fraction of nodes of $\mathcal{S}_{11}$ that are within $\mathcal{S}'_{11}$.

Lemma 4.7. *The expected fraction $\mathbb{E}(p_c)$ of nodes of $\mathcal{S}_{11}$ that are within the set $\mathcal{S}'_{11}$ is*

$$\mathbb{E}\left(p_c\right) = 1 - \frac{p}{1 + (c-1)p}\,. \tag{4.42}$$

Proof. In the following we describe the model for the behavior of the channel in more detail. Let $c_j = 0, \ldots, c$ denote the number of ticks the channel stays unchanged after the beginning of slot j for a given interferer. When the node starts sending the first time in slot j, $c_j = c$. In each of the following slots this number is reduced by 1 until it reaches 1, i.e. $c_{j+k} = c - k$ for $k = 1, \ldots, c-1$. This reduction is performed independently of whether the node transmits or not. If the node directly starts a new transmission within time slot $j + c$, we have $c_{j+c} = c$ and thus the value 0 does not occur. Otherwise, $c_{j+c} = c_{j+c+1} = \cdots = 0$ until the node starts its next transmission.

With this model the channel state changes after the slot $t - 1$ if and only if $c_{t-1} = 1$. Therefore, we have to derive the probability $\mathbb{E}(p_c) = 1 - \mathbb{P}(c_{t-1} = 1)$. This can be achieved by combining the following three facts:

1. The sum of the probabilities of all possible values for c_{t-1} gives 1, i.e. $\sum_{i=0}^{c} \mathbb{P}(c_{t-1} = i) = 1$;
2. If c_j has the value c, it afterwards also takes the values $c-1, \ldots, 1$, i.e. $\mathbb{P}(c_{t-1} = i) = \mathbb{P}(c_{t-1} = i+1)$ for all $i = 1, \ldots, c-1$; and
3. In order for c_{t-1} to take the value c, it has to have one of the values 0 or 1 one time slot before and the node under consideration has to transmit, i.e. $\mathbb{P}(c_{t-1} = c) = p\big(\mathbb{P}(c_{t-2} = 0) + \mathbb{P}(c_{t-2} = 1)\big)$.

By combining these three properties we can obtain

$$\mathbb{P}(c_{t-1} = 1) = \frac{p}{1 + (c-1)p}\,. \tag{4.43}$$

□

4.2.8.1 Random Node Locations

Case $(2, 2, 1)$ can be interpreted as a combination of cases $(2, 0, 1)$ and $(2, 1, 1)$.

Theorem 4.8. *The correlation coefficient for case* $(2, 2, 1)$ *is given by*

$$\rho(2, 2, 1) = \frac{p}{2}\left(2 - \frac{p}{1 + (c-1)p}\right) . \tag{4.44}$$

Proof. The nodes in $\mathcal{S}'_{11}$ cause a correlation of p similar to case $(2, 0, 1)$; the others cause a correlation of $\frac{p}{2}$ similar to case $(2, 1, 1)$. Thus, the correlation is

$$\rho(2, 2, 1) = \mathbb{E}(p_c)\, p + \big(1 - \mathbb{E}(p_c)\big)\frac{p}{2} . \tag{4.45}$$

By substituting Equation (4.42) into Equation (4.45) we get the result. □

A plot of the correlation for case $(2, 2, 1)$ for different values of c and p can be seen in Figure 4.4. For large values of c the correlation coefficient approaches p whereas for small c the correlation coefficient is smaller. This is due to the fact that if the channel coherence time c is very long the channel stays constant over a high number of transmissions. Thus, we have a very similar situation as in case $(2, 0, 1)$ where no fading is present and the channel stays constant all the time. Therefore, with increasing channel coherence time we approach $\rho(2, 0, 1) = p$. In mathematical terms we have $\lim_{c\to\infty} \rho(2, 2, 1) = p$, as depicted in Figure 4.4.

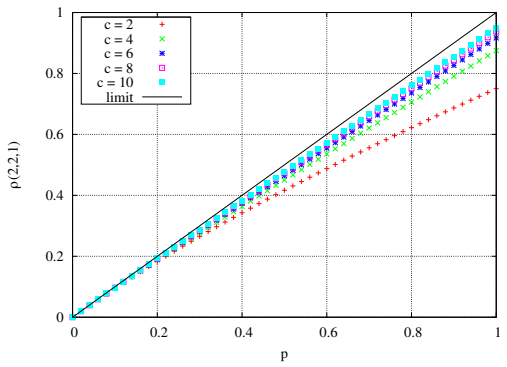

Figure 4.4: Interference correlation in case $(2, 2, 1)$.

4.2.8.2 Nonrandom Node Locations

For case $(0, 2, 1)$ we partition the transmitting nodes of the slots $t - 1$ and t into subsets as presented at the beginning of Section 4.2. Since in each time slot each node transmits with probability p, it is clear that $\mathbb{E}(S_{11}) = p^2$ and $\mathbb{E}(S_{10}) = \mathbb{E}(S_{01}) = p - p^2$. Let p_c denote the fraction of nodes of $\mathcal{S}_{11}$ that have the same channel

conditions within both time slots. Then the nodes in $\mathcal{S}_{11}$ split into two subsets of size $\mathbb{E}(S'_{11}) = p^2\mathbb{E}(p_c)$ and $\mathbb{E}(S''_{11}) = p^2(1 - \mathbb{E}(p_c))$. The value of $\mathbb{E}(p_c)$ has already been derived in Lemma 4.7.

Since in case $(0, 2, 1)$ we do not consider the node distribution to be random, the interference power of a node $x \in \mathcal{N}$ is $I(x) = p_t\, l(\|x\|)T_x(S_{..})$. Here, $l(\|x\|)$ is constant and $T_x(S_{..})$ denotes an indicator variable for $S_{..}$ being one of $\mathcal{S}_{10}$, $\mathcal{S}_{01}$, $\mathcal{S}^*_{11}$, and $\mathcal{S}^{**}_{11}$.

Lemma 4.8. *The expected variance of interference for given node locations is given by*

$$\mathbb{E}\big(\mathrm{var}(I(\mathcal{N}_s) \mid \mathcal{N})\big) = p_t^2\, \mathbb{E}\left(\sum_{x\in\mathcal{N}} l^2(\|x\|)\right) p(2-p)\,. \tag{4.46}$$

Proof. The variance can be obtained by substituting $s = 1$ into Equation (4.30). □

Lemma 4.9. *The expected covariance of interference for given node locations is*

$$\begin{aligned}\mathbb{E}\big(\mathrm{cov}(I'_{11} + I''_{11} + I_{10}, I'_{11} + I''_{11} + I_{01} \mid \mathcal{N})\big) &= \\ = \quad p_t^2\, \mathbb{E}\left(\sum_{x\in\mathcal{N}} l^2(\|x\|)\right) &\frac{p^2(1 + p(c-2))}{1 + p(c-1)}\,.\end{aligned} \tag{4.47}$$

Proof. The overall covariance can be split into

$$\begin{aligned}&\mathbb{E}\big(\mathrm{cov}(I'_{11} + I''_{11} + I_{10}, I'_{11} + I''_{11} + I_{01} \mid \mathcal{N})\big) = \\ &= \ \mathbb{E}\big(\mathrm{var}(I'_{11} \mid \mathcal{N})\big) + 2\,\mathbb{E}\big(\mathrm{cov}(I'_{11}, I''_{11} \mid \mathcal{N})\big) + \mathbb{E}\big(\mathrm{var}(I''_{11} \mid \mathcal{N})\big) \\ &\quad + 2\,\mathbb{E}\big(\mathrm{cov}(I'_{11}, I_{10} \mid \mathcal{N})\big) + 2\,\mathbb{E}\big(\mathrm{cov}(I''_{11}, I_{10} \mid \mathcal{N})\big) + \mathbb{E}\big(\mathrm{cov}(I_{10}, I_{01} \mid \mathcal{N})\big).\end{aligned} \tag{4.48}$$

The covariances can be calculated by applying Equation (4.24). Note that the variances substituted into this formula have to be calculated without considering fading, since fading does not change the covariances, as shown in Theorem 4.2. The correlations needed in Equation (4.24) are derived by applying Theorem 4.1 with the fractions $\mathbb{E}(S'_{11}) = p^2 p_c$, $\mathbb{E}(S''_{11}) = p^2(1 - p_c)$, and $\mathbb{E}(S_{10}) = \mathbb{E}(S_{01}) = p - p^2$ yielding

$$\mathrm{cor}(\mathcal{S}^*_{11}, \mathcal{S}^{**}_{11} \mid \mathcal{N}) = -\sqrt{\frac{p^4 p_c(1-p_c)}{p^4 p_c(1-p_c) - p^2 p_c}}\,, \tag{4.49}$$

$$\mathrm{cor}(\mathcal{S}^*_{11}, \mathcal{S}_{10} \mid \mathcal{N}) = -\sqrt{\frac{p^3(1-p)p_c}{p^2 - p + 1 - p_c(p^4 - p^3 - p^2)}}\,, \tag{4.50}$$

$$\mathrm{cor}(\mathcal{S}^{**}_{11}, \mathcal{S}_{10} \mid \mathcal{N}) = -\sqrt{\frac{p^3(1-p)(1-p_c)}{-p^4 + p^3 - p + 1 - p_c(p^4 - p^3 - p^2)}}\,, \tag{4.51}$$

$$\mathrm{cor}(\mathcal{S}_{10}, \mathcal{S}_{01} \mid \mathcal{N}) = -\frac{p(1-p)}{p^2 - p + 1}\,. \tag{4.52}$$

The expected variances for given node locations can be derived by substituting the values of $\mathbb{E}(S_{11}^{**})$, $\mathbb{E}(S_{10})$, and $\mathbb{E}(S_{01})$ into Equation (4.20), and substituting $\mathbb{E}(S_{11}^{*})$ with Equation (4.31) into Equation (4.20), yielding

$$\mathbb{E}\big(\mathrm{var}(I'_{11}\,|\,\mathcal{N})\big) = p_t^2\,\mathbb{E}\left(\sum_{x\in\mathcal{N}} l^2(\|x\|)\right)\left(p^2 - \frac{p^3}{1+(c-1)p}\right)\left(1 - p^2 - \frac{p^3}{1+(c-1)p}\right), \tag{4.53}$$

$$\mathbb{E}\big(\mathrm{var}(I''_{11}\,|\,\mathcal{N})\big) = p_t^2\,\mathbb{E}\left(\sum_{x\in\mathcal{N}} l^2(\|x\|)\right)\left(\frac{p^3}{1+(c-1)p}\right)\left(1 - \frac{p^3}{1+(c-1)p}\right), \tag{4.54}$$

$$\mathbb{E}\big(\mathrm{var}(I_{10}\,|\,\mathcal{N})\big) = \mathbb{E}\big(\mathrm{var}(I_{01}\,|\,\mathcal{N})\big) = p_t^2\,\mathbb{E}\left(\sum_{x\in\mathcal{N}} l^2(\|x\|)\right)\left(p - p^2\right)\left(1 - p + p^2\right). \tag{4.55}$$

Note that the variances of $\mathcal{S}''_{11}$, $\mathcal{S}_{10}$, and $\mathcal{S}_{01}$ are calculated without considering fading, but the variance of $\mathcal{S}'_{11}$ has to be calculated with regard to the fact that the channel state is equal in both slots under consideration, which increases the variance. By substituting all these results into Equation (4.48) we get the overall covariance. □

Theorem 4.9. *The correlation coefficient for case* $(0,2,1)$ *is given by*

$$\rho(0,2,1) = \frac{p(1+p(c-2))}{(2-p)(1+p(c-1))}. \tag{4.56}$$

Proof. Dividing Equation (4.47) by Equation (4.46) yields the result. □

In Figure 4.5 a plot of the correlation coefficient $\rho(0,2,1)$ is presented. It can be seen that the correlation increases with increasing p and it is smaller for fast changing channels, i.e. smaller values of c. Asymptotically we have $\lim_{c\to\infty} \rho(0,2,1) = \frac{p}{2-p}$, as shown in the figure. The correlation coefficient is higher in case $(2,2,1)$ for same values of c and p since the node positions are an additional source of correlation.

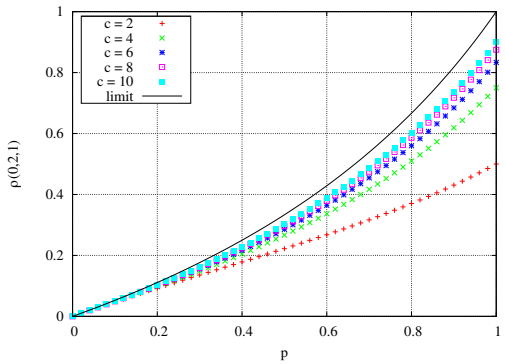

Figure 4.5: Interference correlation in case $(0,2,1)$.

4.2.9 The Correlation Caused by Fading and Traffic; Case $(0, 2, 2)$.

In case $(0, 2, 2)$ the temporal correlation of the interference has two sources: fading and overlapping traffic. These two sources strongly depend on each other and can thus not be analyzed each by its own. Similarly to case $(0, 0, 2)$ we subdivide the transmitting nodes into the subsets $\mathcal{S}_{11}$, $\mathcal{S}_{10}$, and $\mathcal{S}_{01}$. The expected fraction of nodes in these sets are given in Lemma 4.1.

Let $\mathcal{S}'_{11}$ denote the set of nodes having the same channel states in both time slots $t-1$ and t and $\mathcal{S}''_{11}$ denote the set of nodes having different channel states, similar to case $(0, 2, 1)$. Then we have $\mathcal{S}_{11} = \mathcal{S}'_{11} \cup \mathcal{S}''_{11}$.

The major task in the following is to determine $\mathbb{E}(S''_{11})$, which also allows us to compute $\mathbb{E}(S'_{11}) = \mathbb{E}(S_{11}) - \mathbb{E}(S''_{11})$. Therefore, let c_j denote the number of slots the channel stays unchanged from the beginning of slot j onward, similarly to case $(0, 2, 1)$. We have to compute the probability that a node x transmits in both slots and the channel changes after the first slot, i.e.,

$$\mathbb{E}(S''_{11}) = \mathbb{P}\big((x \in \mathcal{S}_{11}) \wedge (c_{t-1} = 1) \big) . \tag{4.57}$$

The value of c_{t-1} is determined by the transmission history of the node, i.e. by the sequences of slots of transmitting and non-transmitting states before time slot $t-1$. In the following we will denote these sequences of slots simply by *sequences*. It is, however, not necessary to consider the full history but only the part from slot $t-1$ back to a block of $c-1$ consecutive slots in which the node does not transmit. This results from the fact that after $c-1$ consecutive slots of staying quiet the value c_j is equal to zero independent of the previous behavior of the node.

Hence, we have to find all sequences after a block with $c-1$ consecutive slots with no transmission that lead to $c_{t-1} = 1$. Then we can calculate the probabilities that these sequences occur and sum these probabilities up, resulting in our desired probability.

All possible sequences can be built up by concatenating the following blocks: a transmission of length s, a transmission of length s followed by one empty slot, ..., a transmission of length s followed by $c-2$ empty slots. We identify each of these blocks with its length in terms of slots modulo c. This identification (ID) indicates the change on c_j during the block. Note that for given c and s the IDs are unique. Let $\mathcal{B}$ denote the set of all IDs. The probability of occurrence for a given block with ID $m \in \mathcal{B}$ can be computed by $p(1-p)^{(m-s) \bmod c}$. The lengths, probabilities of occurrence and IDs can be seen in Table 4.2.

Table 4.2: Blocks for node behavior.

Block length	s	$s+1$	$\cdots$	$s+c-2$
Probability	p	$p(1-p)$	$\cdots$	$p(1-p)^{c-2}$
Change of c_j	$s \bmod c$	$s+1 \bmod c$	$\cdots$	$s+c-2 \bmod c$

Let M denote the set of all IDs appearing for given c and s.

Definition 4.1. Let (m_i) denote a sequence of blocks, i.e., $m_i \in \mathcal{B}$ for all $i \in \mathbb{N}$. Then, $\mathcal{M}$ denotes the *set of all sequences* (m_i). Further, let $|m_i|$ denote the *length* of (m_i) in terms of blocks and $\|m_i\|$ its *length* in terms of slots.

Then we have

$$\|m_i\| := \sum_{i=1}^{|m_i|} s + (m_i - s \mod c)\,. \tag{4.58}$$

We try to find *sequences* (m_i) with $m_i \in M$ for all i that have some desired properties. The probability of occurrence of a sequence is denoted by $\mathbb{P}(m_i)$.

Definition 4.2. A sequence (m_i) is called an (u, e)-sequence, if $c_j = u$ at the beginning of the sequence implies $c_{j+\|m_i\|} = e$ at the end of the sequence. The set of all (u, e)-sequences can be defined as

$$\mathcal{M}(u, e) := \left\{(m_i) \in \mathcal{M} : u + \sum_{i=1}^{|m_i|} m_i \equiv e \mod c\right\}. \tag{4.59}$$

Definition 4.3. A *minimal* (u, e)-sequence is a sequence (m_i) for which no subsequence $(m_j)_{j\in I\subsetneq\{1,\ldots,|m_i|\}}$ is an (u, e)-sequence. We define the set of all minimal (u, e)-sequences as

$$\begin{aligned}\mathcal{M}^!(u, e) \;:=\; &\left\{(m_i) \in \mathcal{M}(u, e) : u + \sum_{i\in I} m_i \not\equiv e \mod c\right.\\ &\left.\forall\, I \subsetneq \{1, \ldots, |m_i|\},\ I \neq \emptyset\right\}.\end{aligned} \tag{4.60}$$

Lemma 4.10. *A minimal (u, e)-sequence (m_i) has a length of at most $|m_i| \leq c + 1$.*

Proof. Let us assume $|m_i| > c + 1$. Since $0 \leq c_j \leq c$ it follows that c_j has the same value in at least two different time slots. If we remove the subsequence inbetween these two slots, we get a subsequence that is again an (u, e)-sequence, which is a contradiction to our assumption. □

The probability that one of the minimal sequences of $\mathcal{M}^!(u, e)$ occurs as the transmission behavior of a node is given by

$$\begin{aligned}\mathbb{P}\big(\mathcal{M}^!(u, e)\big) &= \sum_{(m_i)\in\mathcal{M}^!(u,e)} \prod_{j=1}^{|m_i|} p(1-p)^{(m_i-s) \bmod c} \\ &= \sum_{(m_i)\in\mathcal{M}^!(u,e)} p^{|m_i|}(1-p)^{\sum_{j=1}^{|m_i|}(m_i-s) \bmod c}\,.\end{aligned} \tag{4.61}$$

Definition 4.4. A (minimal) *neutral sequence regarding* u is a (minimal) (u,u)-sequence.

The probability of occurrence of all neutral sequences regarding u can be derived from the occurrence probability of the minimal (u,u)-sequences as the sum of the infinite geometric series

$$\mathbb{P}\big(\mathcal{M}(u,u)\big) = \frac{1}{1-\mathbb{P}\big(\mathcal{M}^{!}(u,u)\big)}\,. \tag{4.62}$$

This expression does, however, not hold for the probabilities $\mathbb{P}\big(\mathcal{M}(u,e)\big)$ with $u \neq e$. To compute those probabilities we first have to introduce another concept.

Definition 4.5. Let $\mathcal{M}^{!}(u,u,E) \subseteq \mathcal{M}^{!}(u,u)$ with $E \subset \mathcal{B}$ denote the set of all minimal neutral sequences regarding u in which the values in E never occur for c_j, i.e.

$$\begin{aligned}\mathcal{M}^{!}(u,u,E) \;:=\; \Big\{(m_i) \in \mathcal{M}^{!}(u,u) : u + \sum_{j=1}^{k} \not\equiv e \mod c \\ \forall\, e \in E, 1 \leq k \leq |m_i|\Big\}\,.\end{aligned} \tag{4.63}$$

We can construct the set $\mathcal{M}(u,e)$ with $u \neq e$ in the following way: We take a sequence $(m_i) \in \mathcal{M}^{!}(u,e)$ and fill neutral sequences regarding the value of c_j between each pair of blocks and at the beginning and end, with the following exception: the neutral sequences in which a value for c_j occurs that previously occurred within the sequence $\mathcal{M}^{!}(u,e)$ have to be excluded from the insertion process. The reason is that otherwise the constructed sequence contains a neutral subsequence other than the ones inserted. Hence the construction process would not be unique for each sequence, i.e. we could construct the same sequence out of two different elements in $\mathcal{M}^{!}(u,e)$.

Definition 4.6. The concatenation of two sequences is defined as

$$\begin{aligned}(m_i) \cup (m'_j) := (m^{*}_k) \text{ with } m^{*}_k = m_k \text{ for } 1 \leq k \leq |m_i| \text{ and} \\ m^{*}_{k+|m_i|} = m'_k \text{ for } 1 \leq k \leq |m'_j|\,.\end{aligned} \tag{4.64}$$

Definition 4.7. Let $C(u,(m_i),r)$ denote the value of c_{j+r} at position r of the sequence (m_i) with $c_j = u$, i.e.

$$C(u,(m_i),r) := u + \sum_{i=1}^{r} m_i \mod c\,, \tag{4.65}$$

and $C(u,(m_i),0) := u$.

Let the notation $(m_i)_l$ indicate the l^{th} element of a list of sequences. In mathematical terms the set $\mathcal{M}(u,e)$ with $u \neq e$ can be constructed as

$$\begin{aligned}\mathcal{M}(u,e) = \Big\{ &(m_i)_0 \cup \bigcup_{k=1}^{|m'_j|} (m'_k \cup (m_i)_k) \ : \\ &\forall (m'_j) \in \mathcal{M}^!(u,e), \\ &\forall (m_i)_k \in \mathcal{M}^!\Big(C(u,(m'_j),k),\ C(u,(m'_j),k), \\ &\qquad \{C(u,(m'_j),o)\ \forall\, 0 \leq o \leq k-1\}\Big)\Big\}. \end{aligned} \tag{4.66}$$

Hence, we can compute the probability $\mathbb{P}\big(\mathcal{M}(u,e)\big)$ with $u \neq e$ by

$$\begin{aligned}\mathbb{P}\big(\mathcal{M}(u,e)\big) = \sum_{(m_i)\in\mathcal{M}^!(u,e)} \mathbb{P}\Bigg(&(m_i) \prod_{j=0}^{|m_i|} \mathbb{P}\mathcal{M}^!\Big(C(u,(m_i),j), \\ &C(u,(m_i),j), \{C(u,(m_i),o)\ \forall\, 0 \leq o \leq j-1\}\Big)\Bigg). \end{aligned} \tag{4.67}$$

The probabilities $\mathbb{P}\big(\mathcal{M}(0,e)\big)$ can be interpreted as the probabilities that $c_j = e$ occurs.

Theorem 4.10. *The expected fraction of nodes in the set $\mathcal{S}''_{11}$ is given by*

$$\begin{aligned}\mathbb{E}(S''_{11}) \ = \ & p(1-p)^{c-1}\Bigg(\sum_{i=1}^{s-1} \mathbb{P}\Big(\mathcal{M}\big(0,(i-1 \mod c)+1\big)\Big) \\ &+ \mathbb{P}\Big(\mathcal{M}\big(0,(s-1 \mod c)+1\big)\Big)\,\frac{p}{1-(s-1)p}\Bigg). \end{aligned} \tag{4.68}$$

Proof. As already mentioned in Equation (4.57), we are interested in the probability that a node is transmitting in both time slots $t-1$ and t and that $c_{t-1} = 1$. This comprises several situations: A transmission could start at slot $t-1$ with $c_{t-1} = 1$, or up to $s-1$ slots before with $c_{t-s} = (s-1 \mod c)+1$. The values for c_j are chosen to achieve $c_{t-1} = 1$.

The last case is an exception as it is the only one where it is not implicitly the case that the node also transmits in slot t. The reason is that a transmission started in slot $t-s$ ends after slot $t-1$.

Hence, to compute $\mathbb{E}(S^{**}_{11})$ we take the sum over all probabilities of occurrence of these situations, with the last one additionally multiplied with the probability that the node transmits in slot t. Then we multiply this sum with the probability that the $c-1$ empty slots at the beginning occur and the node transmits afterwards, which leads to the result. □

Since we now know the values for $\mathbb{E}(S'_{11})$, $\mathbb{E}(S''_{11})$, $\mathbb{E}(S_{10})$, and $\mathbb{E}(S_{01})$ we can apply Theorem 4.1 to compute the covariances between the sets and hence similar to case $(0,2,1)$ the overall correlation coefficient

$$\begin{aligned}\rho(0,2,2) &= \frac{\mathbb{E}\big(\mathrm{cov}(I'_{11}+I''_{11}+I_{10}, I'_{11}+I''_{11}+I_{01}\,|\,\mathcal{N})\big)}{p_t^2\lambda\int_{\mathbb{R}^2} l^2(\|x\|)\,\mathrm{d}x\,\big(2sp-(sp)^2\big)} \\ &\overset{\alpha\geq 2}{=} \frac{\mathbb{E}\big(\mathrm{cov}(I'_{11}+I''_{11}+I_{10}, I'_{11}+I''_{11}+I_{01}\,|\,\mathcal{N})\big)}{p_t^2\lambda\,\frac{\alpha}{\alpha-1}\pi\,\big(2sp-(sp)^2\big)}\,,\end{aligned} \tag{4.69}$$

where the variance is derived in Equation (4.30).

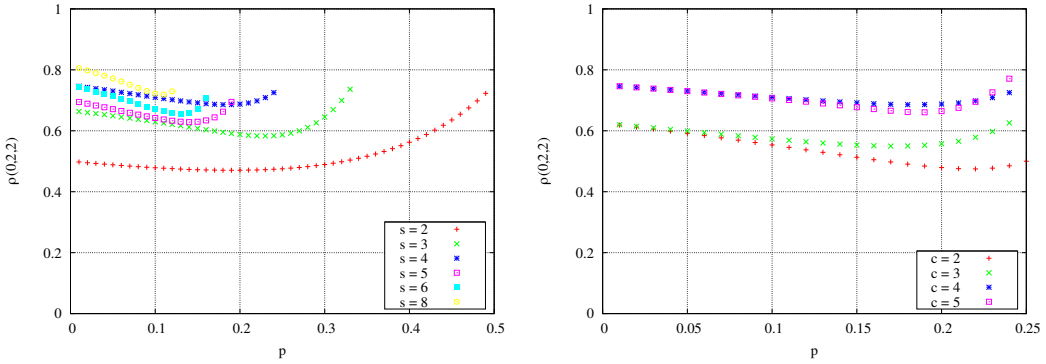

(a) Plot of $\rho(0,2,2)$ for different s with $c=4$. (b) Plot of $\rho(0,2,2)$ for different c with $s=4$.

Figure 4.6: Interference correlation in case $(0,2,2)$.

Figure 4.6(a) shows a plot of the correlation coefficient $\rho(0,2,2)$ for different values of the message length s. The channel coherence time c is held constant at 4. Note that the curves end at $ps=1$. The correlation coefficient is generally higher for longer and thus more overlapping messages, with the following exception: When s is a integer multiple of c the messages and channel states synchronize and for each new transmission a new channel state occurs. Hence, in this case the increase of the correlation compared to a smaller value of s is even higher. A further increase of s by one shows no further increase or even a decrease of the correlation for some values of p, as can be seen, e.g. for $s=4$ and $s=5$. The slight decrease of correlation with increasing p for small values of sp is due to the decrease of the correlation caused by traffic, as can be observed in case $(0,0,2)$. For even higher values of p the increase of the correlation introduced by the channel is larger than this decrease and hence the curve again shows an increase of the correlation coefficient. The dependence on the channel coherence time c is depicted in Figure 4.6(b). In general the correlation is higher for higher values of c, again with the following exception: When c is an integer multiple of s a larger increase of the correlation can be observed due to the synchronized behavior of channels and packets.

4.2.10 The Correlation Caused by Node Distribution, Fading, and Traffic; Case $(2,2,2)$.

Case $(2,2,2)$ can be interpreted as a mixture of the two cases $(0,2,2)$ and $(2,1,2)$. The expected fraction of nodes in $\mathcal{S}_{10}$, $\mathcal{S}_{01}$, $\mathcal{S}'_{11}$, and $\mathcal{S}''_{11}$ is similar as derived for case $(0,2,2)$. The derivation of the covariance $\mathrm{cov}\big(I'_{11}+I''_{11}+I_{10}, I'_{11}+I''_{11}+I_{01}\big)$ is similar to case $(2,1,2)$ except that nodes in the set $\mathcal{S}'_{11}$ are facing the same fading conditions in both slots $t-1$ and t whereas the fading conditions change for nodes in the set $\mathcal{S}''_{11}$. Hence, at the beginning of the expression of the covariance we have $\mathbb{E}(h^4 S'_{11}+S_{10})$, yielding

$$\begin{aligned}&\mathrm{cov}\left(I'_{11}+I''_{11}+I_{10}, I'_{11}+I''_{11}+I_{01}\right) = \\ &= \mathbb{E}\left(h^4 S'_{11}+S''_{11}\right)\mathbb{E}\left(\sum_{x\in\mathcal{N}} l^2(\|x\|)\right) + \left(\mathbb{E}(S_{10})-sp\right)\left(\mathbb{E}\left(\sum_{x\in\mathcal{N}} l(\|x\|)\right)\right)^2 . \quad (4.70)\end{aligned}$$

Hence, the corresponding correlation coefficient is

$$\rho(2,2,2) \overset{\alpha>2}{=} \frac{\mathbb{E}\left(h^4 S'_{11}+S''_{11}\right)\lambda p_t^2 \frac{\alpha\pi}{\alpha-1} + \left(\mathbb{E}\left(S_{10}\right)-dp\right)\lambda^2\left(\frac{\alpha\pi}{\alpha-2}\right)^2}{2sp\lambda p_t^2 \frac{\alpha\pi}{\alpha-1}} . \quad (4.71)$$

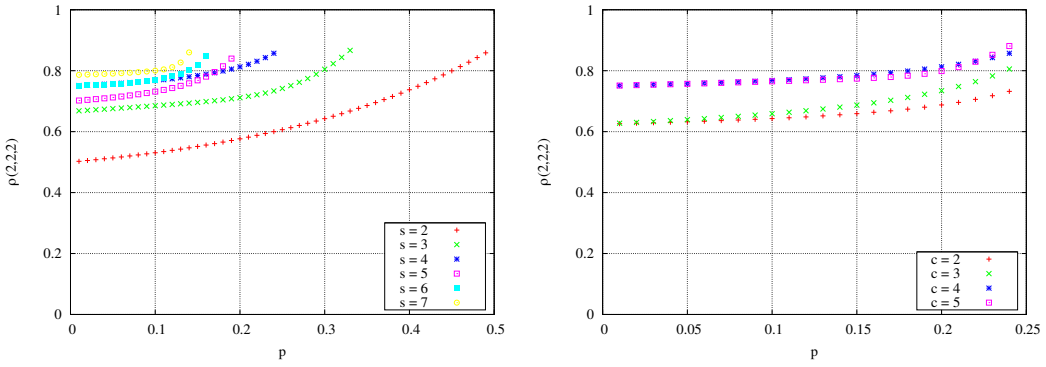

(a) Plot of $\rho(2,2,2)$ for different s with $c=4$. (b) Plot of $\rho(2,2,2)$ for different c with $s=4$.

Figure 4.7: Interference correlation in case $(2,2,2)$.

Similar to case $(0,2,2)$ the correlation coefficient is dependent on p, c, and s. In Figure 4.7(a) the dependence on s is depicted. As can be seen, the correlation is again higher for longer message lengths s. The only exception is when s is an integer multiple of c where messages and channel synchronize and and a higher increase of correlations appear. Thus, in these cases the correlation is for some values of p even higher than for larger values of s.

In Figure 4.7(b) the influence of the channel coherence time c on the correlation coefficient $\rho(2,2,2)$ is shown. The curves can be partitioned into groups, where the

major increase of correlation is determined by the integer value $\lfloor \frac{c}{s} \rfloor$. Every time c is an integer multiple of s a significant increase of the correlation can be observed.

When comparing case $(2, 2, 2)$ to case $(0, 2, 2)$ the major difference is that the correlation coefficient is generally higher in case $(2, 2, 2)$ when all parameters are held constant. The reason is that the node positions are an additional source of correlation. The increase is larger for higher values of the sending probability p, since the correlation caused by the node positions is increasing with p, as has been derived in Section 4.2.4.

4.3 Related Work for Interference Models and Analysis

4.3.1 Interference Models

Several researchers proposed interference models for random wireless networks. Example publications are as follows: Rickenbach *et al.* [RSWZ05] present a *receiver-centric model of interference*. The network is modeled as a unit disk graph and the interference is determined as the number of disks overlapping the regarded receiver. Based on this model, an approximation of the optimal connectivity-preserving topology in a highway model is derived.

Dousse *et al.* [DBT05] study the impact of interferences on the *connectivity* of large-scale multihop networks. The total noise is modeled as the weighted sum of the interference levels and the background noise. The paper shows that, for small enough weighting factors, node spatial densities exist for which the network contains a large cluster of nodes, enabling distant nodes to communicate via multiple hops.

In [QZW+07] Qiu *et al.* propose a model that allows an *estimation of several traffic parameter* like throughput as function of the interference within an WLAN network. The model is based on measurements on a testbed using the 802.11a standard. A Markov chain is used to model the interactions between different senders and receivers allowing a quite sophisticated traffic modeling.

A *conflict graph* is applied by Jain *et al.* in [JPPQ03] to model interference. The authors present methods for computing lower and upper bounds on the optimal throughput for a given network and workload under the assumption that packet transmissions at the individual nodes can be finely controlled and carefully scheduled by an omnipotent central entity. Paper [VT06] studies the impact of interference on the *throughput* of a multihop network by means of simulations. The authors conclude that intra-path interference is the major limiting factor for the throughput of multihop paths.

Win *et al.* [WPS09] propose a *theoretical model* representing the interference in wireless networks. The model is based on general assumptions, especially a very general channel model. The authors conduct four case studies, analyzing the interference of cognitive radio networks, the interference in wireless packet networks,

the spectrum of the aggregate radio-frequency emission, and the coexistence of narrowband and ultrawideband systems. A comprehensive analysis of one of these case studies, namely the coexistence of narrowband and ultrawideband systems, based on methods from stochastic geometry, is presented by Pinto *et al.* in [PGWC09].

All these interference models analyze only the expected interference without considering spatial and temporal correlations. The correlations are, however, of great importance when assessing the performance of a wide range of communication methods.

4.3.2 Analytical Work on Interference Correlation

Recent work by Haenggi *et al.* is very closely related to this article. The letter [GH09a] analyzes the *temporal and spatial correlation* of interference in wireless networks. It applies modeling assumptions corresponding to those of our cases $(2, j, k)$ with $j, k \in \{0, 1\}$ investigated in Section 4.2.4. The article [Hae09] studies different performance measures in random wireless networks. Analytical results are based on an "uncertainty cube," which classifies and quantifies the network stochastics with respect to node placement, fading, and medium access protocols. The results of these papers are also explained in [HG09]. The analysis in the previous section can be considered as a logical continuation and extension of these publications.

The paper [YP03] analyzes the *second order statistics* of interference, which is a measure for temporal dependency of the interference, for nodes distributed according to a Poisson point process. They show that interference can be correlated and derive analytical expressions for the correlation.

4.3.3 Practical Work on Interference and its Correlation

Further related work is by Grossglauser and Tse [GT02]. They show that the per-user *throughput* in wireless ad-hoc networks can increase when nodes are mobile rather than fixed. The authors conclude that this improvement is obtained through the exploitation of time variation of the users' channels due to mobility. The impact of mobility can be explained by a decrease of the temporal correlation of interference due to a shorter channel coherence time.

A lot of work is concerned with *cochannel interference* in cellular networks. In the following we provide some work concerning with this topic although the work at hand does not consider cellular networks, since some results may be easily modified to also apply to ad-hoc networks. In [YS92] Yao *et al.* apply the *Nakagami fading model* with different fading parameters for each interferer. Based on this model they study the impact of diversity on the outage probability in terms of a numerical study.

In [GRC03] the authors use a special interference model to calculate the *minimum reuse distance* in a cellular network. From their simulation-based studies they conclude that in interference limited scenarios transmission power has only minor impact on the spatial reuse. Decreasing the distance between nodes and higher path

loss exponents both improve, however, the spatial reuse. An investigation of the interference in cellular networks is presented by Prasad *et al.* in [PK91]. The authors assume a Rayleigh fading channel, log-normal shadowing and a path loss exponent $\alpha = 4$. The authors derive probabilities for the co-channel interference for incoherent cumulation of different interfering signals.

In the paper [BvRWZ04] the authors investigate whether interference can be reduced by means of *topology control*. They show that sparse topologies actually do not automatically reduce interference, which is an assumption that is stated by other papers. Additionally, the authors give a construction method for topologies and show that they are optimal in terms of interference.

Minimizing the interference by a particular *channel assignment* is proposed by the authors of [SGDC08]. There, the authors assume that a number of channels is reserved for the communication of the nodes in a multihop network. Each user decides for each transmission individually which channel it uses. If this decision is done in an optimal way the interference caused by each transmission can be minimized. Finding an optimal schedule for the channel usage is, however, known to be NP-complete. Simulations show that the algorithms proposed in the paper well approximate this minimal values. A similar approach is followed by the authors of [XTZ07]. The major difference is that the focus is more on interference coming from external sources, i.e., not within the wireless network itself. If the interference increases above a certain threshold the whole network or only the affected part switches to another channel. Therefore, the communication tries to avoid interference if it is limited to one or a few channels.

Zhu *et al.* [ZZHZ10] perform an *empirical study* on point-to-multipoint transmission. They conclude that the reception events are highly correlated. It is thus not needed for each of the neighbors to individually acknowledge reception. A protocol that reduces the number of acknowledgments is proposed and evaluated by empirical and simulation-based studies. Srinivasan *et al.* [SJC+10] propose an empirical measure for the *correlation of the successful reception* for different links. They compare this measure to two commonly used empirical measures. Results show that the proposed measure performs better in terms of predicting the performance of certain protocols. Both papers perform empirical studies on the interlink correlation of transmission success. The paper at hand provides a first step toward the goal of backing up these empirical results with a theoretical background.

Chapter 5

Case Study: Analysis of the Overall Network Throughput

When considering only a single transmission, cooperative relaying is able to improve the throughput between the two nodes involved. When such a cooperative relaying transmission is performed within a larger network, it might have, however, an impact on other concurrent transmissions. The relay causes additional interference that worsens the channel conditions of all neighboring nodes. If we assume low-cost radios that have neither MIMO capabilities nor the support of sophisticated combining techniques, this additional interference reduces the throughput of concurrent transmissions, since they have to reduce their coding or modulation rate according to the channel.

Hence, we are going to analyze the overall network capacity (in terms of concurrent transmissions) for high node densities. We compare the four transmission methods presented in Section 2.8: conventional direct transmission, double data rate transmission, time-diversity direct transmission, and cooperative relaying by simulations. In particular, we investigate the tradeoff between adding diversity to the transmissions and additional interference caused by this diversity.

Preliminary results have been obtained in cooperation with G. Brandner and C. Bettstetter. They have been published in [9].

5.1 Simulation Setup

In the following we perform a simulation based study to investigate the overall network throughput in terms of the number of concurrent transmissions. Therefore, four scenarios are simulated, which differ in the distribution of the nodes and the selection criterion for the destination nodes (see Table 5.1). Nodes are distributed in two different manners, which are explained in Section 2.1: The nodes can be either distributed according to a *homogeneous Poisson point process* or according to the *inhomogeneous node distribution* based on thinning as introduced in Chapter 3.1.

Table 5.1: Simulation scenarios

	node distribution	dest. selection
Scenario 1	*homogeneous*	*no criteria*
Scenario 2	*homogeneous*	*only idle nodes*
Scenario 3	*inhomogeneous*	*no criteria*
Scenario 4	*inhomogeneous*	*only idle nodes*

The selection of the destination is performed randomly from the set of nodes located within the maximum pathloss range of the sender. In scenarios with *no criteria*, the destination is selected randomly from *all* nodes within this range, independent of whether the node is already active, i.e., receiving or transmitting. In scenarios with *only idle nodes*, the destination is randomly chosen from the nodes in range that are currently not active.

All important simulation parameters are presented in Table 5.2. Some parameters must be chosen carefully to achieve meaningful simulation results:

- The transmission range is selected to be the maximum range possible without considering interference.
- The node density is chosen to achieve a good tradeoff between a reasonable number of neighbors per sender and a feasible simulation time.
- The expected interference power at a given time instant can be chosen by defining the number of nodes transmitting simultaneously (only in discrete steps). Hence, the simulation area has to be large enough to allow for a sufficiently high granularity of the simulated interference.
- All other parameters have been chosen from state-of-the-art wireless technologies.

A simulation comprises 10 000 time periods for each traffic load ($n_s = 1, \ldots, 40$) and each transmission method. For each time period a fixed number n_s of senders and corresponding destinations are randomly selected. For direct transmission we apply quadrature phase shift keying (QPSK), while for all other transmission methods quadrature amplitude modulation (16-QAM) is chosen, which doubles the bit rate. This is done for fairness reasons, since for diversity techniques each bit is sent twice and we want to spend the same amount of transmission energy per bit as for direct transmission. The duration of a transmission is two time periods for direct transmission and one time period for all other methods. The simulator collects the following data: the overall number of transmissions, the number of successful transmissions, the number of successful packet deliveries for time diversity and cooperative relaying, and the average distances between the nodes.

Table 5.2: Simulation parameters

Parameter	**Symbol**	**Value**
Number of nodes	n	2000
Area	A	$30\,000^2$ m^2
Node density	$\lambda = n/A$	$2.2 \cdot 10^{-6}$
Duration		10 000 time periods
Transmitters per time unit	n_s	1 - 40
Transmission power	p_t	0 dBm
Receiver sensitivity	$p_t^{\min}$	-94 dBm
Maximum transmission range	$d_{\max}$	1360 m
Packet length		1024 bit
Pathloss exponent	α	3
Bit rate with QPSK	b_r	250 kbps
Noise spectral density	N_0	$4.003886 \cdot 10^{-21}$ J
Bandwidth	B	2 MHz
Thinning range	r	1000 m
Thinning limit	k	13

5.2 Simulation Results

The first simulation setup compares all four transmission methods within Scenario 1. Figure 5.1 compares the transmission methods regarding (a) the number of successful transmissions and (b) the fraction of successful transmissions as a function of the number of concurrent transmissions n_s.

We can roughly partition the plot into three regimes: the *low interference* regime ($n_s = 1 \ldots 8$), the *medium interference* regime ($n_s = 8 \ldots 15$), and the *high interference* regime ($n_s > 15$). In the low interference regime, the main limiting factor for

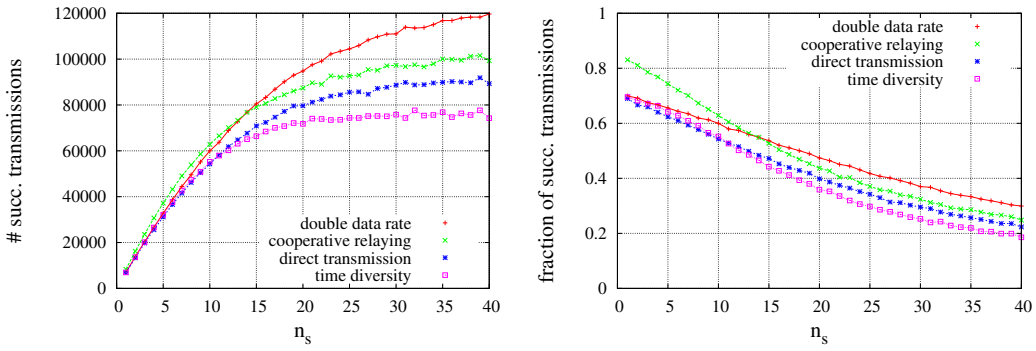

(a) Overall success rates.

(b) Relative success frequencies.

Figure 5.1: Successful transmissions in Scenario 1.

transmission success is the channel state due to Rayleigh fading. Here, cooperative relaying shows the best performance, since it best counteracts the effects of fading. All other methods are performing worse, and at about the same level.

If we consider the medium interference regime, we can observe two major changes: First, double data rate transmission outperforms both direct transmission and time diversity. The reason for this behavior is that double data rate transmissions cause only half the interference than all other methods. Therefore, the slope of the curve is reduced, leading to a better performance in medium and high interference situations. Second, direct transmission is outperforming time diversity, since the interference of two consecutive time slots is highly correlated. Hence, if the first transmission fails, the second is also very likely to fail, and vice versa.

In the high interference regime, double data rate transmission clearly outperforms cooperative relaying due to lower interference. As the traffic load increases much further, the number of successful transmissions does no longer increase but experiences a saturation effect.

For high traffic loads in Scenario 1, the source is likely to select a non-idle node as destination (*no criteria*). In contrast, for low traffic load this probability is low. In Scenario 2 only idle nodes are allowed to be selected as destinations. Hence, in the high interference regime we can observe a slight improvement of the performance compared to Scenario 1, as can be seen in Figure 5.2(a). The difference is, however, very small; but it would be significantly higher for a higher number of concurrent transmissions (not shown on the figure). In the low and medium interference regimes there is no difference at all.

For double data rate transmissions there can be no difference observed in Figure 5.2(a) due to the reduced interference. Again, for a higher number of concurrent transmissions a difference would occur. When comparing Scenarios 3 and 4 similar effects can be observed; a plot with this comparison is presented in Figure 5.2(b).

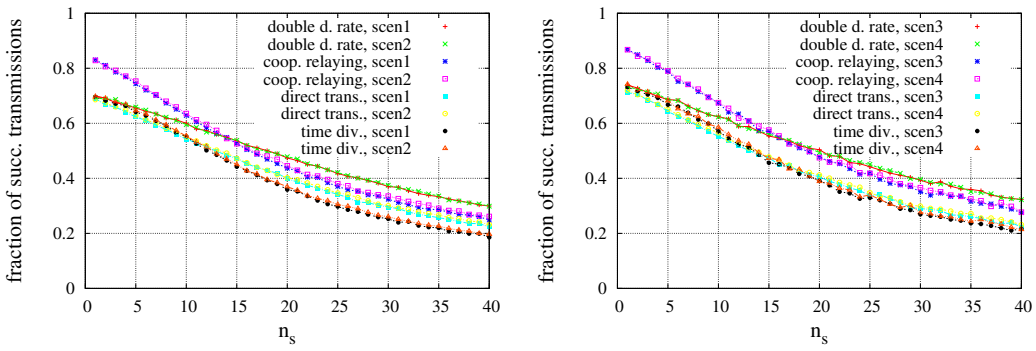

(a) Comparison of Scenarios 1 and 2.

(b) Comparison of Scenarios 3 and 4.

Figure 5.2: Relative success frequencies for Scenarios 1-4.

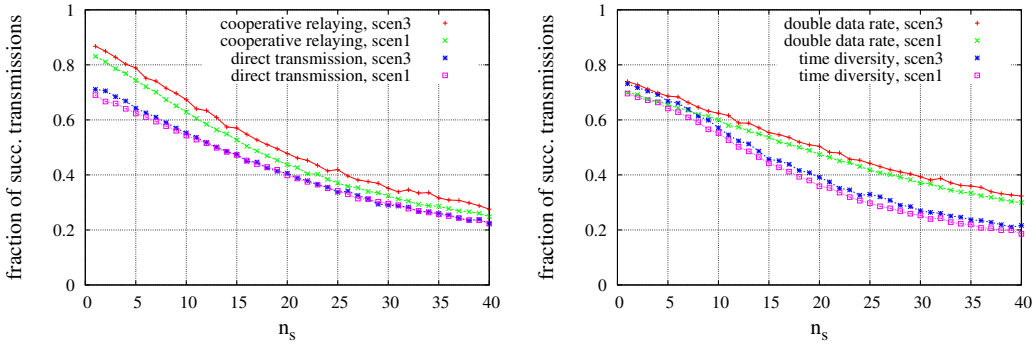

(a) Cooperative relaying vs. direct transmission. (b) Time diversity vs. double data rate.

Figure 5.3: Relative success frequencies for Scenarios 1 and 3.

Figure 5.3 compares the transmission methods for homogeneously and inhomogeneously distributed nodes (Scenario 1 vs. Scenario 3). The trends are similar for both scenarios. There is, however, a significant difference: All methods except direct transmission improve their performance for inhomogeneously distributed nodes, which are the methods that use 16-QAM. This effect can be explained by an improved SINR due to a lower average distance between source and destination, between source and relay, and between relay and destination. The lack of improvement for direct transmission is due to the fact that a lower-order modulation scheme has a weaker dependence on a good SINR than a higher-order modulation scheme. Therefore, the advantage of both double data rate and cooperative relaying over direct transmission is higher for inhomogeneously distributed nodes.

In Scenario 4 an increase of the performance in the high interference regime compared to Scenario 3 can be observed. This difference is again due to non-idle destination nodes in this scenario. Overall, Scenario 4 leads to the highest network capacity of all scenarios considered.

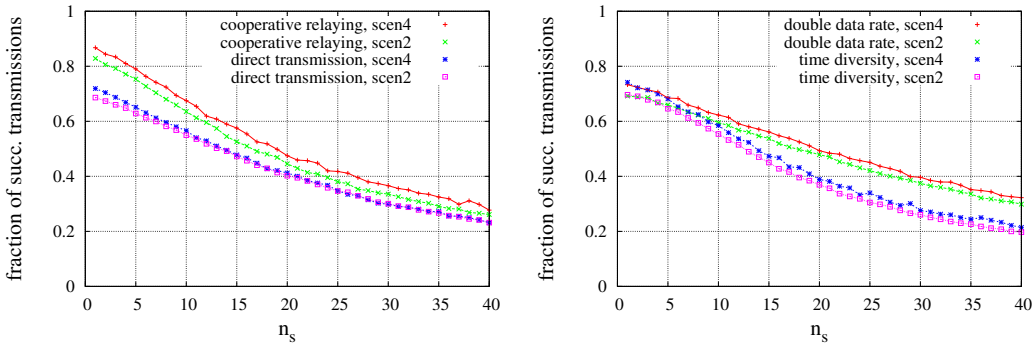

(a) Cooperative relaying vs. direct transmission. (b) Time diversity vs. double data rate.

Figure 5.4: Relative success frequencies for Scenarios 2 and 4.

As shown in Figure 5.4, an inhomogeneous node distribution shows an advantage especially for cooperative relaying, independent of the traffic load. A similar behavior can also be observed for double data rate and time diversity (shown in Figure 5.4(b)). However, direct transmission performs similar for homogeneous and inhomogeneous node distributions. The reasons for this behavior are the same as described in the comparison of Scenarios 1 and 3.

5.3 Related Work for Network Capacity Analysis

5.3.1 Analysis of the Network Capacity

Gastpar *et al.* analyze in [GV02] the *capacity of wireless networks* under the relay traffic pattern. In the underlying model there is only one source-destination pair present, while the other nodes act as relays during the transmission. The authors derive upper and lower bounds for the network capacity and show that these bounds are equal when the number of nodes approaches infinity.

If directional antennas are applied it can improve the network capacity in ad hoc wireless networks, as shown by Yi *et al.* in [YPK03]. The authors compare the network capacity when using directed and undirected antennas on an analytical basis. The analysis is based on the well-know concept of *Voronoi tessellation*.

In [OMPT05] Ochiai *et al.* *beamforming*, which is a method classically applied with antenna array, is performed cooperatively by several nodes. It is shown that under some theoretic assumptions a beamforming pattern with a lobe structure similar to that of an antenna array can be achieved. A cooperative relaying strategy that tries to optimize the energy consumption of the nodes is presented by Madan *et al.* in [MMMZ08]. The distinctive feature of this approach is that several relay nodes are collectively forwarding the message to the destination node. By doing that they cooperatively beamform the radiated signal to save energy, as introduced in [OMPT05]. The main contribution of the paper is to minimize the overall consumed energy by specifically select the relay nodes that perform the beamforming strategy.

5.3.2 The Impact of Cooperative Diversity

A lot of related work is concerning about cooperative approaches in networks, especially about cooperative relaying. Zheng *et al.* simulate in [ZZSW05] the performance of cooperative diversity strategies in *interference-limited ad-hoc networks*. They conclude that the gain of cooperative diversity depends heavily on the chosen cooperative strategy and on the resource allocation strategy. Contrary to our work, the nodes are distributed on a grid in a deterministic manner and each node can only transmit to the surrounding 8 nodes.

In [IH06] Islam *et al.* simulate the throughput performance of a *10-user ad hoc network* employing cooperative diversity techniques; 20 random topologies are regarded. The average throughput for different system loads with cooperative relaying is obtained and compared to the IEEE 802.11 standard without relaying.

The performance of three *different relaying strategies* are investigated by Gormus *et al.* in [GKMM06]. The results are based on the study of the transmissions of one source-destination pair, where either one or two relay nodes are placed in between. These results, however, do not consider the effects of interference caused by concurrent transmissions of other nodes in the network.

The authors of the paper [JQC+04] investigate the impact of the nodes' transmission powers on the performance of cooperative relaying schemes. Their approach is to measure the channel conditions and adjust the transmission power individually for each packet based on this information. Numeric results show that under the given assumptions their approach outperforms both direct and relay communication.

In the article [ZHF05] Zimmermann *et al.* investigate the performance of cooperative relaying protocols by comparing them to direct transmission and conventional relaying in terms of the SNR gain. The SNR gain is used to benchmark a new protocol in the following way: the improvement of some performance metric (e.g. bit error probability) achieved by the new protocol is expressed in the necessary improvement of the SNR to achieve a similar performance with the reference protocol. The impact of *space-time codes* on cooperative relaying is analyzed by Miyano *et al.* in [MMA04]. It is assumed that the number of hops in the communication path is more than two. The performance of the scheme increases with the number of hops, as the simulation results in the paper show.

In the paper [NJGM07] Ng *et al.* compare *transmitter and receiver cooperation* for different SNR ranges. The results show that transmitter cooperation performs better than receiver cooperation under most SNR conditions, except if the cooperation channel, i.e. the channel between the two cooperating nodes, suffers from severe fading. Deploying both techniques together improves the performance only for low SNR values. Two cooperative relaying schemes that provide an interference free received signal at the user terminals are proposed by Zhao *et al.* in [ZKWB07]. The performance of the schemes is analyzed by a simulation based study that shows that the proposed schemes outperform the reference schemes in the selected scenarios.

Dohler *et al.* examine the *bit error rates* for a cooperative relaying network with space-time block codes in [DHDA04]. They assume Rayleigh or Nakagami fading channels and full or partial cooperation of the mobile terminals.

The latter papers do not consider the overall network performance metrics but instead assume that improving the performance of a *single link* does improve the performance of the whole network. As our simulation results in Chapter 5 show, this is not always the case, as improving a single link's performance may cause additional interference.

The following papers utilize measures that consider the overall performance of the network including interfering effects between concurrent transmissions in their

results. In the paper [AY07] Adinoyi *et al.* investigate cooperative relaying schemes with *relays being fixed terminals* each having more than one antenna. It is argued that due to the fixed nature of the relays it is feasible to have several antennas on the them. Some numerical analyses are present to compare the performance of the most important combining strategies (maximum ratio combining vs. selection combining). For all investigations the Nakagami fading model is deployed.

In [GE07] Gündüz *et al.* investigate the performance of *combined source and channel coding* in cooperative relaying schemes over a slowly fading channel. They apply the diversity-multiplexing tradeoff to characterize the distortion exponent of the channel. They conclude that layered source coding and a careful matching of the code rates and cooperation schemes is very effective to improve the distortion exponent.

The tradeoff between capacity and fairness in *cellular networks* when applying cooperative relaying is analyzed by Song *et al.* in [SSLC07]. The authors conclude that an adequate scheduling algorithm may lead to good results regarding this tradeoff. Further, they propose a scheduling algorithm that improves both capacity and fairness at the expense of cooperation among the users.

An analysis of the performance of cooperative relaying based on *real measurements* is presented by Kyritsi *et al.* in [KEGL06]. The measurements are conducted in an office environment using a testbed consisting of two access points and two user terminals each equipped with four antennas. The results show that the links between the user terminals suffer from stronger fading effects than the links between user terminals and access points. Hence, a appropriate choice of the relays and transmission powers can significantly increase the achievable rates.

In the paper [RF06] Rost *et al.* propose a cooperative relaying scheme for *infrastructure based wireless systems*. The major characteristic of this scheme is that it applies two relay nodes and has no need for an increase of the spectral efficiency in comparison to direct transmission. Such an increase is usually needed to allow for a fair comparison of the two schemes. A simulation based analysis is performed that shows that the proposed scheme outperforms direct transmission, conventional relaying, and time diversity in terms of outage probability in the low SNR regime. In the high SNR regime, however, the proposed scheme performs worse than some of the reference schemes.

In [AM08] Atia *et al.* investigate the *performance degradation* for cooperative relaying schemes, if only *imperfect channel state information* in the downlink of wireless networks is available. The authors derive an upper bound of the overall throughput for a two-phase transmission system. This bound is utilized to optimize an adaptive beamforming strategy with the result that it performs almost similar than with having perfect channel state information.

5.3.3 Interference Related Capacity Analysis

Rickenbach *et al.* propose and study a *receiver-centric model of interference* in [RSWZ05], where each node possibly disturbs the transmission of other nodes that are located within a defined interference radius. The degree of interference at a certain receiver depends on the number of interference radii that cover this receiver. In contrast to the paper at hand there is a strict border that determines if a sender interferes with other nodes.

For *theoretical approaches for modeling interference*, the following papers can be considered: In the article [Hae09] Haenggi *et al.* derive *analytical expressions* for different measures of the network throughput in wireless networks. It classifies the networks in an *uncertainty cube* regarding node placement, fading, and MAC protocols and derives analytical results. A comprehensive overview of these results can also be found in [HG09]. In contrast to our work transmission success is determined based on a threshold value for SINR. Further, we contribute by also considering inhomogeneous node distributions.

In the paper [JS97] Jones *et al.* proposes an interference model for *microcellular networks*, which incorporates user terminal mobility and radio propagation parameters.

Parissidis *et al.* introduce in [PKM+08] a *multiple circle model* similar to the model introduced by Schilcher *et al.* in [7]. The authors use it to compute transmission success probability and apply the model to a MAC protocol. The major difference to the model presented in [7] is the hard cutoff for the SINR value instead of a mapping from SINR to bit error probability.

In [Ham02] Hamdi derives the *probability density functions* for the SINR and the bit error probability for Rayleigh fading channels. An additive interference model and a capture threshold model for random access networks and scheduled networks are discussed in [IRK09].

In [AvB87] Arnbak *et al.* show that a *Rayleigh fading environment* might improve the network capacity. The improvement is caused by an improvement of the SINR due to the degradation of the interfering signals caused by other concurrent transmissions.

5.3.4 Network Capacity in Sparse Networks

In the following we give a short overview of analysis of the network capacity for *sparse networks*: In [GGL08, GGL09] Garetto *et al.* analyze the behavior of the network capacity under *different degrees of mobility* in sparse mobile ad hoc networks. They also consider the shape of the spatial distribution around one or more so-called home-points as a major influence factor on the capacity. These home-points are locations at which nodes are located most of the time, e.g., private homes, workplaces, and warehouses in the case of people.

A similar analysis has been performed by Huang *et al.* in [Hua09]. In contrast to Garetto et al. they investigated networks with *infrastructure support*, which is

modeled via several base stations that are connected with unlimited bandwidth. Additionally, the mobility model is modified to support hybrid networks (including static base stations).

Subramanian *et al.* propose a *framework* for analyzing the throughput of sparse mobile networks in [SVF09]. The framework utilizes embedded Markov chains to model the behavior of the nodes. Throughput is defined as the rate a source node is able to send data packets to a destination node to which no multihop path exists. Instead, moving nodes are used to store and carry messages from one cliques within the network to another. Mobility is modeled via random direction (see also [SF08]) and two versions of the random waypoint model.

In the paper [JMR10] Jacquet *et al.* derive theoretical upper bounds for the *information propagation speed* in delay tolerant networks. Mobility is modeled via the random waypoint model, the random walk model, and Brownian motion. The results are also derived for one- and three-dimensional networks.

Chapter 6

Conclusion and Future Work

In the thesis at hand we focused on modeling different aspects of wireless networks. The motivation for these investigations was that realistic and accurate models are the main ingredient when performing simulations of wireless networks. Since such simulations are a very important aspect of developing new protocols, methods and techniques for wireless networks, it is imminent that such models are of great importance within the research community.

The research questions addressed were manifold:

1. How can nodes of a network be placed on a given area to realistically reflect the behavior of real network nodes?
2. How can we measure the inhomogeneity of a given node distribution?
3. How does interference change over time and space?
4. What is the impact of interference on the overall throughput of a wireless network?

By giving attention to the first two questions we came to the conclusion that users do not uniformly distribute over a given area, which contradicts to the assumptions made in many studies performed on wireless networks. From a spatial viewpoint, there seem to be locations that attract several users, while other locations are rarely visited. From a node viewpoint, there are often nodes quite isolated while others tend to be in groups.

Therefore, we perceived the need for a model that allows to inhomogeneously distribute nodes on a given area. The model proposed in Chapter 3.1 generates node distributions with different inhomogeneity levels depending on two scalar parameters. By using these parameters it is possible to generate a broad range of node distributions, from distributions with a few large clusters to distributions with many small clusters. These inhomogeneity levels can be measured by a metric proposed within Chapter 3.2. This inhomogeneity measure has been compared to human perception

by means of an online survey and showed a good match. By applying these two tools it is easily possible to generate a node distribution that possesses all desired properties as, e.g., number of nodes, inhomogeneity level, cluster size, etc.

The third research question was discussed in Chapter 4. There, we derived closed-form expressions for the temporal correlation of interference in wireless networks. For that purpose we considered three sources of correlation — node locations, channel, and traffic — and based the analysis on commonly-used modeling assumptions, as homogeneously distributed nodes, Rayleigh block fading, and slotted ALOHA. This work can be considered as an extension of results published by Haenggi *et al.* in [GH09a, HG09, Hae09]. Our investigations have shown that the temporal correlation of interference, under the given assumptions, only depend on the sending probability, the message duration, and the radio channel's temporal behavior. Node density and distribution, transmission power, and receiver sensitivity have no influence on the temporal correlation of interference.

Finally, the last research question was answered by a simulation based study presented in Chapter 5, which compared time and space-time diversity techniques to conventional communication methods. The results show that in an interference limited scenario, methods that reduce the overall interference as, e.g., higher modulation schemes, are able to increase the overall network throughput significantly. They are even performing better than many space-time diversity techniques, which have the disadvantage of causing a lot of interference especially in very harsh fading environments.

Regarding correlation of interference, more interesting research can be conducted in the future. This comprises several possibilities: First, the results presented in Chapter 4 can be generalized with regard to the offset of the two compared time instants, the fading model, the MAC protocol, and the node distribution. Second, it could be of interest to derive the spatial correlation for two given locations in the area for all cases addressed in Chapter 4. Third, the impact of interference correlation on the correlation of outage could be investigated, which can then be applied to performance analyses of time and space-time diversity methods. These formal analyses could be used to backup the simulation results presented in the case study in Chapter 5.

Appendix A

Simulations of Inhomogeneous Node Distributions

In the following we are going to compare the stochastic properties derived in Section 3.1.2 to the outcome of our simulations. In order to get representative data we have simulated 25000 nodes on an area with size 100×100 length units, which gives $\lambda = 2.5$, and $r = 2$. k was chosen in a way that at most 99.9% and at least 10% of the nodes survive, which can be achieved by $k \in \{17, \ldots, 38\}$. With only 10% or less of the initial nodes remaining a comparison to simulations has no meaning since the samples are too scattered.

Tables A.1 and A.2 compare simulated and calculated results with each other. The first column of Table A.1 presents the number of nodes remaining after thinning.

Table A.1: Comparison of simulated and calculated values, part 1.

	Remaining Nodes			**Common neighbors**		
k	Sim	Calc	%	Sim	Calc	%
17	24962	24952,8	0,04	28,2096	28,3067	0,34
18	24891	24907,7	0,07	28,2559	28,3302	0,26
19	24839	24828,9	0,04	28,3565	28,3685	0,04
20	24681	24698,6	0,07	28,4217	28,4277	0,02
21	24569	24493,9	0,31	28,4000	28,5145	0,40
22	24188	24187,7	0,00	28,5719	28,6357	0,22
23	23753	23750,5	0,01	28,7501	28,7978	0,17
24	23128	23153,3	0,11	29,0248	29,0058	0,07
25	22375	22371,5	0,02	29,2225	29,2637	0,14
26	21441	21389,2	0,24	29,4978	29,5732	0,26
27	20032	20202,1	0,85	30,1372	29,9346	0,68
28	18710	18821,0	0,59	30,5124	30,3467	0,55
29	17192	17271,3	0,46	30,8791	30,8071	0,23
30	15468	15592,6	0,81	31,5554	31,3126	0,78
31	13668	13834,6	1,22	32,2497	31,8594	1,23
32	11954	12053,1	0,83	32,7710	32,4438	1,01
33	10280	10304,0	0,23	33,6112	33,0618	1,66
34	8543	8638,9	1,12	34,0361	33,7098	0,97
35	6959	7100,4	2,03	34,6040	34,3843	0,64
36	5826	5719,4	1,83	35,7125	35,0823	1,80
37	4822	4514,3	6,38	36,1572	35,8010	0,99
38	3681	3491,0	5,16	37,1587	36,5378	1,70

Table A.2: Comparison of simulated and calculated values, part 2.

	1st neighbor correlation			2nd neighbor correlation			Neighbor distance		
k	Sim	Calc	%	Sim	Calc	%	Sim	Calc	%
17	0,9992	0,9990	0,02	0,9978	0,9990	0,12	0,3158	0,3164	0,19
18	0,9977	0,9982	0,05	0,9951	0,9980	0,29	0,3176	0,3165	0,33
19	0,9965	0,9969	0,04	0,9930	0,9965	0,36	0,3164	0,3167	0,11
20	0,9938	0,9947	0,10	0,9874	0,9941	0,68	0,3186	0,3170	0,50
21	0,9913	0,9916	0,04	0,9832	0,9904	0,73	0,3185	0,3175	0,33
22	0,9858	0,9873	0,15	0,9719	0,9852	1,37	0,3181	0,3181	0,02
23	0,9805	0,9815	0,11	0,9633	0,9783	1,55	0,3193	0,3190	0,12
24	0,9721	0,9741	0,20	0,9461	0,9692	2,45	0,3190	0,3199	0,31
25	0,9608	0,9649	0,43	0,9289	0,9580	3,12	0,3204	0,3211	0,20
26	0,9509	0,9539	0,32	0,9062	0,9444	4,22	0,3220	0,3223	0,09
27	0,9388	0,9412	0,25	0,8885	0,9285	4,50	0,3198	0,3258	1,88
28	0,9243	0,9268	0,26	0,8615	0,9105	5,69	0,3238	0,3282	1,35
29	0,9094	0,9108	0,15	0,8336	0,8904	6,81	0,3271	0,3308	1,12
30	0,8939	0,8934	0,06	0,8124	0,8685	6,91	0,3275	0,3335	1,83
31	0,8778	0,8748	0,35	0,7775	0,8451	8,69	0,3277	0,3363	2,64
32	0,8626	0,8551	0,87	0,7565	0,8203	8,44	0,3306	0,3391	2,57
33	0,8458	0,8346	1,33	0,7261	0,7944	9,40	0,3305	0,3417	3,39
34	0,8224	0,8134	1,10	0,6905	0,7677	11,18	0,3406	0,3441	1,02
35	0,8007	0,7916	1,13	0,6513	0,7404	13,67	0,3531	0,3461	1,99
36	0,8015	0,7695	3,99	0,6561	0,7127	8,62	0,3476	0,3477	0,02
37	0,7712	0,7472	3,12	0,6140	0,6848	11,53	0,3559	0,3607	1,35
38	0,7576	0,7247	4,35	0,5976	0,6569	9,92	0,3709	0,3636	1,94

The number of nodes remaining in the simulation (Sim) differs only slightly from the calculated expectation (Calc) for smaller values of k. The relative deviation is given in percent. As k increases the number of nodes remaining fluctuates a lot from simulation to simulation and thus the deviation becomes bigger.

The second column of Table A.1 presents the number of neighbors a node and its nearest neighbor have in common. As before, the simulated (Sim) and calculated (Calc) values are compared and the relative difference in percent is given in the column titled %. Again, the calculated values are closer to the simulation results for smaller values of k.

In Equation (3.21) in Section 3.1.2.5 we use the survival correlation between a node and its i^{th} nearest neighbor. The simulated and calculated probabilities that the first and second nearest neighbor survive are listed in the first two columns of Table A.2, respectively.

The nearest neighbor distance in the original distribution does not depend on k and is therefore not listed in the table. In the simulation the mean nearest neighbor distance was 0.3165 while the calculated value is 0.3162 and thus only shows a relative deviation of 0.09%.

The third column of Table A.2 shows the simulated nearest neighbor distances (Sim) in the inhomogeneous distribution and their calculated expectation (Calc). Our approximation is relatively good for smaller values of k but worsens a bit as more nodes are removed.

List of Symbols

A	Area.
a	Horizontal size of A.
$A_{0e}^{(l)}$	Subarea of C_l that is not common with node N_l.
$A_c^{(l)}$	Common area of node N_0 and node N_l.
$A_{ce}^{(l)}$	Common area of node N_0 and node N_l within C_l.
A_i	Subarea index i in a segmentation.
A'_j	Subarea index i in a refined segmentation.
$a_n(t)$	Amplitude of an electromagnetic wave at time instant t.
B	Bandwidth occupied by a single transmission.
$\mathcal{B}$	Set of possible block IDs.
b	Vertical size of A.
b_r	Bitrate of a single transmission.
$B_{n,p}$	Binomial distribution with parameters n and p.
c	Channel coherence time in slots.
c'	Channel coherence time in time units.
c_j	Duration in slots the channel stays unchanged after time slot j.
C_l	Circle around node N_0 with radius $d(N_0, N_l)$.
D	The destination node of a given transmission.
d	Distance.
$d(\cdot, \cdot)$	Distance metric.
D_i	Random distance between the nodes N_0 and N_i.
d_i	Distance between the nodes N_0 and N_i.
$d_{\max}$	Maximum transmission range.
D_l	Random variable denoting the distance to the l^{th} neighbor in an homogeneous point process.
d_{ref}	Reference distance.
$d_w(\cdot, \cdot)$	Wrap-around distance metric.
$\mathcal{E}$	Set of excluded block IDs.
$\mathbb{E}(\cdot)$	Expected value.
$\overline{\mathbb{E}}(\cdot)$	Upper bound of an expected value.
$\underline{\mathbb{E}}(\cdot)$	Lower bound of an expected value.
$\hat{\mathbb{E}}(\cdot)$	Approximation of an expected value.
E_b	Energy per transmitted bit.

E_s	Energy per transmitted symbol.
f_0	Transmission frequency.
f_0'	Doppler frequency.
$f_{d(N_1,N_i)}(d)$	Probability density function of the distance between the nodes N_1 and N_i.
$f_{D_l}(d)$	Probability density function of l^{th} neighbor in an homogeneous point process.
$f_{D_k'}(d)$	Probability density function of l^{th} neighbor in an inhomogeneous point process.
$F_r(\Delta t)$	The autocorrelation function of the channel.
$F_{r_I}(\Delta t)$	The autocorrelation function of the in-phase component $r_I(t)$.
$F_{r_Q}(\Delta t)$	The autocorrelation function of the quadrature component $r_Q(t)$.
$F_{r_I,r_Q}(\Delta t)$	The crosscorrelation function of the channel.
$\vec{G}$	The random vector of all values G_i.
$\vec{g}$	A realization of the random vector $\vec{G}$.
G_i	The random number of nodes within circle i in the interference model.
g_i	The i^{th} element of the vector $\vec{g}$.
g_r	The antenna gain of the receiver.
g_{ref}	Reference gain.
$g_s^{(\text{dB})}$	The gain caused by shadowing in (dB).
g_s	The gain caused by shadowing (linear).
g_t	The antenna gain of the transmitter.
h	Channel state.
$I(\cdot)$	Interference power.
$\overline{I}(\mathcal{S},d)$	Upper bound for the interference.
$\underline{I}(\mathcal{S},d)$	Lower bound for the interference.
$I_0(z)$	The modified Bessel function of order zero.
I_{10}	Interference caused by the nodes in the set $\mathcal{S}_{10}$.
I_{01}	Interference caused by the nodes in the set $\mathcal{S}_{01}$.
I_{11}	Interference caused by the nodes in the set $\mathcal{S}_{11}$.
I_{11}^*	Interference caused by the nodes in the set $\mathcal{S}_{11}^*$.
I_{11}^{**}	Interference caused by the nodes in the set $\mathcal{S}_{11}^{**}$.
I_{11}'	Interference caused by the nodes in the set $\mathcal{S}_{11}'$.
I_{11}''	Interference caused by the nodes in the set $\mathcal{S}_{11}''$.
I_i	Interval for possible bit error probabilities.
$I_{\max}(d)$	Maximum interference in order to achieve at least a given data rate.
K	Random variable of the number of neighbors of a node.
k	Minimum number of neighbors for surviving the thinning process.
K_i	The i^{th} circle in the interference model.
L	Traffic load.
$l(\cdot)$	Path loss function.
$\mathcal{M}$	Set of all sequences.

m	Parameter for Nakagami fading.
(m_i)	A sequence.
$\|m_i\|$	Length of the sequence in blocks.
$\|\|m_i\|\|$	Length of the sequence in time slots.
$\mathcal{N}$	Poisson point process of the node locations.
n	Number of nodes.
$\bar{n}(z)$	Expected number of nodes in each subarea in a segmentation.
n'	Number of nodes after the thinning process.
N_0	Spectral noise density.
n_i	Number of nodes in subarea A_i.
$\bar{n}_i(z)$	Expected number of nodes in subarea i of a segmentation.
$n_{i,(x_o,y_o)}$	Number of nodes in subarea A_i for a segmentation with offset (x_o, y_o).
$n'_{j,(x,y)}$	Number of nodes in subarea A_i for a refined segmentation with offset (x_o, y_o).
$N(a_i, b_i]$	Number of events in the interval $(a_i, b_i]$.
N_i	Some node.
n_s	Number of currently sending nodes.
$n_s^{(i)}$	Number of currently sending nodes not located within the first i circle rings.
$\mathcal{N}_{\text{fail}}$	Set of all possible distributions of nodes on circle rings such that the interference caused by them is above a certain threshold.
$\mathcal{N}_{\text{ok}}$	Set of all possible distributions of nodes on circle rings such that the interference caused by them is below a certain threshold.
N_{μ,σ^2}	Normal distribution with mean μ and variance σ^2.
p	Transmission probability.
$\mathbb{P}(\cdot)$	Probability.
$\overline{\mathbb{P}}(\cdot)$	Upper bound of a probability.
$\underline{\mathbb{P}}(\cdot)$	Lower bound of a probability.
p_b	Bit error probability.
$p_c^{(l)}$	Probability that a node is located within $A_c^{(l)}$.
$p_{ce}^{(l)}$	Probability that a node is located within $A_{ce}^{(l)}$.
p_c	Fraction of nodes of $\mathcal{S}_{11}$ that are within $\mathcal{S}'_{11}$.
p_{col}	Collision probability.
p_{com}	Probability that a neighbor of N_0 is also a neighbor of N_1.
P_i	Waypoint distribution in the inhomogeneous RWP model.
$p_i(d, \theta)$	Probability for a node being in the i^{th} circle ring around node N_0.
p_p	Packet error probability.
p_r	Reception power.
$p_r^{\min}$	Receiver sensitivity.
p_s	Symbol error probability.
p_t	Transmission power.
P_λ	Poisson distribution with parameter λ.
q	Number of circles considered in the interference model.

r	Neighborhood radius.
$r_i(d,\theta)$	Radius of the i^{th} circle in the circle based interference model.
r_I	Interference radius.
$r_I(t)$	In-phase component of a received electromagnetic wave.
$r_Q(t)$	Quadrature component of a received electromagnetic wave.
$\mathcal{S}$	Set of all sending nodes.
S	The source node of a given transmission.
s	Duration of a single transmission in time slots.
SNR	Signal to noise ratio.
SIR	Signal to interference ratio.
SINR	Signal to interference and noise ratio.
$\mathcal{S}_{10}$	Nodes transmitting in time slot $t-1$ but not in time slot t.
$\mathcal{S}_{01}$	Nodes transmitting in time slot t but not in time slot $t-1$.
$\mathcal{S}_{11}$	Nodes transmitting in both time slots $t-1$ and t.
$\mathcal{S}_{11}^{*}$	Subset of the nodes in $\mathcal{S}_{11}$ that transmit the same message in both time slots.
$\mathcal{S}_{11}^{**}$	Subset of the nodes in $\mathcal{S}_{11}$ that transmit two different messages in the two time slots.
$\mathcal{S}_{11}'$	Subset of the nodes in $\mathcal{S}_{11}$ that have the same channel conditions in both time slots.
$\mathcal{S}_{11}''$	Subset of the nodes in $\mathcal{S}_{11}$ that have different channel conditions in the two time slots.
S_{10}	The fraction of nodes within set $\mathcal{S}_{10}$.
S_{01}	The fraction of nodes within set $\mathcal{S}_{01}$.
S_{11}	The fraction of nodes within set $\mathcal{S}_{11}$.
S_{11}^{*}	The fraction of nodes within set $\mathcal{S}_{11}^{*}$.
S_{11}^{**}	The fraction of nodes within set $\mathcal{S}_{11}^{**}$.
S_{11}'	The fraction of nodes within set $\mathcal{S}_{11}'$.
S_{11}''	The fraction of nodes within set $\mathcal{S}_{11}''$.
T	The temperature in K.
$\mathcal{T}$	Inhomogeneous node distribution on a finite area.
t	Current time (slot).
$t-1$	Previous time slot.
T_b	Time duration of the transmission of one bit.
T_i	Random moving duration for mobility models.
T_s	Time duration of the transmission of one symbol.
$T_{p,i}$	Random pause time in the inhomogeneous RWP model for node i.
T_p	Common random pause time in the inhomogeneous RWP.
T_{fail}	The event that a transmission fails.
T_{ok}	The event that a transmission succeeds.
$T_x(S)$	Indicator variable that is equal to 1 for $x \in S$ and equal to 0 otherwise.
$\mathcal{U}$	Homogeneous node distribution on a finite area.

v	Vector of values of $\{0,1\}$, where v_i indicates that node N_i survives the thinning process.
$V(k-1)$	Set of all vectors v with $k-1$ elements being equal to 1.
v_0	Speed of a node.
v_c	The speed of light.
V_i	Random velocity.
$v_{\max}$	Maximum value for the random velocity.
$v_{\min}$	Minimum value for the random velocity.
w	Weight for the weighted sum of the inhomogeneity measure.
x_o	Offset in x-direction.
y_o	Offset in y-direction.
z	Segmentation index for the inhomogeneity measure.
z'	Segmentation index for refined segmentation.
$z_{\max}$	Maximal refined segmentation.
α	Path loss exponent.
β	Movement angle of destination in relation to the source.
γ_b	SNR per bit.
$\bar{\gamma}_b$	Average SNR per bit.
γ_s	SNR per symbol.
$\bar{\gamma}_s$	Average SNR per symbol.
δ	Packet duration in time units.
Δi	The granularity of the circle model.
Δp	The granularity of the bit error probability intervals.
Θ	Throughput of a MAC protocol.
θ	Threshold value for SNR/SINR.
κ	The Boltzmann constant.
λ	Node density.
λ_T	Traffic density.
μ	Expected number of neighbors of a node.
ν	Parameter for Rician fading.
ρ	Correlation coefficient.
σ^2	Variance of the Gaussian distribution used for modeling fading.
σ_s^2	Variance of the Gaussian distribution used for modeling shadowing.
τ	Common moving duration for mobility models.
$\tau_n(t)$	Delay of the n^{th} multipath component at time t.
Φ_i	Random angle for mobility models.
ϕ_0	Phase offset.
$\phi_n(t)$	Phase of the n^{th} multipath component at time t.
$\phi_{D_n}(t)$	Doppler shift of the n^{th} multipath component at time t.
ψ	Inhomogeneity measure.
$\psi(z)$	Inhomogeneity measure for a given segmentation.
$\psi_{(x_o,y_o)}(z)$	Inhomogeneity measure for a given segmentation and a given offset.

List of Own Publications

[1] C. Bettstetter, M. Gyarmati, and U. Schilcher. An inhomogeneous node distribution and its stochastic properties. In *Proc. ACM/IEEE Intern. Symp. on Modeling, Analysis, and Simuation of Wireless and Mobile Systems (MSWiM)*, Chania, Greece, October 2007.

[2] U. Schilcher, M. Gyarmati, C. Bettstetter, Y. W. Chung, and Y. H. Kim. Measuring inhomogeneity in spatial distributions. In *Proc. IEEE Vehicular Technology Conference (VTC)*, pages 2690–2694, Singapore, May 2008.

[3] M. Gyarmati, U. Schilcher, G. Brandner, C. Bettstetter, Y. W. Chung, and Y. H. Kim. Impact of random mobility on the inhomogeneity. In *Proc. IEEE Global Comm. Conf. (GLOBECOM)*, New Orleans, LA, USA, December 2008.

[4] G. Brandner, U. Schilcher, M. Gyarmati, and C. Bettstetter. Non-colliding first messages in slotted aloha: Further insights toward a practical solution. In *Proc. IEEE Vehicular Technology Conf. (VTC)*, Barcelona, Spain, April 2009.

[5] S. Crisóstomo, U. Schilcher, C. Bettstetter, and J. Barros. Analysis of probabilistic flooding: How do we choose the right coin? In *Proc. IEEE Intern. Conf. on Communications (ICC)*, Dresden, Germany, June 2009.

[6] G. Brandner, U. Schilcher, and C. Bettstetter. Extended abstract: Radio channel measurements: First results of a car-to-car scenario. In *Proc. ACM Annual Intern. Conf. on Mobile Computing and Networking (MobiCom)*, Beijing, China, September 2009.

[7] U. Schilcher, M. Gyarmati, G. Brandner, and C. Bettstetter. Extended abstract: Modeling interference in wireless networks. In *Proc. ACM Annual Intern. Conf. on Mobile Computing and Networking (MobiCom)*, Beijing, China, September 2009.

[8] G. Brandner, U. Schilcher, and C. Bettstetter. Cooperative relaying in car-to-car communications: Initial results from an experimental study. In *Proc. IEEE Intern. Symp. on Communications, Control, and Signal Processing (ISCCSP)*, Limassol, Cyprus, March 2010.

[9] U. Schilcher, G. Brandner, and C. Bettstetter. Diversity schemes in interference-limited wireless networks with low-cost radios. In *Proc. IEEE Wireless Communications and Networking Conf. (WCNC)*, Cancún, Mexico, March 2011.

[10] U. Schilcher, C. Bettstetter, and G. Brandner. Temporal correlation of interference in wireless networks with Rayleigh fading. *Submitted to IEEE Trans. on Mobile Computing*, 2011.

[11] S. Crisóstomo, U. Schilcher, C. Bettstetter, and J. Barros. Probabilistic flooding in stochastic networks: Analysis of global information outreach. *Submitted to Elsevier Journal of Computer Networks*, 2011.

Curriculum Vitae

Personal Information

Name:	Udo Schilcher
Degree:	DDI
Address:	Plescherken 15a 9074 Keutschach Austria
Date of birth:	11.01.1978
Place of birth:	Wolfsberg
Phone:	+43-676-5294191
E-mail:	udo.schilcher@uni-klu.ac.at
Citizenship:	Austria

Education

1997	Graduation diploma at the HTBLVA Villach IT and organization
Oct. 1997 – May 1998	Military service at the Lutschounigkaserne Villach
Oct. 1998 - Apr. 2005	Study of Applied Informatics, University of Klagenfurt Master degree with distinction, Title of the thesis: 'The IKEv2 protocol and its extensions' Supervisor: Prof. Dr. Patrick Horster
Oct. 2003 - Mar. 2004	Internship at the Siemens AG, Munich Implementation of the EAP-IKEv2 protocol Supervisor: DI Hannes Tschofenig
Mar. 2000 - May 2006	Study of Technical Mathematics, University of Klagenfurt Master degree with distinction, Title of the thesis: 'The Factorization of Integers' Supervisor: Prof. Dr. Johannes Schoissengeier
Since Dec. 2005	PhD at the Mobile Systems Group, University of Klagenfurt Supervisor: Prof. Dr.-Ing. Christian Bettstetter

Professional Experience

1997 - 2004	During summer job as a programmer, PATRIA / Frantschach AG / Mondi Packaging Frantschach-St. Gertraud, Austria
Since Dec. 2005	Scientific and teaching staff member, Mobile Systems group, Institute of Networked and Embedded Systems, University of Klagenfurt – Performed research on many different aspects of Mobile Systems leading to several international publications (see list below). – Taught courses in Mobile and Wireless Systems and Network Simulation over 4 years. – Participated in system administration tasks.
Since Oct. 2010	Teacher for Mathematics (side job) at the adult education center (Kärntner Volkshochschulen) Klagenfurt, Austria

Additional Skills and Experiences

English
Scientific working
Teaching undergraduate courses

Social competences

Working in Teams
Empathy
Flexibility

Hobbys

Martial arts (Taekwondo, Karate)
Cycling, Jogging, Dancing
Playing e-guitar

Bibliography

[3GPP10] 3GPP. TS 36.211 v10.0.0: Evolved universal terrestrial radio access (E-UTRA); physical channels and modulation. *www.3gpp.org*, December 2010.

[Abr70] N. Abramson. The ALOHA system: Another alternative for computer communications. In *Proc. Fall Joint Comput. Conf. of the AFIPS*, volume 37, pages 281–285, Houston, TX, USA, November 1970.

[ABS08] H. Adam, C. Bettstetter, and S. M. Senouci. Adaptive relay selection in cooperative wireless networks. In *Proc. IEEE Intern. Symp. on Personal, Indoor and Mobile Radio Communications (PIMRC)*, pages 1–5, Cannes, France, September 2008.

[ABS09] H. Adam, C. Bettstetter, and S. M. Senouci. Multi-hop-aware cooperative relaying. In *Proc. IEEE Vehicular Technology Conf. (VTC)*, pages 1–5, Barcelona, Spain, April 2009.

[Ada97] A. Adas. Traffic models in broadband networks. *IEEE Commun. Mag.*, 35(7):82–89, July 1997.

[AEBS09] H. Adam, W. Elmenreich, C. Bettstetter, and S. M. Senouci. CoRe-MAC: A MAC-protocol for cooperative relaying in wireless networks. In *Proc. IEEE Global Telecommunications Conf. (GLOBECOM)*, pages 1–6, Honolulu, HI, USA, December 2009.

[AGL09a] G. Alfano, M. Garetto, and E. Leonardi. Capacity scaling of wireless networks with inhomogeneous node density: Lower bounds. In *Proc. IEEE Infocom*, pages 1890–1898, Rio de Janeiro, Brazil, April 2009.

[AGL09b] G. Alfano, M. Garetto, and E. Leonardi. Capacity scaling of wireless networks with inhomogeneous node density: upper bounds. *IEEE J. Select. Areas Commun.*, 27(7):1147–1157, 2009.

[AGLM10] G. Alfano, M. Garetto, E. Leonardi, and V. Martina. Capacity scaling of wireless networks with inhomogeneous node density: Lower bounds. *IEEE/ACM Trans. Networking*, 18(5):1624–1636, October 2010.

[AHP99] B. O. Adrian, S.-G. Haggman, and A. Pietila. Study of the impact of non-uniform spatial traffic distribution on the system parameters of cdma cellular networks. In *Proc. IEEE Intern. Conf. on Personal Wireless Communication*, pages 394–398, Jaipur, India, 1999.

[Ala98] S. M. Alamouti. A simple transmit diversity technique for wireless communications. *IEEE J. Select. Areas Commun.*, 16(8):1451–1458, October 1998.

[Ali96] A. A. Ali. Optimum time diversity for channels subject to pulse-burst interference. *IEE Proc. Communications*, 143(1):43–46, February 1996.

[AM01] D. Avidor and S. Mukherjee. Hidden issues in the simulation of fixed wireless systems. *ACM Wireless Netw.*, 7(2):187–200, April 2001.

[AM08] G. Atia and A. Molisch. Cooperative relaying with imperfect channel state information. In *Proc. IEEE Global Telecommunications Conf. (GLOBECOM)*, pages 1–6, New Orleans, LA, USA, December 2008.

[AvB87] J. Arnbak and W. van Blitterswijk. Capacity of slotted ALOHA in Rayleigh-fading channels. *IEEE J. Select. Areas Commun.*, 5(2):261–269, February 1987.

[AY07] A. Adinoyi and H. Yanikomeroglu. Cooperative relaying in multi-antenna fixed relay networks. *IEEE Trans. Wireless Commun.*, 6(2):533–544, February 2007.

[Bak41] G. A. Baker. Test of homogeneity for normal populations. *The Annals of Mathematical Statistics*, 12(2):233–236, June 1941.

[BB97] A. Baier and K. Bandelow. Traffic engineering and realistic network capacity in cellular radio networks with inhomogeneous traffic distribution. In *Proc. IEEE Vehicular Technology Conf. (VTC)*, pages 780–784, May 1997.

[BBV08] C. Bettstetter, G. Brandner, and R. Vilzmann. On colliding first messages in slotted ALOHA. In *Proc. IEEE Intern. Symp. on Personal, Indoor and Mobile Radio Commun. (PIMRC)*, Cannes, France, March 2008.

[Bet01] C. Bettstetter. Mobility modeling in wireless networks: Categorization, smooth movement, and border effects. *ACM Mobile Computing and Commun. Rev.*, 5(3):55–67, July 2001.

[Bet02] C. Bettstetter. On the minimum node degree and connectivity of a wireless multihop network. In *Proc. ACM Intern. Symp. on Mobile Ad Hoc Networking and Computing (MobiHoc)*, Lausanne, Switzerland, June 2002.

[Bet04] C. Bettstetter. On the connectivity of ad hoc networks. *The Computer Journal*, 47(4):432–447, July 2004. Oxford University Press.

[BHPC04] C. Bettstetter, H. Hartenstein, and X. Pérez-Costa. Stochastic properties of the random waypoint mobility model. *ACM Wireless Networks*, 10(5):555–567, September 2004.

[BL02] M. Borschbach and W. M. Lippe. A model of inhomogeneity for ad hoc networks. In *IEEE Intern. Conf. on Networks (ICON)*, pages 255–260, Grand Copthorne Waterfront, Singapore, 2002.

[BR04] P. Basu and J. Redi. Effect of overhearing transmissions on energy efficiency in dense sensor networks. In *Proc. ACM Intern. Symp. on Information Processing in Sensor Networks (IPSN)*, pages 196–204, Berkeley, CA, USA, April 2004.

[BRS02] D. M. Blough, G. Resta, and P. Santi. A statistical analysis of the long-run node spatial distribution in mobile ad hoc networks. In *Proc. ACM Workshop on Modeling Analysis and Simulation of Wireless and Mobile Systems (MSWiM)*, pages 30–37, Atlanta, GA, USA, September 2002.

[BRS03] C. Bettstetter, G. Resta, and P. Santi. The node distribution of the random waypoint mobility model for wireless ad hoc networks. *IEEE Trans. Mobile Comput.*, 2(3):257–269, July–September 2003.

[BvRWZ04] M. Burkhart, P. von Rickenbach, R. Wattenhofer, and A. Zollinger. Does topology control reduce interference? In *Proc. ACM Intern. Symp. on Mobile ad hoc Networking and Computing (MobiHoc)*, pages 9–19, Tokyo, Japan, May 2004.

[BZ02] C. Bettstetter and J. Zangl. How to achieve a connected ad hoc network with homogeneous range assignment: An analytical study with consideration of border effects. In *Proc. IEEE Intern. Conf. on Mobile and Wireless Commun. Networks (MWCN)*, pages 125–129, Stockholm, Sweden, September 2002.

[CB97] M. E. Crovella and A. Bestavros. Self-similarity in world wide web traffic: evidence and possible causes. *IEEE/ACM Trans. Networking*, 5(6):835–846, December 1997.

[Cla68] R. H. Clarke. A statistical theory of mobile-radio reception. *Bell Syst. Tech. J.*, 47(6):957–1000, July–August 1968.

[Cox55] D. R. Cox. Some statistical methods related with series of events. *J. Royal Statistics Soc.*, 17:129–157, 1955.

[Cre91] N. A. C. Cressie. *Statistics for Spatial Data*. Wiley, 1991.

[CS01] K.-H. Chiang and N. Shenoy. A random walk mobility model for location management in wireless networks. In *Proc. IEEE Intern. Symp. on Personal, Indoor and Mobile Radio Communications (PIMRC)*, volume 2, pages E–43–E–48, San Diego, CA, USA, October 2001.

[DBT05] O. Dousse, F. Baccelli, and P. Thiran. Impact of interferences on connectivity in ad hoc networks. *IEEE/ACM Trans. Netw.*, 13(2):425–436, April 2005.

[DDKS00] N. D. Doulamis, A. D. Doulamis, G. E. Konstantoulakis, and G. I. Stassinopoulos. Efficient modeling of VBR MPEG-1 coded video sources. *IEEE Trans. on Circuits and Systems for Video Technology*, 10(1):93–112, February 2000.

[DHDA04] M. Dohler, M. Hussain, A. Desai, and H. Aghvami. Performance of distributed space-time block codes. In *Proc. IEEE Vehicular Technology Conf. (VTC)*, volume 2, pages 742–746, Milan, Italy, May 2004.

[DiP89] R. C. DiPietro. An FFT based technique for suppressing narrow-band interference in PN spread spectrum communications systems. In *Proc. Intern. Conf. on Acoustics, Speech, and Signal Processing (ICASSP)*, volume 2, pages 1360–1363, Glasgow, Scotland, UK, May 1989.

[DJC+92] P. B. Danzig, S. Jamin, R. Cceres, D. J. Mitzel, and D. Estrin. An empirical workload model for driving wide-area tcp/ip network simulations. *Internetworking: Research and Experience*, 3:1–26, September 1992.

[DTH02] O. Dousse, P. Thiran, and M. Hasler. Connectivity in ad-hoc and hybrid networks. In *Proc. IEEE Joint Conf. of the IEEE Computer and Communications Societies (INFOCOM)*, volume 2, pages 1079–1088, Shanghai, China, November 2002.

[DVJ03] D. J. Daley and D. Vere-Jones. *An Introduction to the Theory of Point Processes, Volume I: Elementary Theory and Methods.* Springer, 2nd edition, 2003.

[DVJ08] D. J. Daley and D. Vere-Jones. *An Introduction to the Theory of Point Processes, Volume II: General Theory and Structure.* Springer, 2nd edition, 2008.

[DW09] H. Dang and H. Wu. Mobility models for delay-tolerant mobile networks. In *Proc.Intern. Conf. on Sensor Technologies and Applications (SENSORCOMM)*, pages 55–60, Athens, Greece, June 2009.

[Ein56] A. Einstein. *Investigations on the Theorey of Brownian Movement.* Dover, 1956.

[Eth05] IEEE std 802.3 - 2005 part 3: Carrier sense multiple access with collision detection (CSMA/CD) access method and physical layer specifications. *IEEE Std 802.3-2005 (Revision of IEEE Std 802.3-2002 including all approved amendments)*, pages 1–594, December 2005.

[Fär02] J. Färber. Network game traffic modelling. In *Proc. Workshop on Network and system support for games (NetGames)*, pages 53–57, Braunschweig, Germany, April 2002.

[Fri46] H. T. Friis. A note on a simple transmission formula. *Proc. of the IRE*, 34(5):254–256, May 1946.

[GE07] D. Gündüz and E. Erkip. Source and channel coding for cooperative relaying. *IEEE Trans. Inform. Theory*, 53(10):3454–3475, October 2007.

[GGL08] M. Garetto, P. Giaccone, and E. Leonardi. Capacity scaling of sparse mobile ad hoc networks. In *Proc. IEEE Infocom*, pages 206–210, Phoenix, AZ, USA, April 2008.

[GGL09] M. Garetto, P. Giaccone, and E. Leonardi. Capacity scaling in ad hoc networks with heterogeneous mobile nodes: The super-critical regime. *IEEE/ACM Transactions on Networking*, 17(5):1522–1535, October 2009.

[GH09a] R. K. Ganti and M. Haenggi. Spatial and temporal correlation of the interference in ALOHA ad hoc networks. *IEEE Commun. Letters*, 13(9):631–633, September 2009.

[GH09b] B. Gu and X. Hong. Mobility identification and clustering in sparse mobile networks. In *Proc. IEEE Military Communications Conf. (MILCOM)*, pages 1–7, Boston, MA, USA, October 2009.

[Gil65] E. N. Gilbert. Energy reception for mobile radio. *Bell Syst. Tech. J.*, 44(8):1779–1803, October 1965.

[GKMM06] S. Gormus, D. Kaleshi, J. McGeehan, and A. Munro. Performance comparison of cooperative and non-cooperative relaying mechanisms in wireless networks. In *Proc. IEEE Wireless Commun. and Netw. Conf. (WCNC)*, volume 2, pages 890–896, Las Vegas, NV, USA, April 2006.

[Gol05] A. Goldsmith. *Wireless Communications*. Cambridge University Press, 2005.

[GRC03] X. Guo, S. Roy, and W. S. Conner. Spatial reuse in wireless ad-hoc networks. In *Proc. IEEE Vehicular Technology Conf. (VTC)*, volume 3, pages 1437–1442, Orlando, FL, USA, October 2003.

[GSN05] B. Gloss, M. Scharf, and D. Neubauer. A more realistic random direction mobility model. In *Proc. COST 290 Management Committee Meeting*, Würzburg, Germany, October 2005.

[GT02] M. Grossglauser and D. N. C. Tse. Mobility increases the capacity of ad hoc wireless networks. *IEEE/ACM Trans. Networking*, 10(4):477–486, August 2002.

[GV93] C. Gerthsen and H. Vogel. *Physik*. Springer, 17th edition, 1993.

[GV02] M. Gastpar and M. Vetterli. On the capacity of wireless networks: The relay case. In *Proc. IEEE INFOCOM*, volume 3, pages 1577–1586, November 2002.

[Hae05] M. Haenggi. On distances in uniformly random networks. *IEEE Trans. Inform. Theory*, 51:3584–3586, October 2005.

[Hae09] M. Haenggi. Outage, local throughput, and capacity of random wireless networks. *IEEE Trans. Wireless Commun.*, 8(8):4350–4359, August 2009.

[Ham02] K. A. Hamdi. Exact probability of error of BPSK communication links subjected to asynchronous interference in Rayleigh fading environment. *IEEE Trans. Commun.*, 50(10):1577–1579, October 2002.

[HC96] T.-S. Ho and K.-C. Chen. Performance analysis of IEEE 802.11 CSMA/CA medium access control protocol. In *Proc. IEEE Intern. Symp. on Personal, Indoor and Mobile Radio Communications (PIMRC)*, volume 2, pages 407–411, Taipei, Taiwan, October 1996.

[Hea06] M. Heal. A comment on the throughput of non-persistent CSMA. In *Proc. World Congress in Computer Science, Computer Engineering, and Applied Computing (CIC)*, pages 77–79, Las Vegas, NV, USA, June 2006.

[HG09] M. Haenggi and R. Ganti. *Interference in Large Wireless Networks*. now publishing, 2009.

[HGPC99] X. Hong, M. Gerla, G. Pei, and C.-C. Chiang. A group mobility model for ad hoc wireless networks. In *Proc. ACM MSWiM*, pages 53–60, Seattle, Washington, United States, August 1999.

[HHL08] Y. Huan, J. Hong, and L. Lei. Performance analysis of mobility models in sparse ad-hoc networks. In *Proc. Chinese Control Conf. (CCC)*, pages 216–220, Kunming, China, July 2008.

[HLV06] E. Hyytia, P. Lassila, and J. Virtamo. Spatial node distribution of the random waypoint mobility model with applications. *IEEE Trans. Mobile Comput.*, 5(6):680–694, June 2006.

[HMS+05] W.-J. Hsu, K. Merchant, H.-W. Shu, C.-H. Hsu, and A. Helmy. Weighted waypoint mobility model and its impact on ad hoc networks. *ACM SIGMOBILE Mob. Comput. Commun. Rev.*, 9(1):59–63, January 2005.

[HR86] D. Hong and S. S. Rappaport. Traffic model and performance analysis for cellular mobile radio telephone systems with prioritized and nonprioritized handoff procedures. *IEEE Trans. Veh. Technol.*, 35(3):77–92, August 1986.

[HSPH07] W.-J. Hsu, T. Spyropoulos, K. Psounis, and A. Helmy. Modeling time-variant user mobility in wireless mobile networks. In *Proc. IEEE INFOCOM*, pages 758–766, Anchorage, AK, USA, May 2007.

[Hua09] W. Huang. Capacity of mobile ad hoc network with infrastructure support. In *Proc. Asia-Pacific Conf. on Communications (APCC)*, pages 713–716, Shanghai, China, October 2009.

[IH06] M. R. Islam and W. Hamouda. Performance of cooperative ad-hoc networks in Rayleigh fading channels. In *Proc. IEEE Vehicular Technology Conf. (VTC)*, pages 1–5, Montréal, Canada, September 2006.

[IK09] T. Issariyakul and V. Krishnamurthy. Amplify-and-forward cooperative diversity wireless networks: Model, analysis, and monotonicity properties. *IEEE/ACM Trans. Networking*, 17(1):225–238, February 2009.

[IRK09] A. Iyer, C. Rosenberg, and A. Karnik. What is the right model for wireless channel interference? *IEEE Trans. Wireless Commun.*, 8(5):2662–2671, May 2009.

[JM96] D. B. Johnson and D. A. Maltz. Dynamic source routing in ad hoc wireless networks. In T. Imielinski and H. F. Korth, editors, *Mobile Computing*, volume 353 of *The Kluwer Intern. Series in Engineering and Computer Science*, pages 153–181. Springer US, February 1996.

[JMR10] P. Jacquet, B. Mans, and G. Rodolakis. Information propagation speed in mobile and delay tolerant networks. *IEEE Trans. Inform. Theory*, 56(10):5001–5015, October 2010.

[Joh00] J.-O. Johansson. Measuring homogeneity of planar point-patterns by using kurtosis. *Pattern Recognition Letters*, 21(13):1149–1156, December 2000.

[JPPQ03] K. Jain, J. Padhye, V. Padmanabhan, and L. Qiu. Impact of interference on multihop wireless networkperformance. In *Proc. ACM Intern. Conf. on Mobile Computing and Networking (MobiCom)*, pages 66–80, San Diego, CA, USA, September 2003.

[JQC+04] Z. Jingmei, Z. Qi, S. Chunju, W. Ying, Z. Ping, and Z. Zhang. Adaptive optimal transmit power allocation for two-hop non-regenerative wireless relaying system. In *Proc. IEEE Vehicular Technology Conf. (VTC)*, volume 2, pages 1213–1217, Milan, Italy, May 2004.

[JS97] B. C. Jones and D. J. Skellern. An integrated propagation-mobility interference model for microcell network coverage prediction. *ACM Intern. Journal on Wireless Personal Communications*, 5:223–256, November 1997.

[JZH98] B. Jabbari, Y. Zhou, and F. Hillier. Random walk modeling of mobility in wireless networks. In *Proc. IEEE Vehicular Technology Conf. (VTC)*, volume 1, pages 639–643, Ottawa, Ontario, Canada, May 1998.

[Kal96] G. K. Kaleh. Frequency-diversity spread-spectrum communication system to counter bandlimited gaussian interference. *IEEE Trans. Commun.*, 44(7):886–893, July 1996.

[KB10] J. Klinglmayr and C. Bettstetter. Synchronization of inhibitory pulse-coupled oscillators in delayed random and line networks. In *Proc. Intern. Symp. on Applied Sciences in Biomedical and Communication Technologies (ISABEL)*, pages 1–4, Rome, Italy, November 2010.

[KBT09] J. Klinglmayr, C. Bettstetter, and M. Timme. Globally stable synchronization by inhibitory pulse coupling. In *Proc. Intern. Symp. on Applied Sciences in Biomedical and Communication Technologies (ISABEL)*, pages 1–4, Bratislava, Slovak Republic, November 2009.

[KEGL06] P. Kyritsi, P. Eggers, R. Gall, and J. Lourenco. Measurement based investigation of cooperative relaying. In *Proc. IEEE Vehicular Technology Conf. (VTC)*, pages 1–5, Montréal, Canada, September 2006.

[KM98] M. M. Krunz and A. M. Makowski. Modeling video traffic using m/g/infin; input processes: a compromise between markovian and lrd models. *IEEE J. Select. Areas Commun.*, 16(5):733–748, June 1998.

[LH06] X. Liu and M. Haenggi. Toward quasiregular sensor networks: Topology control algorithms for improved energy efficiency. *IEEE Trans. on Parallel and Distributed Systems*, 17:975–986, September 2006.

[LL10] D. Lee and J. H. Lee. Outage probability for dual-hop relaying systems with multiple interferers over Rayleigh fading channels. *IEEE Trans. Veh. Technol.*, 60(1):333–338, October 2010.

[LS79] P. A. W. Lewis and G. S. Shedler. Simulation of non-homogeneous Poisson processes by thinning. *Naval Res. Logistics Quart.*, 26(3):403–413, September 1979.

[LW00] J. N. Laneman and G. W. Wornell. Energy-efficient antenna sharing and relaying for wireless networks. In *Proc. IEEE Wireless Commun. and Netw. Conf. (WCNC)*, volume 1, pages 7–12, Chicago, IL, USA, September 2000.

[LWT01] J. N. Laneman, G. W. Wornell, and D. N. C. Tse. An efficient protocol for realizing cooperative diversity in wireless networks. In *Proc. IEEE Intern. Symp. on Information Theory (ISIT)*, page 294, Washington, DC, USA, June 2001.

[LYD06] S. Lim, C. Yu, and C. R. Das. Clustered mobility model for scale-free wireless networks. In *Proc. IEEE Local Computer Networks*, pages 231–238, Tampa, FL, USA, November 2006.

[MA05] S. Mukherjee and D. Avidor. Outage probabilities in Poisson and clumped Poisson-distributed hybrid ad-hoc networks. In *Proc. IEEE Conf. on Sensor and ad hoc Commun. and Netw. (SECON)*, pages 563–574, Santa Clara, California, USA, September 2005.

[Mad08] U. Madhow. *Fundamentals of Digital Communication*. Cambridge University Press, 2008.

[Mah97] B. A. Mah. An empirical model of HTTP network traffic. In *Proc. Joint Conf. of the IEEE Computer and Commun. Soc. (INFOCOM)*, volume 2, pages 592–600, Kobe, Japan, April 1997.

[MBM09] M. Menth, A. Binzenhofer, and S. Muhleck. Source models for speech traffic revisited. *IEEE/ACM Trans. Networking*, 17(4):1042–1051, August 2009.

[MMA04] T. Miyano, H. Murata, and K. Araki. Cooperative relaying scheme with space time code for multihop communications among single antenna terminals. In *Proc. IEEE Global Telecommunications Conf. (GLOBECOM)*, volume 6, pages 3763–3767, Dallas, TX, USA, December 2004.

[MMMZ08] R. Madan, N. Mehta, A. Molisch, and J. Zhang. Energy-efficient cooperative relaying over fading channels with simple relay selection. *IEEE Trans. Wireless Commun.*, 7(8):3013–3025, August 2008.

[MNdM04] A. Mendes, B. A. A. Nunes, and L. F. M. de Moraes. Uma avaliação dos efeitos das regras de borda e dos modelos de mobilidade no comportamento dos nós em redes ad hoc. In *Proc. Workshop de Comunicação Sem Fio e Computação Móvel (WCSF)*, pages 117–126, Fortaleza, CE, Brasil, October 2004.

[MRC05] S. Muff, F. Rao, and A. Caflisch. Local modularity measure for network clusterizations. *Phys. Rev. E*, 72(5):1–4, November 2005.

[MYAB09] N. Marchenko, E. Yanmaz, H. Adam, and C. Bettstetter. Selecting a spatially efficient cooperative relay. In *Proc. IEEE Global Telecommunications Conf. (GLOBECOM)*, pages 1–7, Honolulu, HI, USA, December 2009.

[Nak60] M. Nakagami. The m distribution, a general formula of intensity of rapid fading. In W. G. Hoffman, editor, *Statistical Methods in Radio Wave Propagation*, pages 3–36, Oxford, UK, June 1960.

[Neu81] M. F. Neuts. *Matrix-Geometric Solutions in Stochastic Models*. The John Hopkins University Press, 1981.

[NJGM07] C. T. K. Ng, N. Jindal, A. J. Goldsmith, and U. Mitra. Capacity gain from two-transmitter and two-receiver cooperation. *IEEE Trans. Inform. Theory*, 53(10):3822–3827, October 2007.

[NTLL05] P. Nain, D. Towsley, B. Liu, and Z. Liu. Properties of random direction models. In *Proc. IEEE Infocom*, volume 3, pages 1897–1907, Miami, FL, USA, March 2005.

[OMPT05] H. Ochiai, P. Mitran, H. Poor, and V. Tarokh. Collaborative beamforming for distributed wireless ad hoc sensor networks. *IEEE Trans. Signal Processing*, 53(11):4110–4124, November 2005.

[PF95] V. Paxson and S. Floyd. Wide area traffic: the failure of Poisson modeling. *IEEE/ACM Trans. Netw.*, 3:226–244, June 1995.

[PGWC09] P. Pinto, A. Giorgetti, M. Win, and M. Chiani. A stochastic geometry approach to coexistence in heterogeneous wireless networks. *IEEE J. Select. Areas Commun.*, 27(7):1268–1282, September 2009.

[Pia08] R. J. Piasecki. A generalization of the inhomogeneity measure for point distributions to the case of finite size objects. *Physica A: Statistical Mechanics and its Applications*, 387(22):5333–5341, September 2008.

[PK91] R. Prasad and A. Kegel. Improved assessment of interference limits in cellular radio performance. *IEEE Trans. Veh. Technol.*, 40(2):412–419, May 1991.

[PKC+05] T. R. Park, T. H. Kim, J. Y. Choi, S. Choi, and W. H. Kwon. Throughput and energy consumption analysis of IEEE 802.15.4 slotted CSMA/CA. *IEEE Electronics Letters*, 41(18):1017–1019, September 2005.

[PKM+08] G. Parissidis, M. Karaliopoulos, M. May, T. Spyropoulos, and B. Plattner. Interference in wireless multihop networks: A model and its experimental evaluation. In *Proc. Intern. Symp. on a World of Wireless, Mobile and Multimedia Networks (WoWMoM)*, pages 1–12, June 2008.

[PP02] A. Papoulis and S. U. Pillai. *Probability, Random Variables and Stochastic Processes, Fourth Edition*. McGraw-Hill, 2002.

[QZW+07] L. Qiu, Y. Zhang, F. Wang, M. K. Han, and R. Mahajan. A general model of wireless interference. In *Proc. ACM Intern. Conf. on Mobile computing and Networking (MOBICOM)*, pages 171–182, Montréal, Québec, Canada, 2007.

[RF06] P. Rost and G. Fettweis. A cooperative relaying scheme without the need for modulation with increased spectral efficiency. In *Proc. IEEE Vehicular Technology Conf. (VTC)*, pages 1–5, Montréal, Canada, September 2006.

[Ric44] S. O. Rice. Mathematical analysis of random noise. *Bell Syst. Tech. J.*, 23:282–332, July 1944.

[RS02] G. Resta and P. Santi. An analysis of the node spatial distribution of the random waypoint model for ad hoc networks. In *Proc. ACM Workshop on Principles of Mobile Computing (POMC)*, pages 44–50, Toulouse, France, October 2002.

[RSWZ05] P. Rickenbach, S. Schmid, R. Wattenhofer, and A. Zollinger. A robust interference model for wireless ad-hoc networks. In *Proc. IEEE Intern. Parallel Distr. Proc. Symp.*, pages 66–80, Denver, CO, USA, April 2005.

[SB03] P. Santi and D. M. Blough. The critical transmitting range for connectivity in sparse wireless ad hoc networks. *IEEE Trans. Mobile Comput.*, 2(1):25–39, January-March 2003.

[Sch05] M. Schwartz. *Mobile Wireless Communications*. Cambridge University Press, 2005.

[SF08] R. Subramanian and F. Fekri. Unicast throughput analysis of finite-buffer sparse mobile networks using markov chains. In *Proc. Allerton Conf. on Communication, Control, and Computing*, pages 1161–1168, Urbana-Champaign, IL, USA, September 2008.

[SGDC08] A. P. Subramanian, H. Gupta, S. R. Das, and J. Cao. Minimum interference channel assignment in multiradio wireless mesh networks. *IEEE Trans. Mobile Comput.*, 7:1459–1473, December 2008.

[Sio05] I. Siomina. A novel simulation approach for mobility models in an inhomogeneous area. In *Proc. IEEE Intern. Symp. on Personal, Indoor and Mobile Radio Communications (PIMRC)*, volume 4, pages 2116–2120, Berlin, Germany, September 2005.

[SJC+10] K. Srinivasan, M. Jain, J. I. Choi, T. Azim, E. S. Kim, P. Levis, and B. Krishnamachari. The κ factor: Inferring protocol performance using inter-link reception correlation. In *Proc. MobiCom*, Chicago, IL, USA, September 2010.

[SKM95] D. Stoyan, W. S. Kendall, and J. Mecke. *Stochastic Geometry and its Applications*. Wiley, 2nd edition, 1995.

[SSLC07] S. Song, K. Son, H.-W. Lee, and S. Chong. Opportunistic relaying in cellular network for capacity and fairness improvement. In *Proc. IEEE Global Telecommunications Conf. (GLOBECOM)*, pages 4407–4412, Washington, DC, USA, November 2007.

[SVF09] R. Subramanian, B. N. Vellambi, and F. Fekri. A generalized framework for throughput analysis in sparse mobile networks. In *Proc. Intern. Symp. on Modeling and Optimization in Mobile, Ad Hoc, and Wireless Networks (WiOPT)*, pages 1–10, Seoul, Korea, June 2009.

[TAB07] A. Tyrrell, G. Auer, and C. Bettstetter. Biologically inspired synchronization for wireless networks. In F. Dressler and I. Carreras, editors, *Advances in Biologically Inspired Information Systems*, volume 69, pages 47–62. Springer, December 2007.

[TAB10] A. Tyrrell, G. Auer, and C. Bettstetter. Emergent slot synchronization in wireless networks. *IEEE Trans. Mobile Comput.*, 9(5):719–732, May 2010.

[TBA08] F. Tan, Y. Borghol, and S. Ardon. Emo: A statistical encounter-based mobility model for simulating delay tolerant networks. In *Proc. Intern. Symp. on a World of Wireless, Mobile and Multimedia Networks (WoWMoM)*, Newport Beach, CA, USA, June 2008.

[TH80] F. A. Tobagi and V. B. Hunt. Performance analysis of carrier sense multiple access with collision detection. *Journal on Computer Networks*, 4(5):245–259, October 1980.

[Tho56] H. R. Thompson. Distribution of distance to nth neighbour in a population of randomly distributed individuals. *Ecology*, 57(2):391–394, April 1956.

[TK85] H. Takagi and L. Kleinrock. Throughput analysis for pesistent CSMA systems. *IEEE Trans. Commun.*, 33(7):627–638, July 1985.

[Tyr10] A. Tyrrell. *Firefly Synchronization in Wireless Networks*. Dr. Hut Verlag, 2010.

[Vit74] P. Vit. Testing for homogeneity: the geometric distribution. *Biometrika*, 61(3):565–568, December 1974.

[VT06] A. K. Vyas and F. A. Tobagi. Impact of interference on the throughput of a multihop path in a wireless network. In *Proc. Intern. Conf. on Broadband Communications, Networks and Systems (BROADNETS)*, pages 1–10, San José, California, USA, October 2006.

[VWAH06] R. Vilzmann, J. Widmer, I. Aad, and C. Hartmann. Low-complexity beamforming techniques for wireless multihop networks. In *Proc. IEEE SECON*, volume 2, pages 489–497, Reston, VA, USA, September 2006.

[Wimax09] IEEE standard for local and metropolitan area networks part 16: Air interface for broadband wireless access systems. *IEEE Std 802.16-2009 (Revision of IEEE Std 802.16-2004)*, pages 1–2004, May 2009.

[Wlan09] IEEE standard for information technology–telecommunications and information exchange between systems–local and metropolitan area networks–specific requirements part 11: Wireless LAN medium access control (MAC) and physical layer (PHY) specifications amendment 5: Enhancements for higher throughput. *IEEE Std 802.11n-2009 (Amendment to IEEE Std 802.11-2007 as amended by IEEE Std 802.11k-2008, IEEE Std 802.11r-2008, IEEE Std 802.11y-2008, and IEEE Std 802.11w-2009)*, pages 1–502, October 2009.

[Wpan06] IEEE standard for information technology- telecommunications and information exchange between systems- local and metropolitan area networks- specific requirements part 15.4: Wireless medium access control (MAC) and physical layer (PHY) specifications for low-rate wireless personal area networks (WPANs). *IEEE Std 802.15.4-2006 (Revision of IEEE Std 802.15.4-2003)*, pages 1–305, September 2006.

[WPS09] M. Win, P. Pinto, and L. Shepp. A mathematical theory of network interference and its applications. *Proc. IEEE*, 97(2):205–230, February 2009.

[XJZ+10] J. Xiao, X. Ji, X. Zhang, S. Chen, and W. Wang. Queue analysis of finite buffer for self-similar traffic in three-node cooperative relay wireless networks. In *Proc. IEEE Intern. Conf. on Computer and Information Technology (CIT)*, pages 2562–2569, Bradford, UK, July 2010.

[XTZ07] W. Xu, W. Trappe, and Y. Zhang. Channel surfing: defending wireless sensor networks from interference. In *Proc. Intern. Conf. on Information Processing in Sensor Networks (IPSN)*, pages 499–508, Cambridge, Massachusetts, USA, April 2007.

[YB07] S. Yang and J.-C. Belfiore. Towards the optimal amplify-and-forward cooperative diversity scheme. *IEEE Trans. Inform. Theory*, 53(9):3114–3126, September 2007.

[YP03] X. Yang and A. P. Petropulu. Co-channel interference modeling and analysis in a Poisson field of interferers in wireless communications. *IEEE Trans. Signal Processing*, 51(1):64–76, January 2003.

[YPK03] S. Yi, Y. Pei, and S. Kalyanaraman. On the capacity improvement of ad hoc wireless networks using directional antennas. In *Proc. ACM Intern.*

Symp. on Mobile ad hoc Networking & Computing (MobiHoc), pages 108–116, Annapolis, Maryland, USA, June 2003.

[YS92] Y.-D. Yao and A. U. H. Sheikh. Investigations into cochannel interference in microcellular mobile radio systems. *IEEE Trans. Veh. Technol.*, 41(2):114–123, May 1992.

[ZA02] E. Ziouva and T. Antonakopoulos. CSMA/CA performance under high traffic conditions: throughput and delay analysis. *Elsevier Jounal on Computer Communications*, 25(3):313–321, January 2002.

[ZHF05] E. Zimmermann, P. Herhold, and G. Fettweis. On the performance of cooperative relaying protocols in wireless networks. *European Trans. on Telecommunications*, 16(1):5–16, February 2005.

[ZKWB07] J. Zhao, M. Kuhn, A. Wittneben, and G. Bauch. Cooperative transmission schemes for decode-and-forward relaying. In *Proc. IEEE Intern. Symp. on Personal, Indoor and Mobile Radio Commun. (PIMRC)*, pages 1–5, Athens, Greece, September 2007.

[Zwi57] F. Zwicky. *Morphological Astronomy*. Springer, 1957.

[ZYC+09] P. Zhang, J. Yuan, J. Chen, J. Wang, and J. Yang. Analyzing amplify-and-forward and decode-and-forward cooperative strategies in wyner's channel model. In *Proc. IEEE Wireless Commun. and Netw. Conf. (WCNC)*, pages 1–6, Budapest, Hungary, April 2009.

[ZZHZ10] T. Zhu, Z. Zhong, T. He, and Z.-L. Zhang. Exploring link correlation for efficient flooding in wireless sensor networks. In *Proc. USENIX Symp. Networked Sys. Design Implementation*, San Jose, CA, USA, April 2010.

[ZZSW05] H. Zheng, Y. Zhu, C. Shen, and X. Wang. On the effectiveness of cooperative diversity in ad hoc networks: a MAC layer study. In *Proc. IEEE Intern. Conf. on Acoustics, Speech, and Signal Processing (ICASSP)*, volume 3, pages 509–512, Philadelphia, PA, USA, March 2005.